J_k -INTEGRAL FORMULATION AND IMPLEMENTATION FOR THERMALLY LOADED ORTHOTROPIC FUNCTIONALLY GRADED MATERIALS

A THESIS SUBMITTED TO
THE GRADUATE SCHOOL OF NATURAL AND APPLIED SCIENCES
OF
MIDDLE EAST TECHNICAL UNIVERSITY

BY

EYÜP ERHAN ARMAN

IN PARTIAL FULFILLMENT OF THE REQUIREMENTS
FOR
THE DEGREE OF MASTER OF SCIENCE
IN
MECHANICAL ENGINEERING

NOVEMBER 2008

Approval of the thesis:

J_k-INTEGRAL FORMULATION AND IMPLEMENTATION FOR THERMALLY LOADED ORTHOTROPIC FUNCTIONALLY GRADED MATERIALS

submitted by **EYÜP ERHAN ARMAN** in partial fulfillment of the requirements for the degree of **Master of Science in Mechanical Engineering, Middle East Technical University** by,

Prof. Dr. Canan ÖZGEN
Dean, Graduate School of **Natural and Applied Sciences** ________________

Prof. Dr. Süha ORAL
Head of the Department, **Mechanical Engineering** ________________

Assoc. Prof. Dr. Serkan DAĞ
Supervisor, **Mechanical Engineering Dept., METU** ________________

Examining Committee Members:

Prof. Dr. Bülent DOYUM ________________
Mechanical Engineering Dept., METU

Assoc. Prof. Dr. Serkan DAĞ
Mechanical Engineering Dept., METU ________________

Prof. Dr. Suat KADIOĞLU
Mechanical Engineering Dept., METU ________________

Prof. Dr. Haluk DARENDELİLER
Mechanical Engineering Dept., METU ________________

Assoc. Prof. Dr. Bora YILDIRIM
Mechanical Engineering Dept., HU ________________

Date: ________________

I hereby declare that all information in this document has been obtained and presented in accordance with academic rules and ethical conduct. I also declare that, as required by these rules and conduct, I have fully cited and referenced all material and results that are not original to this work.

Name, Last Name: Eyüp Erhan Arman

Signature:

ABSTRACT

J_k-INTEGRAL FORMULATION AND IMPLEMENTATION FOR THERMALLY LOADED ORTHOTROPIC FUNCTIONALLY GRADED MATERIALS

Arman, Eyüp Erhan

M.Sc., Department of Mechanical Engineering

Supervisor: Assoc. Prof. Dr. Serkan Dağ

November 2008, 99 pages

The main aim of this study is to utilize a J_k-integral based computational method in order to calculate crack tip parameters for orthotropic functionally graded materials (FGMs). The crack is subjected to mixed mode thermal loading. Mixed mode thermal fracture analysis requires the calculation of mode-I and mode-II stress intensity factors (K_I, K_{II}). In addition to stress intensity factors, energy release rate and T-stress are calculated by means of J_k-integral. J_k-integral is defined as a line integral over a vanishingly small curve. Since it is difficult to deal with a line integral on a vanishing curve , J_k-integral is converted to a domain independent form containing area and line integrals by the help of plane thermoelasticity constitutive relations. Steady-state temperature distribution profiles in FGMs and the components of the J_k-integral are computed by means of the finite element method.

In both thermal and structural analyses, finite element models that possess graded isoparametric elements are created in the general purpose finite element analysis software ANSYS. In the formulation of J_k-integral, all required engineering material properties are assumed to possess continuous spatial variations through the functionally graded medium. The numerical results are compared to the results obtained from Displacement Correlation Technique (DCT). The domain independence of J_k-integral is also demonstrated. The results obtained in this study show the effects of crack location and material property gradation profiles on stress intensity factors, energy release rate and T-stress.

Keywords: Functionally Graded Materials (FGMs), Finite Element Method, J_k-Integral, Mixed-Mode Stress Intensity Factors, Thermal Stresses.

ÖZ

FONKSİYONEL DERECELENDİRİLMİŞ MALZEMELERDE ISISAL YÜKLEME ALTINDA J_k-İNTEGRAL FORMÜLASYONU VE UYGULAMASI

Arman, Eyüp Erhan

Yüksek Lisans, Makina Mühendisliği Bölümü

Tez Yöneticisi: Doç. Dr. Serkan Dağ

Kasım 2008, 99 Sayfa

Bu çalışmanın amacı, J_k-integral metodunu kullanarak Fonksiyonel Derecelendirilmiş Malzemelerdeki çatlak ucu parametrelerini hesaplamaktır. Çatlak, karışık modda termal yüklemeye maruz kalmaktadır. Karışık modda termal yüklemeler altındaki çatlak analizleri mod-I ve mod-II gerilme şiddeti factörlerinin (K_I, K_{II}) hesap edilmesini gerektirmektedir. Gerilme şiddeti faktörlerinin hesabına ek olarak enerji bırakma miktarı ve T-gerilimsi de J_k-integral metodu ile hesap edilmektedir. J_k-integral sonsuz küçüklükte bir eğri üzerinde eğri integrali olarak tanımlanmıştır. Eğri üzerinde tanımlanmış integral ile çalışmanın mümkün olmamasından, J_k-integral, düzlemsel termal elastikiyet kuramları ile alan ve çizgi integralleri içeren ve alandan bağımsız bir integral haline dönüştürülmüştür. Fonsiyonel Derecelendirilmiş Malzemelerdeki sürekli haldeki sıcaklık dağılım profilleri ve J_k-integrali oluşturan unsurlar sonlu elemanlar yöntemi ile hesap edilmektedir.

Genel amaçlı sonlu eleman analiz yazılımı olan ANSYS'te yapılan termal ve yapısal analizlerde derecelendirilmiş izoparametrik elemanlara sahip sonlu eleman modelleri oluşturulmuştur. J_k-integral formülasyonunda gerekli olan bütün malzeme özelliklerinin, fonksiyonel derecelendirilmiş ortamda sürekli uzaysal değişimlere sahip oldukları varsayılmıştır. Elde edilen sayısal sonuçlar Yer Değiştirme Bağıntısı Tekniği ile elde edilen sonuçlarla karşılaştırılmıştır. J_k-integralinin alandan bağımsız olma özelliği de gösterilmiştir. Bu çalışmada elde edilen sonuçlar çatlak pozisyonunun ve malzeme özelliklerinin derecelendirilme profillerinin gerilme şiddeti faktörlerine, enerji bırakma miktarına ve T-gerilmesine etkilerini göstermektedir.

Anahtar Kelimeler: Fonksiyonel Derecelendirilmiş Malzemeler, Sonlu Elemanlar Methodu, J_k-Integrali, Karışık-Mod Gerilme Şiddeti Faktörleri, Termal Gerilmeler.

To My Family

ACKNOWLEDGEMENTS

I express sincere appreciation to my supervisor Assoc. Prof. Dr. Serkan DAĞ and Assoc. Prof. Dr. Bora YILDIRIM for their great guidance, advice, criticism, systematic supervision, encouragements, and insight throughout the study.

I am thankful to my company ASELSAN Inc. for letting and supporting of my thesis.

The cooperation and friendly support of my colleagues in ASELSAN during my thesis study also deserves to be acknowledged.

I also want to thank my beloved family, my mother Gönül Arman, my father Necat Arman, my sister Esra Arman for their encouragement and faith in me.

TABLE OF CONTENTS

APPENDICES

LIST OF FIGURES

FIGURES

LIST OF TABLES

TABLES

LIST OF SYMBOLS

a	*Half crack length*
h	*Total thickness of the FGM medium*
h_1	*Thickness of the FGM medium above the crack*
h_2	*Thickness of the FGM medium below the crack*
W	*Mechanical strain energy density function*
W^+	*Mechanical strain energy density function at the upper crack face*
W^-	*Mechanical strain energy density function at the lower crack face*
J_k	J_k *- Integral*
q	*q function*
z_k	*Complex variable*
x_k	*Real part of complex variable*
y_k	*Imaginary part of complex variable*
μ_k	*Roots of the characteristic equation*
α_k	*Real part of roots of the characteristic equation*
β_k	*Imaginary part of roots of the characteristic equation*
a_{ij}	*Compliance coefficients*
E_i	*Modulus of Elasticity*
K_I	*Mode I stress intensity factor*
K_{II}	*Mode II stress intensity factor*
x_1	*Global coordinate x in indicial notation*
x_2	*Global coordinate y in indicial notation*
T_{str}	*T- stress*
R	*Length of integration path*

δ_k	*Length of portions over which* $(W^+ - W^-)$ *is approximated*
Γ_ε	*The curve on which* J_k *- Integral is defined*
Ω	*Domain integral area*
Γ	*Closed curve which surrounds the area* Ω
σ_{ij}	*Stress tensor*
ε_{ij}	*Strain tensor*
n_i	*Unit outward normal to the integration path*
u_i	*Displacement components*
δ	*Kronecker's delta*
ν_{ij}	*Poisson's ratios*
α_i	*Thermal expansion coefficients*
ΔT	*Temperature difference*

CHAPTER 1

INTRODUCTION

1.1 Functionally Graded Materials

In recent years, there is an increasing demand for high performance materials that can deal with severe thermal environmental conditions. Some examples of these conditions are combustion chambers, aerospace structures, modern power generation and propulsion applications. Special focus has been given on Functionally Graded Materials (FGMs) which can provide thermal protection. Functionally Graded Materials are heterogeneous composites that have spatial variations in thermal and mechanical properties in a continuous manner. In general, Functionally Graded Materials demonstrate ceramic/metal material property gradation exploiting the favorable properties of both ceramics and metals.

Initially, FGMs have been introduced to take the advantages of ceramic and metallic components. Ceramic layer provides heat and corrosion resistance. On the other hand metallic substrate provides mechanical strength and toughness. With such materials, it is possible to improve thermal or mechanical stress relaxation, and to increase bonding strength and toughness along a coating/substrate interface. Therefore, FGMs have an ability to reduce the magnitude of residual and thermal stresses and to increase the bonding strength and fracture toughness.

FGMs have many potential applications in various industries such as the aerospace industry. Since FGMs enable to produce light weight, strong and durable materials, they are preferred to be used in aeronautics. Another possible technological application is the cutting tools. The demand for increased strength and thermal resistant cutting tools leads to use of FGMs in cutting tools. In biomaterial industry FGMs are used as components in bones and joints. Also, in combustion chambers, solid oxide fuel cells, piezoelectric devices and pressure vessels, FGMs are utilized.

There are various techniques of processing FGMs. Some of the methods are plasma spray forming, electron beam physical vapor deposition, combustion sintering, centrifugal casting and electrophoretic deposition. Some of these deposition methods are known to result in a highly anisotropic structure with reduced thermal and mechanical properties. For instance, plasma sprayed coatings have a lamellar microstructure, on the contrary electron beam physical vapor deposition method leads to a columnar microstructure. Due to the deposition methods, FGMs lose their isotropy and it is necessary to consider the orthotropic properties when studying the mechanics of FGMs.

Better understanding of FGMs is needed to allow wider use of such materials. Structural performance of material compounds is affected by various defects that already exist within the material. Therefore, fracture remains as a key failure mode of FGMs. Fracture mechanisms of these materials have to be carefully investigated. In recent years, there has been a great interest in determining the thermal stress distribution near the vicinity of a crack located in FGMs. By calculating the crack tip parameters such as stress intensity factors, it is possible to determine failure characteristics and structural reliability of FGMs.

In this study, J_k-integral is used to determine crack tip parameters. J_k-integral is a highly effective method to carry out fracture analysis. Originally, J_k-integral is not used for thermally loaded materials. This is due to the fact that, it is not possible for J_k-integral to keep its path independence under thermal stress conditions. In this study, J_k-integral is converted to domain independent form consisting of line and area integrals.

1.2 Literature Survey

Extensive research efforts are currently devoted to the experimental characterization, analytical interpretation and numerical simulation of fracture in FGMs. Because of the complexity of fracture analysis of FGMs, these researches are limited to simple geometries that contain a single crack or a series of cracks. Also, loading conditions of these geometries are simple. In the fracture analysis of FGMs different methods, such as Displacement Correlation Technique (DCT) and J_k-integral, are employed. In almost all of these methods, a numerical method (generally FEM) is used to obtain results. Below is a review of the literature related to the problem under consideration.

An important study was performed by Nikishkov and Atluri [1]. They used the equivalent domain integral method to calculate crack tip parameters, which quantify the severity of the stress/strain fields near the crack-tip under thermo-mechanical loading. 8-node isoparametric finite elements were used in the computational algorithm of this study. It is shown that the equivalent domain integral representation yields the most accurate, stable, and path-independent numerical values for the crack-tip parameters.

In the paper by Kim and Paulino [2], slanted and non-slanted cracks in orthotropic FGM plates under mechanical loading were studied. J_k-integral formulation was made for cracks that did not need to be oriented parallel to the principal orthotropy directions. Mode-I and mode-II stress intensity factors were calculated with the help of the finite element method. In the finite element procedure, isoparametric formulation was used. Material properties were chosen to be exponentially and linearly varying. The numerical results obtained from J_k-integral were validated by the results obtained from the Displacement Correlation Technique. It was shown that plate size, material property gradation and boundary conditions play significant roles in fracture behavior of FGMs.

One of the three dimensional fracture analyses was made by Walters et al [3]. In this study, the crack under consideration was subjected to thermomechanical loading which were tension loading and temperature gradient dependent loading. Results were obtained by using the domain integral approach. Therefore, a new form of J-integral was proposed. Displacement correlation technique was used to validate the results obtained from domain integral. For different crack sizes, aspect ratios and material property gradations under tensile, bending and spatially varying temperature loading, the 2D and 3D normalized stress intensity factors were calculated. The results demonstrate the accuracy of proposed J-integral in 2D and 3D.

Another important study was performed by Kim and Paulino [4]. They developed an interaction integral (M-integral) formulation by using the Lekhnitskii and Stroh formalisms to evaluate elastic T-stress for arbitrarily oriented straight and curved cracks in orthotropic nonhomogeneous materials. Exponential and hyperbolic-tangent functions are utilized to model the material property gradation.

Several fracture problems were investigated to validate the proposed integral formulation. The computed T-stress values were compared to available reference solutions. It was shown that the computed values are highly accurate.

An experimental study was carried out by Abanto-Bueno and Lambros [5]. Mechanical behaviour of the FGMs was characterized by uniaxial tensile testing. Real time data acquisitions were required for the utilization of this testing method. With the help of full-field digital image correlation technique, data for displacement field around the crack tip were acquired while the crack propagated into the graded material. Stress intensity factor and T-stress were calculated with the obtained data. It was shown that T-stress term in the asymptotic expansions for stresses had to be taken into account in order to obtain fracture resistance in FGMs.

A J-integral based method for thermal fracture analysis of orthotropic FGMs is presented by Dağ [6]. Two models were considered. The first one was a single edge crack in an FGM layer. The second one consists of periodic cracks in an FGM layer bonded to a homogeneous substrate. In both of these analyses, the FGM layer is assumed to be orthotropic. Again, the J-integral was converted to a domain independent area integral to calculate the crack tip parameters. The J-integral was computed by the finite element method. The mode-I stress intensity factors for different crack geometries and material property variation profiles were compared to the results obtained from enriched finite element method. Numerical results illustrate the influences of thermal conductivity, thermal expansion coefficient, relative crack length and crack periodicity on the mode-I stress intensity factors.

Mixed mode thermal fracture analysis of isotropic FGMs was carried out by Dağ [7] using the J_k-integral. Mode-I and Mode-II stress intensity factors were calculated for an embedded crack in an FGM layer under steady state thermal loading conditions and for periodic cracks in an FGM Thermal Barrier Coating subjected to thermal shock heating. The necessary modifications were carried out to convert the J_k-integral to a domain independent form that contains area and line integrals. Then, the components of the J_k-integral were calculated by the finite element method. The results illustrate the influences of material property variation profiles and crack geometry on the crack tip parameters, such as mode-I and mode-II stress intensity factors, energy release rate and T-stress.

Another important study is presented in the paper by Kim [8]. They calculated the non-singular T-stress and mixed-mode stress intensity factors in functionally graded materials (FGMs) by means of interaction integral in conjunction with finite element method. In this study, spatial gradation of thermomechanical properties was represented by graded finite elements. It was shown that material gradation affects the magnitudes and signs of T-stress and stress intensity factors. The path independence of M-integral was demonstrated for both SIFs and T-stress. It was also demonstrated that T-stress is more dependent on the size of domain compared to the SIFs and for the same mesh discretization, the accuracy of SIFs is higher than that of the T-stress.

In all of the studies mentioned above, materials are either isotropic or orthotropic. In isotropic models, mode-I and mixed-mode thermal stress intensity factors, energy release rate and T-stress have been calculated under both thermal loading and mechanical loading. In the case of orthotropic models, under thermal loading only mode-I fracture analysis has been performed.

The work reported in this study presents the formulation and implementation of the J_k-integral for mixed-mode fracture analysis of orthotropic functionally graded materials under thermal stress conditions.

1.3 Scope of the Study

The main objective of this study is to evaluate the crack tip parameters, namely mode-I and mode-II stress intensity factors, energy release rate and T-stress under thermal loading conditions by considering orthotropic functionally graded materials.

All the crack tip parameters are calculated using the J_k-integral approach. J_k-integral formulation is integrated into ANSYS by utilizing Ansys Parametric Design Language (APDL). Subroutines are written to calculate the integrands of J_k-integral. Numerical method of Gauss Quadrature is used to evaluate J_k-integral components. In addition, continuous variations in the material properties are taken into account by assigning the properties at the centroids of the finite elements.

The code written for the analysis is composed of two parts. In the first part, thermal boundary conditions are assigned to the related surfaces of the functionally graded medium and steady-state temperature distribution is determined. In the second part, using the calculated temperature field, structural analysis is performed and crack tip parameters are calculated. In order to validate the stress intensity factors, those obtained from J_k-integral are compared to the results obtained from the Displacement Correlation Technique [8]. The effects of crack location and material nonhomogeneity are depicted by related plots.

This study introduces a new approach to the calculation of the fracture mechanics parameters of thermally loaded orthotropic FGMs. Mixed-mode fracture analysis of orthotropic FGMs under mechanical loading have been performed by utilizing J_k-integral approach . In the literature, mode-I and mixed-mode fracture mechanics analysis of isotropic FGMs under mechanical and thermal loading conditions have been considered [7]. Therefore, this will be a new study where J_k-integral approach is used for mixed-mode fracture analysis of a crack embedded in an orthotropic functionally graded medium under thermal loading. The particular crack problem considered in the present study is shown in Figure 1.1.

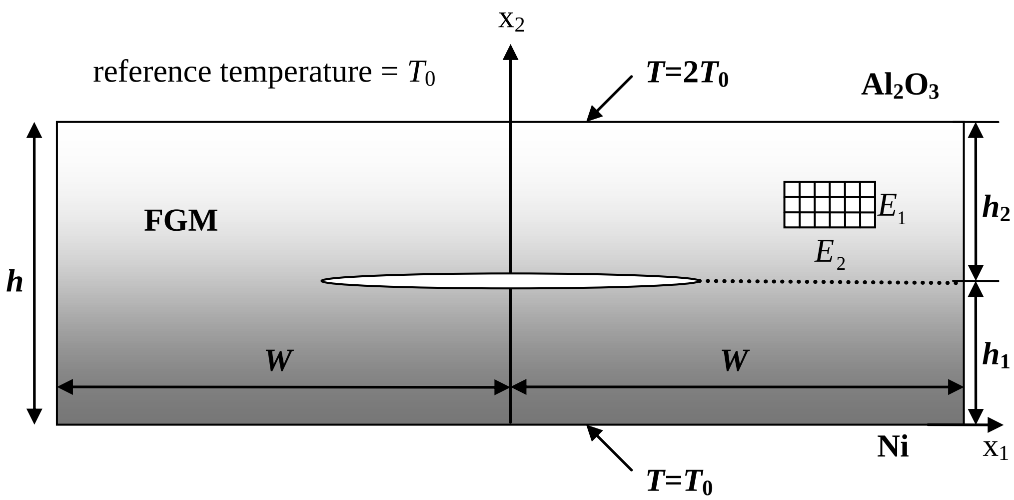

Figure 1.1 Geometry of the crack problem considered in the present study.

The material property gradation is in x_2 direction. Therefore the crack is lying perpendicular to the direction of the property gradation. The temperatures of the top and bottom surfaces are different and these are designated by $T = 2T_0$ on the top surface and $T = T_0$ on the bottom surface. The top and bottom surfaces are kept at different but constant temperatures. Reference temperature is T_0. The problem is solved under steady-state conditions. The lateral surfaces of the model are assumed to be insulated. The two dimensional model of the orthotropic FGM layer is created by using the general purpose finite element analysis software ANSYS. 8-node quadrilateral elements are used in mesh generation.

CHAPTER 2

FORMULATION

2.1 Constitutive Relations of Plane Orthotropic Thermoelasticity

Constitutive relations characterize the individual material and its reaction to the applied loads. Materials for which the constitutive behavior is only a function of the current state of deformation are known as elastic. These elastic materials deform under stress and when the stress is removed they return to their original shape. The amount of deformation during the application of the stress is strain. The homogeneity and non-homogeneity of the material significantly affect the constitutive behavior. A body is called homogeneous when the material properties are the same throughout the body, in other words, the material properties are independent of the position within the body. In case of a heterogeneous or nonhomogeneous body, the material properties are functions of position. For instance, a body composed of layers is nonhomogeneous. The layers can have uniform thicknesses of different materials. The directional dependency of material properties in a body yields anisotropy. An anisotropic body possesses different values of a material property in different directions at a point. An isotropic body possesses same values of a material property in all directions at a point.

One of the most frequently encountered non-homogeneous materials are orthogonal anisotropic or, in other words, orthotropic materials. In case of thermal elasticity, the stress-strain relation of orthotropic materials is given by Lekhnitskii [10] as follows:

$$
\begin{Bmatrix} \varepsilon_1 \\ \varepsilon_2 \\ \varepsilon_3 \\ \varepsilon_4 \\ \varepsilon_5 \\ \varepsilon_6 \end{Bmatrix} = \begin{Bmatrix} \frac{1}{E_1} & \frac{-\nu_{21}}{E_2} & \frac{-\nu_{31}}{E_3} & 0 & 0 & 0 \\ \frac{-\nu_{21}}{E_2} & \frac{1}{E_2} & \frac{-\nu_{32}}{E_3} & 0 & 0 & 0 \\ \frac{-\nu_{13}}{E_1} & \frac{-\nu_{23}}{E_2} & \frac{1}{E_3} & 0 & 0 & 0 \\ 0 & 0 & 0 & \frac{1}{G_{23}} & 0 & 0 \\ 0 & 0 & 0 & 0 & \frac{1}{G_{13}} & 0 \\ 0 & 0 & 0 & 0 & 0 & \frac{1}{G_{12}} \end{Bmatrix} \begin{Bmatrix} \sigma_1 \\ \sigma_2 \\ \sigma_3 \\ \sigma_4 \\ \sigma_5 \\ \sigma_6 \end{Bmatrix} + \begin{Bmatrix} \alpha_1 \Delta T \\ \alpha_2 \Delta T \\ \alpha_3 \Delta T \\ 0 \\ 0 \\ 0 \end{Bmatrix} \tag{2.1}
$$

where

$\Delta T = T - T_0$, T_0 is the reference temperature.

$$
\varepsilon_1 = \varepsilon_{11},\ \varepsilon_2 = \varepsilon_{22},\ \varepsilon_3 = \varepsilon_{33},\ \varepsilon_4 = 2\varepsilon_{23},\ \varepsilon_5 = 2\varepsilon_{13},\ \varepsilon_6 = 2\varepsilon_{12} \tag{2.2}
$$

$$
\sigma_1 = \sigma_{11},\ \sigma_2 = \sigma_{22},\ \sigma_3 = \sigma_{33},\ \sigma_4 = \sigma_{23},\ \sigma_5 = \sigma_{13},\ \varepsilon_6 = \sigma_{12} \tag{2.3}
$$

In the case of plane stress and plane strain, the constitutive relations of plane orthotropic thermoelasticity are given by Dağ [6]. For the case of plane stress, the relation is given as follows:

$$
\begin{Bmatrix} \varepsilon_{11} \\ \varepsilon_{22} \\ 2\varepsilon_{12} \end{Bmatrix} = \begin{Bmatrix} \frac{1}{E_1} & \frac{-\nu_{12}}{E_1} & 0 \\ \frac{-\nu_{12}}{E_1} & \frac{1}{E_2} & 0 \\ 0 & 0 & \frac{1}{G_{12}} \end{Bmatrix} \begin{Bmatrix} \sigma_{11} \\ \sigma_{22} \\ \sigma_{12} \end{Bmatrix} + \begin{Bmatrix} \alpha_1 \Delta T \\ \alpha_2 \Delta T \\ 0 \end{Bmatrix} \tag{2.4}
$$

where ε_{ij} $(i, j = 1,2)$ are the combination of mechanical and thermal strains, namely total strain components. E_{ij}, ν_{ij} and G_{ij} $(i, j = 1,2)$ are engineering constants. $\Delta T = T - T_0$ is the temperature difference from a reference temperature.

The constitutive relation for the case of plane strain is given by Dağ [6] as follows:

$$\begin{Bmatrix} \varepsilon_{11} \\ \varepsilon_{22} \\ 2\varepsilon_{12} \end{Bmatrix} = \begin{Bmatrix} \dfrac{(1-\nu_{31}\nu_{13})}{E_1} & \dfrac{-(\nu_{12}+\nu_{13}\nu_{32})}{E_1} & 0 \\ \dfrac{-(\nu_{12}+\nu_{13}\nu_{32})}{E_1} & \dfrac{(1-\nu_{23}\nu_{32})}{E_2} & 0 \\ 0 & 0 & \dfrac{1}{G_{12}} \end{Bmatrix} \begin{Bmatrix} \sigma_{11} \\ \sigma_{22} \\ \sigma_{12} \end{Bmatrix} + \begin{Bmatrix} (\nu_{31}\alpha_3+\alpha_1)\Delta T \\ (\nu_{32}\alpha_3+\alpha_2)\Delta T \\ 0 \end{Bmatrix}$$

(2.5)

The relationships between the engineering constants of orthotropic materials are given by:

$$\frac{\nu_{12}}{E_1} = \frac{\nu_{21}}{E_2} \qquad \frac{\nu_{13}}{E_1} = \frac{\nu_{31}}{E_3} \qquad \frac{\nu_{23}}{E_2} = \frac{\nu_{32}}{E_3} \tag{2.6}$$

The two-dimensional anisotropic elasticity problems can be formulated in terms of the analytic functions, $\Phi(z_k)$, of complex variable, $z_k = x_k + i y_k$ (k=1,2), where

$$x_k = x + \alpha_k y, \qquad y_k = \beta_k y, \qquad (k=1,2) \tag{2.7}$$

α_k and β_k (k=1,2) are the real and imaginary parts of $\mu_k = \alpha_k + i\beta_k$. μ_k are the roots of the characteristic equation given below. The roots are selected such that $\beta_k > 0$ [2]. μ_k are always complex or purely imaginary in conjugate pairs as $\mu_1, \bar{\mu}_1; \mu_2, \bar{\mu}_2$. Moreover, μ_1 *and* μ_2 must be evaluated at the crack tip location.

μ_k can be considered as numbers which characterize the degree of anisotropy in the case of plane problems. According to their values one can judge how much a given body differs from that of the isotropy, for which $\mu_1 = \mu_2 = i$ [10].

$$a_{11}^{tip}\mu^4 + (2a_{12}^{tip} + a_{66}^{tip})\mu^2 + a_{22}^{tip} = 0 \tag{2.8}$$

The compliance coefficients a_{ij}^{tip} are given as follows for plane stress:

$$a_{11}^{tip} = \frac{1}{E_1^{tip}}, \quad a_{12}^{tip} = \frac{-\nu_{12}^{tip}}{E_1^{tip}}, \quad a_{22}^{tip} = \frac{1}{E_2^{tip}}, \quad a_{66}^{tip} = \frac{1}{G_{12}^{tip}} \tag{2.9}$$

In case of plane strain these constants are given by

$$a_{11}^{tip} = \frac{1-\nu_{31}^{tip}\nu_{13}^{tip}}{E_1^{tip}}, \quad a_{12}^{tip} = -\frac{\nu_{12}^{tip} + \nu_{13}^{tip}\nu_{32}^{tip}}{E_1^{tip}}, \quad a_{22}^{tip} = \frac{1-\nu_{23}^{tip}\nu_{32}^{tip}}{E_2^{tip}}, \quad a_{66}^{tip} = \frac{1}{G_{12}^{tip}} \tag{2.10}$$

When the material is orthotropic and the directions of axes x_1 and x_2 coincide with the principal directions of elasticity, then the following three possibilities exist for the roots μ_1 and μ_2 [10]:

Case I: $\mu_1 = \kappa i$, $\mu_2 = \lambda i$, roots are purely imaginary and unequal.

Case II: $\mu_1 = \mu_2 = \kappa i$, roots are purely imaginary and equal.

Case III: $\mu_1 = \varphi + \kappa i$, $\mu_2 = -\varphi + \kappa i$

Since β_k are taken as positive, κ and λ values are positive as well. In this study, Case I is obtained.

2.2 J_k-Integral Formulation

The J_k-integral is a line integral which is defined over a vanishingly small curve at a crack tip. In Figure 2.1, an orthotropic functionally graded medium is depicted. It is assumed that the FGM medium shown in Figure 2.1 is linear elastic. Also, the medium is assumed to be under mixed-mode thermal stresses. x_1 and x_2 constitute a local crack tip coordinate system. Γ_ε is an arbitrary curve around the crack tip. It starts from the lower crack face and ends up at the upper crack face. $\vec{n}$ is the unit outward normal of the curve Γ_ε.

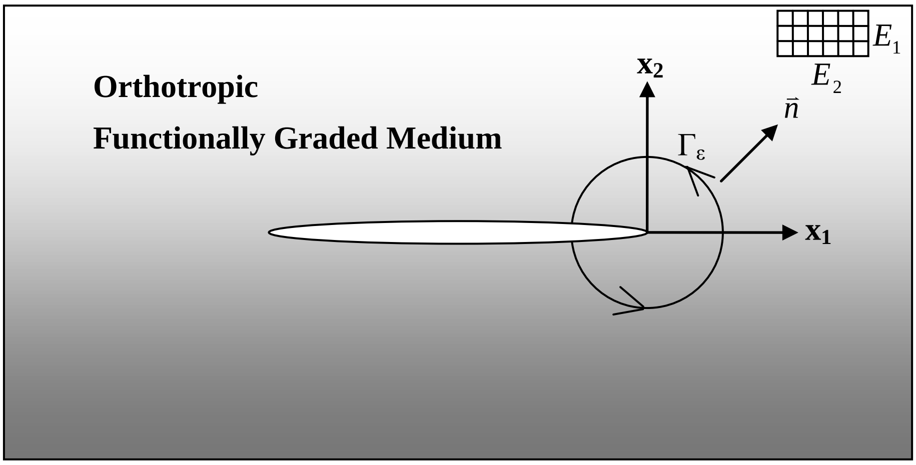

Figure 2.1 A curve Γ_ε around a crack tip in an orthotropic functionally graded medium.

Then J_k-integral is defined on the curve Γ_ε in the case of plane stress or plane strain as follows:

$$J_k = \lim_{\Gamma_\varepsilon \to 0} \left\{ \int_{\Gamma_\varepsilon} \left(W n_k - \sigma_{ij} n_j u_{i,k} \right) d\Gamma \right\} \qquad (i,j,k=1,2) \qquad (2.11)$$

where W : mechanical strain energy density function.

n_k : unit normal outward to the curve Γ_ε .

σ_{ij} : stress components.

$u_{i,k}$: displacement components.

Γ : arc length of the curve.

$$(\ )_{,k} \equiv \frac{\partial (\ )}{\partial x_k}$$

One of the main variables required in the calculation of J_k-integral is the mechanical strain energy density function, *W*. In case of a general 3-D state of stress, the mechanical strain energy density function can be written in the following form:

$$W = \frac{1}{2} \sigma_{ij} \varepsilon_{ij}^m \qquad (i,j=1,2,3) \qquad (2.12)$$

where ε_{ij}^m is the mechanical strain. The components of the mechanical strain are given as

$$\varepsilon_{11}^m = \varepsilon_{11} - \alpha_1 \Delta T \text{ , } \varepsilon_{22}^m = \varepsilon_{22} - \alpha_2 \Delta T \text{ , } \varepsilon_{33}^m = \varepsilon_{33} - \alpha_3 \Delta T$$

$$\varepsilon_{12}^m = \varepsilon_{12} \text{ , } \varepsilon_{13}^m = \varepsilon_{13} \text{ , } \varepsilon_{23}^m = \varepsilon_{23} \qquad (2.13)$$

where $\varepsilon_{33} = 0$ for plane strain.

The mechanical strain energy density function takes the following form for plane stress and strain:

$$W = \begin{cases} \frac{1}{2}\left[\sigma_{11}\varepsilon_{11}^{m} + \sigma_{12}\varepsilon_{12}^{m} + \sigma_{21}\varepsilon_{21}^{m} + \sigma_{22}\varepsilon_{22}^{m}\right], \textit{plane stress} \\ \frac{1}{2}\left[\sigma_{11}\varepsilon_{11}^{m} + \sigma_{12}\varepsilon_{12}^{m} + \sigma_{21}\varepsilon_{21}^{m} + \sigma_{22}\varepsilon_{22}^{m} + \sigma_{33}\varepsilon_{33}^{m}\right], \ \textit{plane strain} \end{cases} \tag{2.14}$$

The stress-strain relations for the cases of plane stress and plane strain are given by equations (2.4) and (2.5) respectively. In the case of plain strain, $\varepsilon_{33} = \varepsilon_{13} = \varepsilon_{23} = 0$ and σ_{33} can be obtained by equating ε_{33} to zero as follows:

$$\sigma_{33} = \frac{E_3}{E_1}\nu_{13}\sigma_{11} + \frac{E_3}{E_2}\nu_{23}\sigma_{22} - E_3\alpha_3\Delta T \tag{2.15}$$

Then W can be written in terms of strain components for the case of plane strain in the following form [6]

$$\begin{aligned} W = {} & \frac{E_1\bar{\varepsilon}_{11}}{2\Lambda}\left\{(1 - \frac{E_2\nu_{13}\nu_{32}^2}{E_1\nu_{31}})E_1\bar{\varepsilon}_{11} + (\nu_{12} + \nu_{13}\nu_{32})E_2\bar{\varepsilon}_{22}\right\} + G_{12}(\varepsilon_{12}^2 + \varepsilon_{21}^2) \\ & + \frac{E_1E_2\bar{\varepsilon}_{22}}{2\Lambda}\left\{(\nu_{12} + \nu_{13}\nu_{32})\bar{\varepsilon}_{11} + (1 - \nu_{31}\nu_{13})\bar{\varepsilon}_{22}\right\} + \frac{E_1\nu_{31}}{2\nu_{13}}\alpha_3^2(\Delta T)^2 \end{aligned} \tag{2.16}$$

where

$$\Lambda = E_1(1 - \nu_{31}\nu_{13}) - E_2\left(\frac{\nu_{32}^2\nu_{13}}{\nu_{31}} + \nu_{12}^2 + 2\nu_{12}\nu_{13}\nu_{32}\right) \tag{2.17}$$

$$\bar{\varepsilon}_{11} = \varepsilon_{11} - (\nu_{31}\alpha_3 + \alpha_1)\Delta T \ , \ \bar{\varepsilon}_{22} = \varepsilon_{22} - (\nu_{32}\alpha_3 + \alpha_2)\Delta T \tag{2.18}$$

Using the equations (2.16)-(2.18), W can be represented in the following form:

$$W = W\left(\varepsilon_{11}, \varepsilon_{12}, \varepsilon_{21}, \varepsilon_{22}, E_1, E_2, \nu_{31}, \nu_{13}, \nu_{12}, \nu_{32}, G_{12}, \alpha_1, \alpha_2, \alpha_3, \Delta T\right) \tag{2.19}$$

In the case of plain stress, $\sigma_{33} = \sigma_{13} = \sigma_{23} = 0$ and W can be written in terms of strain components in the following form [6]

$$\begin{aligned} W = &\frac{E_1^2(\varepsilon_{11} - \alpha_1 \Delta T) + \nu_{12} E_1 E_2 (\varepsilon_{22} - \alpha_2 \Delta T)}{2(E_1 - \nu_{12}^2 E_2)} (\varepsilon_{11} - \alpha_1 \Delta T) + G_{12}(\varepsilon_{12}^2 + \varepsilon_{21}^2) \\ &+ \frac{\nu_{12} E_1 E_2 (\varepsilon_{11} - \alpha_1 \Delta T) + E_1 E_2 (\varepsilon_{22} - \alpha_2 \Delta T)}{2(E_1 - \nu_{12}^2 E_2)} (\varepsilon_{22} - \alpha_2 \Delta T) \end{aligned} \tag{2.20}$$

Using equation (2.20), W can be represented in the following form

$$W = W\left(\varepsilon_{11}, \varepsilon_{12}, \varepsilon_{21}, \varepsilon_{22}, E_1, E_2, \nu_{12}, G_{12}, \alpha_1, \alpha_2, \Delta T\right) \tag{2.21}$$

The expression of the J_k-integral given in equation (2.11) is not suitable to be used in the numerical analysis. Because stress and strain components can not be calculated over a vanishingly small curve. It is necessary to express the J_k-integral in terms of domain and line integrals. In order to express the J_k-integral in terms of area and line integrals, we consider a positively oriented closed curve Γ around the crack tip as shown in Figure 2.2.

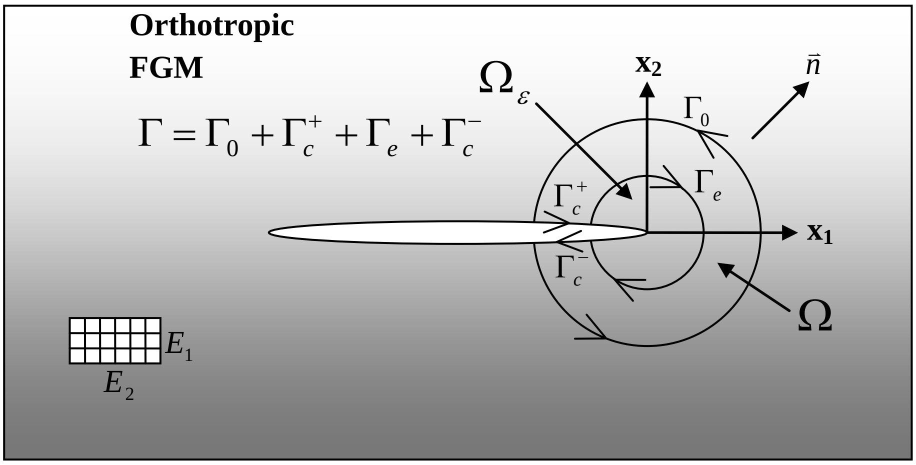

Figure 2.2 A closed curve Γ around the crack tip.

The closed curve Γ surrounds the area Ω. The curve Γ is piecewise smooth and represented as follows:

$$\Gamma = \Gamma_0 + \Gamma_c^+ + \Gamma_e + \Gamma_c^- \tag{2.22}$$

Before expressing the J_k-integral in terms of area and line integrals, some manipulations have to be carried out. Therefore, another line integral I_k is defined over the closed curve Γ. In addition to defining a new line integral, a new function q is defined. q is a piecewise smooth function which changes from unity on Γ_e and to zero on Γ_0. The integral I_k is defined as follows:

$$I_k = \oint_\Gamma \left\{ \sigma_{ij} u_{i,k} - W \delta_{kj} \right\} q n_j \, d\Gamma \ , \qquad (i,j,k = 1,2) \tag{2.23}$$

where δ_{kj} is the Kronecker's Delta.

By utilizing the Divergence Theorem (see APPENDIX A for the Divergence Theorem) in plane, I_k can be converted into an area integral as follows:

$$I_k = \iint_{\Omega} \frac{\partial}{\partial x_j}(\sigma_{ij} u_{i,k} q - W\delta_{kj} q) d\Omega , \qquad (i,j,k = 1,2) \qquad (2.24)$$

Note that the equations of equilibrium read as:

$$\sigma_{ij,j} = 0 , \qquad (\mathrm{i,j}= 1,2) \qquad (2.25)$$

Let's define the integrand of the integral I_k as Z_k

$$Z_k = \frac{\partial}{\partial x_j}(\sigma_{ij} u_{i,k} q - W\delta_{kj} q) \qquad (i,j,k = 1,2) \qquad (2.26)$$

Carrying out the differentiation, one obtains

$$Z_k = \{\sigma_{ij,j} u_{i,k} + \sigma_{ij} u_{i,kj} - W_{,j}\delta_{kj} - W\delta_{kj,j}\} q + \{\sigma_{ij} u_{i,k} - W\delta_{kj}\} q_{,j} \quad (i,j,k=1,2) \quad (2.27)$$

Note the following properties related to the Kronecker's Delta function

$$\delta_{kj,j} = 0 \ , \qquad (k,j = 1,2)$$

$$W_{,j}\delta_{kj} = W_{,k} \ , \qquad (k,j = 1,2)$$

Then, Z_k can be expressed with two components Z_k^1 and Z_k^2 as follows:

$$Z_k = \underbrace{\left\{\sigma_{ij,j}u_{i,k} + \sigma_{ij}u_{i,kj} - W_{,j}\delta_{kj} - W\delta_{kj,j}\right\}q}_{Z_k^1} + \underbrace{\left\{\sigma_{ij}u_{i,k} - W\delta_{kj}\right\}q_{,j}}_{Z_k^2} \qquad (2.28)$$

Z_k^1 contains the partial derivative of W with respect to x_k. This partial derivative can be written for both plane stress and plane strain in the form shown below:

$$W_{,k} = \frac{\partial W}{\partial x_k} = \frac{\partial W}{\partial \varepsilon_{ij}}\frac{\partial \varepsilon_{ij}}{\partial x_k} + \left[\frac{\partial W}{\partial x_k}\right]_{\text{expl}} , \qquad (i,j,k = 1,2) \qquad (2.29)$$

where $\left(W_{,k}\right)_{\text{expl}}$ is the explicit derivative of the mechanical strain energy density function. Assuming that all the thermomechanical material parameters are continuous functions of the coordinate x_1 and x_2 in the FGM layer and using the equations (2.19) and (2.21), $\left(W_{,k}\right)_{\text{expl}}$ can be written as follows for plane stress

$$\begin{aligned} \left[\frac{\partial W}{\partial x_k}\right]_{\text{expl}} &= \frac{\partial W}{\partial E_1}\frac{\partial E_1}{\partial x_k} + \frac{\partial W}{\partial E_2}\frac{\partial E_2}{\partial x_k} + \frac{\partial W}{\partial \nu_{12}}\frac{\partial \nu_{12}}{\partial x_k} + \frac{\partial W}{\partial G_{12}}\frac{\partial G_{12}}{\partial x_k} + \frac{\partial W}{\partial \alpha_1}\frac{\partial \alpha_1}{\partial x_k} \\ &+ \frac{\partial W}{\partial \alpha_2}\frac{\partial \alpha_2}{\partial x_k} + \frac{\partial W}{\partial (\Delta T)}\frac{\partial (\Delta T)}{\partial x_k} \quad , (k = 1,2) \end{aligned} \qquad (2.30)$$

For the case of plane strain we have

$$
\left[\frac{\partial W}{\partial x_k}\right]_{\text{expl}} = \frac{\partial W}{\partial E_1}\frac{\partial E_1}{\partial x_k} + \frac{\partial W}{\partial E_2}\frac{\partial E_2}{\partial x_k} + \frac{\partial W}{\partial \nu_{12}}\frac{\partial \nu_{12}}{\partial x_k} + \frac{\partial W}{\partial \nu_{13}}\frac{\partial \nu_{13}}{\partial x_k} + \frac{\partial W}{\partial \nu_{31}}\frac{\partial \nu_{31}}{\partial x_k}
$$

$$
+ \frac{\partial W}{\partial \nu_{32}}\frac{\partial \nu_{32}}{\partial x_k} + \frac{\partial W}{\partial G_{12}}\frac{\partial G_{12}}{\partial x_k} + \frac{\partial W}{\partial \alpha_1}\frac{\partial \alpha_1}{\partial x_k} + \frac{\partial W}{\partial \alpha_2}\frac{\partial \alpha_2}{\partial x_k} + \frac{\partial W}{\partial \alpha_3}\frac{\partial \alpha_3}{\partial x_k} \tag{2.31}
$$

$$
+ \frac{\partial W}{\partial(\Delta T)}\frac{\partial(\Delta T)}{\partial x_k} \quad ,(k=1,2)
$$

The derivatives of the strain energy density function can be obtained in closed form [6] (see APPENDIX A for the closed form derivatives of *W*).

By using the property,

$$
\frac{\partial W}{\partial \varepsilon_{ij}} = \sigma_{ij} \tag{2.32}
$$

and kinematic relation for small displacements

$$
\varepsilon_{ij} = \frac{1}{2}\left\{\frac{\partial u_i}{\partial x_j} + \frac{\partial u_j}{\partial x_i}\right\}, \qquad (i,j=1,2) \tag{2.33}
$$

$W_{,k}$ can be expressed as follows

$$
W_{,k} = \sigma_{ij}\frac{1}{2}\frac{\partial}{\partial x_k}\left\{\frac{\partial u_i}{\partial x_j} + \frac{\partial u_j}{\partial x_i}\right\} + \left(W_{,k}\right)_{\text{expl}}, \qquad (i,j,k=1,2) \tag{2.34}
$$

$$
W_{,k} = \sigma_{ij}\frac{1}{2}\frac{\partial}{\partial x_k}\frac{\partial u_i}{\partial x_j} + \sigma_{ij}\frac{1}{2}\frac{\partial}{\partial x_k}\frac{\partial u_j}{\partial x_i} + \left(W_{,k}\right)_{\text{expl}}, \qquad (i,j,k=1,2) \tag{2.35}
$$

By interchanging the dummy indices of the second term in equation (2.35), the following is obtained:

$$W_{,k} = \sigma_{ij} u_{i,kj} + (W_{,k})_{\text{expl}} , \qquad (i,j,k=1,2) \qquad (2.36)$$

Then Z_k^1 becomes

$$Z_k^1 = \left(\sigma_{ij,j} u_{i,k} - \left(W_{,k}\right)_{\text{expl}}\right) q , \qquad (i,j,k=1,2) \qquad (2.37)$$

Using the equation of equilibrium $\sigma_{ij,j} = 0$

$$Z_k^1 = \left(-\left(W_{,k}\right)_{\text{expl}}\right) q , \qquad (k=1,2) \qquad (2.38)$$

Then Z_k^1 equals

$$Z_k = -\left(W_{,k}\right)_{\text{expl}} q + \left(\sigma_{ij} u_{i,k} - W\delta_{kj}\right) q_{,j} , \qquad (i,j,k=1,2) \qquad (2.39)$$

The integral I_k can then be redefined in the following way

$$I_k = \oint_{\Gamma} \left\{ \sigma_{ij} u_{i,k} q - W \delta_{kj} q \right\} n_j d\Gamma = \iint_{\Omega} \left\{ \sigma_{ij} u_{i,k} - W \delta_{kj} \right\} q_{,j} d\Omega - \iint_{\Omega} \left(W_{,k} \right)_{\text{expl}} q d\Omega ,$$

$$(i,j,k=1,2) \qquad (2.40)$$

Let's define a function b_k as

$$b_k = \left(\sigma_{ij} u_{i,k} - W \delta_{kj} \right) q n_j , \qquad (i,j,k=1,2) \qquad (2.41)$$

The integral I_k can be divided into four line integrals by using newly defined function b_k

$$I_k = \oint_{\Gamma} b_k d\Gamma = \oint_{\Gamma_e} b_k d\Gamma + \oint_{\Gamma_c^+} b_k d\Gamma + \oint_{\Gamma_c^-} b_k d\Gamma + \oint_{\Gamma_0} b_k d\Gamma , \qquad (k=1,2) \qquad (2.42)$$

By changing the orientation of Γ_e, a new curve is obtained identical to the curve in Figure 2.1 and knowing that q is equal to zero on Γ_0, I_k can be written as follows

$$I_k = \oint_{\Gamma} b_k d\Gamma = -\oint_{\Gamma_\varepsilon} b_k d\Gamma + \oint_{\Gamma_c^+} b_k d\Gamma + \oint_{\Gamma_c^-} b_k d\Gamma , \qquad (k=1,2) \qquad (2.43)$$

By substituting the value b_k on the integral defined on Γ_ε, the J_k-integral is obtained.

$$\oint_{\Gamma} b_k d\Gamma = \underbrace{\oint_{\Gamma_\varepsilon} \left(W\delta_{kj} - \sigma_{ij} u_{i,k}\right) q n_j d\Gamma}_{J_k - \text{integral}} + \oint_{\Gamma_c^+} b_k d\Gamma + \oint_{\Gamma_c^-} b_k d\Gamma, \qquad (i,j,k=1,2) \qquad (2.44)$$

Then,

$$\begin{aligned} J_k &= \iint_{\Omega} \left(\sigma_{ij} u_{i,k} - W\delta_{kj}\right) q_{,j} dA - \iint_{\Omega} \left(W_{,k}\right)_{\text{expl}} q dA \\ &- \int_{\Gamma_c^+} \left(\sigma_{ij} u_{i,k} - W\delta_{kj}\right) q n_j d\Gamma - \int_{\Gamma_c^-} \left(\sigma_{ij} u_{i,k} - W\delta_{kj}\right) q n_j d\Gamma, \end{aligned} \qquad (i,j,k=1,2) \qquad (2.45)$$

Ω is the area between the crack tip and the curve Γ_0. Since the crack surfaces are free surfaces, the term $\sigma_{ij} u_{i,k} n_j = 0$ in the Γ_c^+ and Γ_c^- integrals. Then J_k-integral can be further simplified as follows

$$\begin{aligned} J_k &= \iint_{\Omega} \left(\sigma_{ij} u_{i,k} - W\delta_{kj}\right) q_{,j} dA - \iint_{\Omega} \left(W_{,k}\right)_{\text{expl}} q dA \\ &+ \int_{\Gamma_c^+} \left(W^+ n_k^+\right) q d\Gamma + \int_{\Gamma_c^-} \left(W^- n_k^-\right) q d\Gamma, \end{aligned} \qquad (i,j,k=1,2) \qquad (2.46)$$

In addition, the first component of unit outward normal, i.e. n_1, is equal to zero on Γ_c^+ and Γ_c^-. Finally J_k-integral is written as follows

$$\begin{aligned} J_k &= \iint_{\Omega} \left(\sigma_{ij} u_{i,k} - W\delta_{kj}\right) q_{,j} dA - \iint_{\Omega} \left(W_{,k}\right)_{\text{expl}} q dA \\ &+ \int_{\Gamma_c} \left(W^+ - W^-\right) q n_k^+ d\Gamma, \end{aligned} \qquad (i,j,k=1,2) \qquad (2.47)$$

There exists a discontinuity denoted by the term (W^+-W^-) in the mechanical strain energy density across the crack faces.

The components of J_k-integral can now be written as follows

$$J_1 = \iint_{\Omega} \left(\sigma_{ij} u_{i,1} - W\delta_{1j}\right) q_{,j} \, d\Omega - \iint_{\Omega} \left(W_{,1}\right)_{\text{expl}} q d\Omega \,, \qquad \text{(i,j=1,2)} \qquad (2.48)$$

$$J_2 = \iint_{\Omega} \left(\sigma_{ij} u_{i,2} - W\delta_{2j}\right) q_{,j} \, d\Omega - \iint_{\Omega} \left(W_{,2}\right)_{\text{expl}} q d\Omega$$
$$- \int_{\Gamma_c} \left(W^+ - W^-\right) q d\Gamma, \qquad \text{(i,j=1,2)} \qquad (2.49)$$

The mechanical strain energy density function used in J_1 and J_2-integrals is given by the equations (2.14) and (2.18) for plane strain and plane stress, respectively. Moreover, the explicit derivatives of W are given by equations (2.28) and (2.29) for plane stress and plane strain, respectively. The area integrals given in J_1 and J_2-integrals will be calculated over a circular domain as shown in Figure 2.3.

Now let's concentrate on the line integral term $\int_{\Gamma_c} (W^+ - W^-) q d\Gamma$ given in the J_2-integral. The integrand of this line integral involves mechanical strain energy density function difference. The most general method to calculate this integral is proposed by Eischen [12]. Eischen suggested that the path of the line integral can be divided into two one of which is close to the crack tip and the other remote from the crack tip. The line integral is then expressed as:

$$\int_{\Gamma_c} (W^+ - W^-) q d\Gamma = \int_0^R (W^+ - W^-) q dx = \int_0^{R-\delta} (W^+ - W^-) q dx + \int_{R-\delta}^R (W^+ - W^-) q dx$$

(2.50)

where R is the length of the integration path. δ is the length of portion over which $(W^+ - W^-)$ is approximated by its asymptotic representation and x is the line integration variable measured from the point where Γ_0 intersects x_1 axis. The integration path is shown in the Figure 2.3. The integral close to the crack tip possessing the limits $R-\delta < x < R$ can then be evaluated using the asymptotic approximation to W. The asymptotic distribution of the stresses near the crack tip are given as follows [2]:

$$\sigma_{ij}(r,\theta) = \frac{K_I}{\sqrt{2\pi r}} f_{ij}^{I}(\theta) + \frac{K_{II}}{\sqrt{2\pi r}} f_{ij}^{II}(\theta) + T_{str}\delta_{1i}\delta_{1j} \ , \qquad (i,j=1,2) \qquad (2.51)$$

$$\begin{aligned}\sigma_{11}(r,\theta) = {} & \frac{K_I}{\sqrt{2\pi r}} \mathrm{Re}\left[\frac{\mu_1^{tip}\mu_2^{tip}}{\mu_1^{tip} - \mu_2^{tip}} \left\{ \frac{\mu_2^{tip}}{\sqrt{\cos\theta + \mu_2^{tip}\sin\theta}} - \frac{\mu_1^{tip}}{\sqrt{\cos\theta + \mu_1^{tip}\sin\theta}} \right\} \right] \\ & + \frac{K_{II}}{\sqrt{2\pi r}} \mathrm{Re}\left[\frac{1}{\mu_1^{tip} - \mu_2^{tip}} \left\{ \frac{\left(\mu_2^{tip}\right)^2}{\sqrt{\cos\theta + \mu_2^{tip}\sin\theta}} - \frac{\left(\mu_1^{tip}\right)^2}{\sqrt{\cos\theta + \mu_1^{tip}\sin\theta}} \right\} \right] + T_{str}\end{aligned} \qquad (2.52)$$

$$\begin{aligned}\sigma_{22}(r,\theta) = {} & \frac{K_I}{\sqrt{2\pi r}} \mathrm{Re}\left[\frac{1}{\mu_1^{tip} - \mu_2^{tip}} \left\{ \frac{\mu_1^{tip}}{\sqrt{\cos\theta + \mu_2^{tip}\sin\theta}} - \frac{\mu_2^{tip}}{\sqrt{\cos\theta + \mu_1^{tip}\sin\theta}} \right\} \right] \\ & + \frac{K_{II}}{\sqrt{2\pi r}} \mathrm{Re}\left[\frac{1}{\mu_1^{tip} - \mu_2^{tip}} \left\{ \frac{1}{\sqrt{\cos\theta + \mu_2^{tip}\sin\theta}} - \frac{1}{\sqrt{\cos\theta + \mu_1^{tip}\sin\theta}} \right\} \right]\end{aligned} \qquad (2.53)$$

$$\begin{aligned}\sigma_{12}(r,\theta) = {} & \frac{K_I}{\sqrt{2\pi r}} \mathrm{Re}\left[\frac{\mu_1^{tip}\mu_2^{tip}}{\mu_1^{tip} - \mu_2^{tip}} \left\{ \frac{1}{\sqrt{\cos\theta + \mu_1^{tip}\sin\theta}} - \frac{1}{\sqrt{\cos\theta + \mu_2^{tip}\sin\theta}} \right\} \right] \\ & + \frac{K_{II}}{\sqrt{2\pi r}} \mathrm{Re}\left[\frac{1}{\mu_1^{tip} - \mu_2^{tip}} \left\{ \frac{\mu_1^{tip}}{\sqrt{\cos\theta + \mu_1^{tip}\sin\theta}} - \frac{\mu_2^{tip}}{\sqrt{\cos\theta + \mu_2^{tip}\sin\theta}} \right\} \right]\end{aligned} \qquad (2.54)$$

where r and θ are the polar coordinates shown in Figure 2.3. T_{str} is the non-singular stress component, namely the T-stress. T-stress influences crack growth under mixed-mode loading, crack path stability and size and shape of plastic zone around the crack tip.

The mechanical strain energy density function difference can be written as follows

$$W^{+} - W^{-} = W(r,\pi) - W(r,-\pi) \tag{2.55}$$

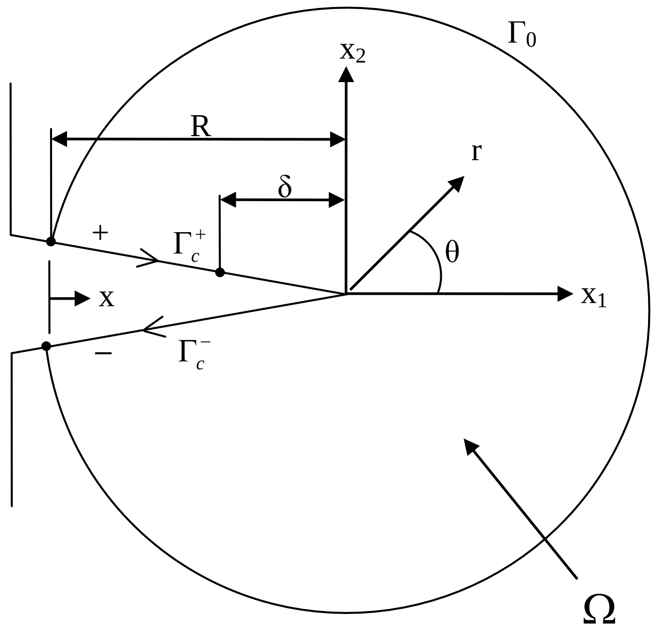

Figure 2.3 Integration path Γ_c and circular area Ω around the crack tip.

In order to calculate $W^{+} - W^{-}$, in addition to knowing that Case I is obtained in this study, the equations (2.12), (2.51) and (2.55) are used. Then the mechanical strain energy density function difference is obtained as

$$W(r,\pi) - W(r,-\pi) = [W^{+} - W^{-}] = \frac{1}{2}\left\{a_{11}\left(4\frac{K_{II}}{\sqrt{2\pi r}}\left\{D\left(\beta_1^2 - \beta_2^2\right)\right\}T_{str}\right)\right\} \tag{2.56}$$

which can be rewritten as

$$\left[W^{+} - W^{-}\right] = \frac{1}{\sqrt{2\pi r}} F \tag{2.57}$$

where

$$F = 2a_{11} K_{II} \left\{ D\left(\beta_1^2 - \beta_2^2\right) \right\} T_{str} \tag{2.58}$$

$$a_{11} = \begin{cases} \dfrac{1}{E_1} & , \, plane\, stress \\ \dfrac{\left(1 - \nu_{31}\nu_{13}\right)}{E_1} & , \, plane\, strain \end{cases} \tag{2.59}$$

$$D = \frac{-1}{\left(\beta_1 - \beta_2\right)} \tag{2.60}$$

where the β_1 and β_2 are given by equation 2.7.

Then the following approximation can be made to the line integral $\int_{\Gamma_c} (W^{+} - W^{-}) q d\Gamma$.

Where

$$q = 1 - \frac{\sqrt{x_1^2 + x_2^2}}{R} \tag{2.61}$$

Then,

$$\int_{\Gamma_c} (W^{+} - W^{-}) q d\Gamma \approx \int_0^{R-\delta} (W^{+} - W^{-}) q dx + \int_{R-\delta}^{R} \frac{F}{\sqrt{2\pi r}} q dx \tag{2.62}$$

Evaluating the integral, one obtains

$$\int_{\Gamma_c}(W^+ - W^-)qd\Gamma \approx \int_0^{R-\delta}(W^+ - W^-)qdx + \sqrt{\frac{\delta}{2\pi}}\frac{2F(3R-\delta)}{3R} \qquad (2.63)$$

Then J_2-integral can finally be written as follow

$$\begin{aligned} J_2 &= \iint_\Omega \left(\sigma_{ij}u_{i,2} - W\delta_{2j}\right)q_{,j}d\Omega - \iint_\Omega \left(W_{,2}\right)_{\text{expl}} qd\Omega \\ &- \int_0^{R-\delta}\left(W^+ - W^-\right)qdx - \sqrt{\frac{\delta}{2\pi}}\frac{2F(3R-\delta)}{3R}, \end{aligned} \qquad (i,j=1,2) \qquad (2.64)$$

2.3 Calculation of the mixed-mode stress intensity factors and the *T*-stress

Notice that J_1-integral can be evaluated by calculating the domain integral given by equation (2.48). On the other hand, J_2-integral can not be directly calculated by using the integral expression (2.64). Because, the final integral expression for J_2-integral contains K_{II} and T_{str} which are unknowns. Therefore a new quantity $\hat{J}_2$ is introduced as follows:

$$\begin{aligned} \hat{J}_2 &= \iint_\Omega \left(\sigma_{ij}u_{i,2} - W\delta_{2j}\right)q_{,j}d\Omega - \iint_\Omega \left(W_{,2}\right)_{\text{expl}} qd\Omega \\ &- \int_0^{R-\delta}\left(W^+ - W^-\right)qdx, \end{aligned} \qquad (i,j=1,2) \qquad (2.65)$$

The quantity $\hat{J}_2$ is evaluated using the equation (2.65) for two values of $\delta(\delta_1,\delta_2)$. The distances δ_1 and δ_2 are shown in Figure 2.4. These values of $\hat{J}_2$ can be written as follows

$$\left(\hat{J}_2\right)_{\delta_1} = J_2 + \sqrt{\frac{\delta_1}{2\pi}}\,\frac{2F\left(3R-\delta_1\right)}{3R} \tag{2.66}$$

$$\left(\hat{J}_2\right)_{\delta_2} = J_2 + \sqrt{\frac{\delta_2}{2\pi}}\,\frac{2F\left(3R-\delta_2\right)}{3R} \tag{2.67}$$

Let's define a new function S as follows

$$S = \frac{2F}{\sqrt{2\pi}} \tag{2.68}$$

The equations (2.66) and (2.67) can be rewritten as follows

$$\left(\hat{J}_2\right)_{\delta_1} = J_2 + \sqrt{\delta_1}\left(1-\frac{\delta_1}{3R}\right)S \tag{2.69}$$

$$\left(\hat{J}_2\right)_{\delta_2} = J_2 + \sqrt{\delta_2}\left(1-\frac{\delta_2}{3R}\right)S \tag{2.70}$$

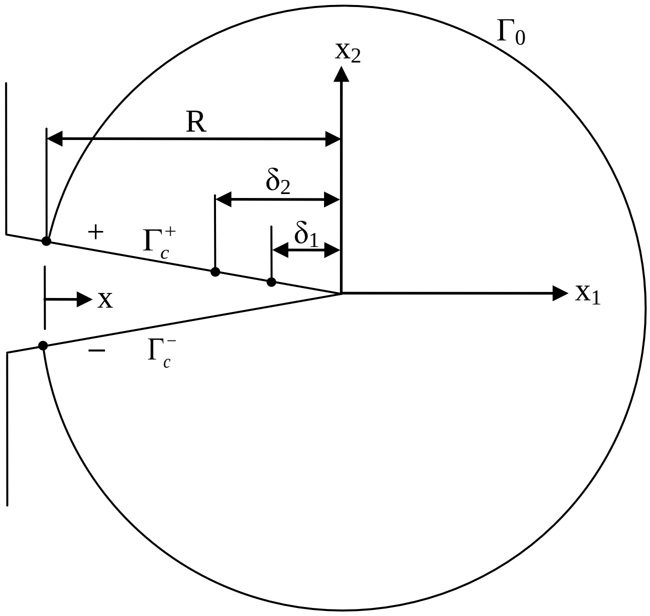

Figure 2.4 The distances δ_1 and δ_2.

J_2 and S can now be easily obtained as follows

$$J_2 = \frac{\sqrt{\delta_1}\left(1-\frac{\delta_1}{3R}\right)\left(\hat{J}_2\right)_{\delta_2} - \sqrt{\delta_2}\left(1-\frac{\delta_2}{3R}\right)\left(\hat{J}_2\right)_{\delta_2}}{\sqrt{\delta_1}\left(1-\frac{\delta_1}{3R}\right) - \sqrt{\delta_2}\left(1-\frac{\delta_2}{3R}\right)} \tag{2.71}$$

$$S = \frac{\left(\hat{J}_2\right)_{\delta_1} - \left(\hat{J}_2\right)_{\delta_2}}{\sqrt{\delta_1}\left(1-\frac{\delta_1}{3R}\right) - \sqrt{\delta_2}\left(1-\frac{\delta_2}{3R}\right)} \tag{2.72}$$

Then, from equations (2.57)-(2.60) and (2.68) T -stress is calculated as follows

$$T_{str} = \frac{S\sqrt{2\pi}}{4a_{11}K_{II}D\left(\beta_1^2 - \beta_2^2\right)} \tag{2.73}$$

In orthotropic FGMs, the relationship between J_k -integral and mode-I and mode-II stress intensity factors have been established as (Obata et al., 1989; Ma and Chen, 1996) [13,14]

$$\begin{aligned} J_1 = -\frac{a_{11}}{2}\,\mathrm{Im}\Big\{&K_I^2\left(\mu_1^{tip} + \mu_2^{tip}\right)\left(\overline{\mu_1^{tip}\mu_2^{tip}}\right) + 2K_I K_{II}\left(\overline{\mu_1^{tip}\mu_2^{tip}}\right) \\ &- K_{II}^2\left(\mu_1^{tip} + \mu_2^{tip}\right)\Big\} \end{aligned} \tag{2.74}$$

$$\begin{aligned} J_2 = -\frac{a_{11}}{4}\,\mathrm{Im}\Big\{&K_I^2\left(\mu_1^{tip}\mu_2^{tip} + \overline{\mu_1^{tip}\mu_2^{tip}}\mu_1^{tip}\mu_2^{tip}\right) \\ &- K_I K_{II}\Big[\mu_1^{tip}\mu_2^{tip}\left(\mu_1^{tip} + \mu_2^{tip} + \overline{\mu_1^{tip}} + \overline{\mu_2^{tip}}\right) \\ &+ \left(\mu_1^{tip} + \mu_2^{tip}\right)\left(\mu_1^{tip}\mu_2^{tip} + 3\overline{\mu_1^{tip}\mu_2^{tip}}\right)\Big] \\ &+ K_{II}^2\Big[\mu_1^{tip}\mu_2^{tip}\left(\mu_1^{tip} + \mu_2^{tip} + \overline{\mu_1^{tip}} + \overline{\mu_2^{tip}}\right) + \overline{\mu_1^{tip}\mu_2^{tip}}\Big]\Big\} \end{aligned} \tag{2.75}$$

where a_{11} is given in equation (2.59), and μ_1 and μ_2 are given by equation (2.8).

Since the stress intensity factors are coupled, they may be solved by means of iteration. Newton iteration is proposed in the paper of Kim and Paulino [2]. But in order to calculate SIFs by means of Newton iteration, initial values of K_I and K_{II} are required. Initial values of K_I and K_{II} are determined by means of Displacement Correlation Technique (DCT) in this paper.

Since in this study μ_1 and μ_2 are obtained purely imaginary, equations (2.74) and (2.75) are further simplified. The relationship between J_k-integral and stress intensity factors can then be rewritten as

$$J_1 = \frac{a_{11}}{2}\left\{K_I^2\left(\beta_1^{tip}+\beta_2^{tip}\right)\left(\beta_1^{tip}\beta_2^{tip}\right)+K_{II}^2\left(\beta_1^{tip}+\beta_2^{tip}\right)\right\} \tag{2.76}$$

$$J_2 = -\frac{a_{11}}{4}\left\{K_I K_{II}\left(\beta_1^{tip}+\beta_2^{tip}\right)4\left(\beta_1^{tip}\beta_2^{tip}\right)\right\} \tag{2.77}$$

where β_1 and β_2 are the imaginary parts of the roots μ_1 and μ_2, respectively.

Here there are two unknowns K_I and K_{II}, and two equations. Therefore from equation (2.77) K_I can be written as

$$K_I = \frac{-J_2}{K_{II}\, a_{11}\left(\beta_1^{tip}+\beta_2^{tip}\right)\beta_1^{tip}\beta_2^{tip}} \tag{2.78}$$

By utilizing the equations (2.76) and (2.78), K_{II} is obtained from the following equation

$$K_{II}^4 - \frac{2J_1}{a_{11}\left(\beta_1^{tip}+\beta_2^{tip}\right)}K_{II}^2 + \left(\frac{-J_2}{a_{11}\left(\beta_1^{tip}+\beta_2^{tip}\right)\beta_1^{tip}\beta_2^{tip}}\right)^2\beta_1^{tip}\beta_2^{tip} = 0 \tag{2.79}$$

All material properties are calculated at the crack tip.

Let’s define a new parameter Θ, such that

$$K_{II}^{2} = \Theta \qquad (2.80)$$

Then, we obtain

$$\Theta^2 - \frac{2J_1}{a_{11}\left(\beta_1^{tip}+\beta_2^{tip}\right)}\Theta + \left(\frac{-J_2}{a_{11}\left(\beta_1^{tip}+\beta_2^{tip}\right)\beta_1^{tip}\beta_2^{tip}}\right)^2 \beta_1^{tip}\beta_2^{tip} = 0 \qquad (2.81)$$

Θ can be obtained in the form,

$$\Theta_{1,2} = \frac{J_1}{a_{11}\left(\beta_1^{tip}+\beta_2^{tip}\right)}\left(1 \pm \left[1-\left(\frac{J_2}{J_1}\right)^2 \frac{1}{\beta_1^{tip}\beta_2^{tip}}\right]^{1/2}\right) \qquad (2.82)$$

K_{II} is obtained as,

$$K_{II} = \pm\left\{\frac{J_1}{a_{11}\left(\beta_1^{tip}+\beta_2^{tip}\right)}\left(1 \pm \left[1-\left(\frac{J_2}{J_1}\right)^2 \frac{1}{\beta_1^{tip}\beta_2^{tip}}\right]^{1/2}\right)\right\}^{1/2} \qquad (2.83)$$

Similarly K_I is obtained as,

$$K_{I} = \pm\left\{\frac{J_1}{a_{11}\left(\beta_1^{tip}+\beta_2^{tip}\right)\beta_1^{tip}\beta_2^{tip}}\left(1 \mp \left[1-\left(\frac{J_2}{J_1}\right)^2 \frac{1}{\beta_1^{tip}\beta_2^{tip}}\right]^{1/2}\right)\right\}^{1/2} \qquad (2.84)$$

The signs of the SIFs and those of the terms within the parenthesis are determined by monitoring relative normal and tangential displacements near the crack tip which are defined as [7, 15, 16]

$$\Delta_I = u_2^{+} - u_2^{-}, \qquad \Delta_{II} = u_1^{+} - u_1^{-} \qquad (2.85)$$

where the superscripts + and – stands for upper and lower crack surfaces, respectively.

Δ_I and Δ_{II} are calculated in the close vicinity of the crack tip. A positive Δ_I implies that crack is open and K_I is positive. Similarly, K_{II} is positive if $\Delta_{II} > 0$. The signs of the terms within the parenthesis in equations (2.83) and (2.84) can be determined by the conditions given below [15]:

$$\text{If } |\Delta_I| \geq |\Delta_{II}| \quad \text{take [+] for } K_{II} \text{ and take [-] for } K_I \tag{2.86}$$

$$\text{If } |\Delta_I| < |\Delta_{II}| \quad \text{take [-] for } K_{II} \text{ and take [+] for } K_I \tag{2.87}$$

CHAPTER 3

FINITE ELEMENT IMPLEMENTATION

3.1 Finite Element Method

In today's studies, modelling the physical phenomena is one of the most important things that the engineers and scientists consider. Almost every phenomenon in the nature, for instance aeronautical, biological, mechanical, chemical, or geological can be described, with the aid of the laws of physics or other fields in terms of algebraic, differential, and/or integral equations relating various quantities of interest. Determining the stress distribution on a cantilever beam subjected to mechanical, aerodynamical or even thermal loading, preparing simulation of weather in advance of a thunderstorm or tornado are the few examples of practical problems.

Physical phenomena can be described analytically. This description is called mathematical model. Mathematical models are composed of a set of equations expressing the important features of the phenomena in terms of variables that describe the system. Mathematical models depend on the fundamental scientific laws of physics. In the case of a dynamics problem, e.g. a simple pendulum, the principle of conservation of linear momentum is used whereas, in case of a heat transfer problem the principle of conservation of energy is utilized. Many engineering problems have been solved with the help of suitable mathematical models and numerical methods by computers for the last three decades. Today, the most general and powerful numerical method in its applications to real world problems involving complicated physics, geometry and boundary conditions is the Finite Element Method.

In the Finite Element Method, the geometrically complex domain under consideration is represented as a set of geometrically simple subdomains, namely finite elements. Every finite element is considered as an independent domain by itself. The governing equation of the problem is approximated over the each subdomains with the help of a suitable variational method. The variational formulation stands for the construction of a functional principle that is equavalent to the governing equations of the problem. In order to obtain the numerical model of the whole domain, the relationships from all elements are assembled using certain interelement relationships.

A finite element analysis typically involves the following steps. Steps 1, 4, and 5 require decisions by the analyst and provide input data for the computer program. Steps 2, 3, 6, and 7 are carried out automatically by the computer program. Stress analysis and heat transfer analysis will be cited as typical applications.

1. Mesh generation programs, called preprocessors, divide the domain into finite elements.
2. The properties of each element are formulated. For instance, in stress analysis, nodal loads associated with all element deformation states that are allowed are determined.
3. Assembly of the elements to obtain the finite element model of the structure is done.
4. Application of the known loads are performed. Nodal forces and/or moments in stress analysis, nodal heat fluxes in heat transfer analysis are determined.
5. All the boundary conditions are specified. In stress analysis, how the structure is supported is specified. This step involves setting several nodal displacements to known values. In heat transfer, where typically certain temperatures are known, all known values of nodal temperature are imposed.

6. Linear algebraic equations to determine nodal degrees of freedom are solved simultaneously.
7. With the help of postprocessors, calculated nodal values are used to sort the output.

The main aim in the numerical analysis carried out in this study is to obtain the results of the area and line integrals given by J_k-integral. Exact evaluation of these integrals is not possible because of the algebraic complexity of the integrands. Numerical evaluation of these integrals involves approximation of the integrand by a polynomial of sufficient degree. This is due to the fact that, the integral of a polynomial can be evaluated exactly. Numerical integration is considered in the present study in order to compute the components of the J_k-integral.

Consider the integral

$$A = \int_{x_a}^{x_b} F(x)\, dx \tag{3.1}$$

Polynomial approximation of $F(x)$ can be written in the following way

$$F(x) \approx \sum_{i=1}^{N} F_i \Psi_i(x) \tag{3.2}$$

where F_i denotes the value of $F(x)$ at the i^{th} point of the interval $[x_a, x_b]$ and $\psi_i(x)$ are polynomials of degree $N-1$.

In general, a quadrature formula has the form

$$A = \int_{x_a}^{x_b} F(x)\,dx \approx \sum_{i=1}^{r} F(x_i) W_i \tag{3.3}$$

where x_i are called the quadrature points and W_i are the quadrature weights.

An accurate representation of irregular domains can be accomplished by using quadrilateral elements. But, derivation of shape functions and evaluation of integrals are difficult over quadrilateral elements. Therefore integral statements defined over quadrilaterals are transferred to rectangle. The transformation is depicted in figure 3.1. In this study, Gauss-Legendre quadrature is used to evaluate the J_k-integrals. Gauss-Legendre quadrature requires the integral to be evaluated over a square region $\hat{\Omega}$ shown in figure 3.1 and the coordinate system (ξ,η) to be defined on the interval $[-1,1]$. In order to use this interval, a coordinate transformation from the global coordinate (x, y) to local coordinate (ξ,η) is carried out. The values of the local coordinate system always lie between -1 and 1 with its origin at the center of the element.

The utilization of the local coordinate system is beneficial in two ways:

1. It is convenient in constructing the interpolation functions.
2. It is required in numerical integration when using Gauss-Legendre Quadrature.

The element $\hat{\Omega}$ is called master element. Each element of the finite element mesh is transformed to $\hat{\Omega}$ only for the purpose of numerically evaluating the J_k-integral.

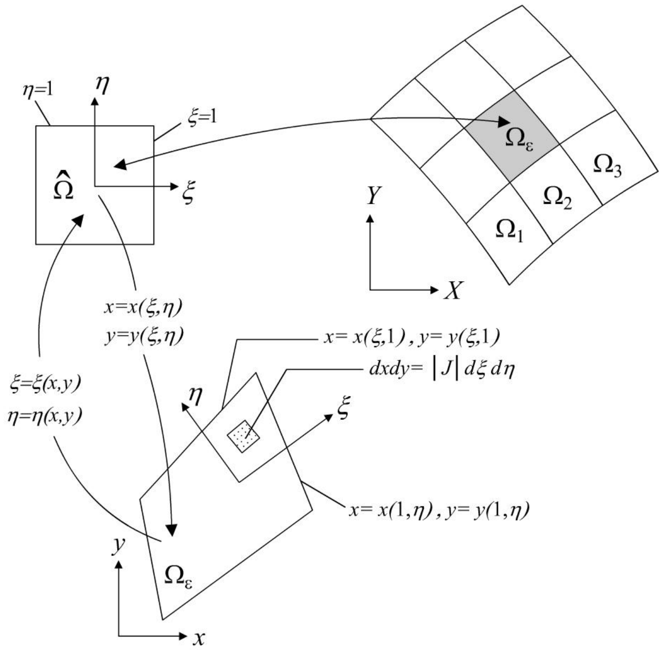

Figure 3.1 Mapping of a master rectangular element to an arbitrary quadrilateral element of a finite element mesh.

The transformation between the element Ω_ε and $\hat{\Omega}$ is performed by a coordinate transformation of the form

$$x = \sum_{i=1}^{m} x_i \psi_i(\xi, \eta) \tag{3.4}$$

$$y = \sum_{i=1}^{m} y_i \psi_i(\xi, \eta) \tag{3.5}$$

where $\psi_i(\xi, \eta)$ denote the shape functions. In general, the dependent variable or variables of the problem are approximated by an expression similar to the expressions (3.4) and (3.5).

The variable or variables are given in the following form:

$$u(\xi,\eta) = \sum_{i=1}^{n} u_i \hat{\psi}_i(\xi,\eta) \tag{3.6}$$

Here the shape functions given by $\hat{\psi}_i$ are different than ψ_i. Therefore depending on the relative degree of approximations used for the geometry and dependent variable(s), the finite element formulations are classified into three categories.

1. Superparametric (*m*>*n*): The approximation used for the geometry is higher order than that used for the dependent variable.
2. Isoparametric (*m*=*n*): The approximation used for the geometry is equal to that of used for the dependent variable.
3. Subparametric (*m*<*n*): The higher order approximation of the dependent variable is used.

In this study isoparametric formulation is used and all the dependent variables of J_k-integral are approximated in a way that is shown in equation (3.6).

Then, with the help of Gauss-Legendre Quadrature, a line integral is represented as

$$\int_a^b F(x)dx = \int_{-1}^{1} \hat{F}(\xi)d\xi \approx \sum_{i=1}^{r} \hat{F}(\xi_i)w_i \tag{3.7}$$

where,

$$\hat{F}(\xi) = F(x(\xi))J(\xi), \quad dx = Jd\xi \tag{3.8}$$

$$J = \sum_{i=1}^{m} x_i \frac{d\psi_i}{d\xi} \tag{3.9}$$

where *r* is the number of base points and w_i are the weight factors.

In the case of an area integral, Gauss-Legendre Quadrature can be expressed as follows

$$\int_{\Omega} F(x,y)dxdy = \int_{\Omega} \hat{F}(\xi,\eta)d\xi d\eta = \int_{-1}^{1}\left[\int_{-1}^{1} \hat{F}(\xi,\eta)d\xi\right]d\eta \approx \int_{-1}^{1}\left[\sum_{i=1}^{N} \hat{F}(\xi_i,\eta)w_i\right]d\eta$$
$$\approx \sum_{j=1}^{M}\sum_{i=1}^{N} \hat{F}(\xi_i,\eta_j)w_i w_j$$

(3.10)

$$\hat{F}(\xi,\eta) = F(x(\xi), y(\eta))\left|J\right|, \quad dxdy = \left|J\right| d\xi d\eta \tag{3.11}$$

where $\left|J\right|$ is the Jacobian matrix determinant. Jacobian matrix and its determinant are given as follows,

$$[J] = \begin{bmatrix} \dfrac{\partial x}{\partial \xi} & \dfrac{\partial y}{\partial \xi} \\ \dfrac{\partial x}{\partial \eta} & \dfrac{\partial y}{\partial \eta} \end{bmatrix} = \begin{bmatrix} \sum x_i \dfrac{\partial \psi_i}{\partial \xi} & \sum y_i \dfrac{\partial \psi_i}{\partial \xi} \\ \sum x_i \dfrac{\partial \psi_i}{\partial \eta} & \sum y_i \dfrac{\partial \psi_i}{\partial \eta} \end{bmatrix} \tag{3.12}$$

$$\left|J\right| = J_{11}J_{22} - J_{21}J_{12} \tag{3.13}$$

In this study, 2nd order Gauss- Legendre Quadrature is used. For the 2nd order Gauss- Legendre Quadrature and for the line integral, the Gauss points and weights are given as

$$\left(\xi_i, \eta_j\right) = \left(\pm \frac{1}{\sqrt{3}}, -1\right) \tag{3.14}$$

$$w_i = 1 \tag{3.15}$$

For the area integral, the Gauss points and weights are given as

$$\left(\xi_i, \eta_j\right) = \left(\pm \frac{1}{\sqrt{3}}, \pm \frac{1}{\sqrt{3}}\right) \tag{3.16}$$

$$w_i = 1, \, w_j = 1 \tag{3.17}$$

In this study, the developed numerical procedure is integrated into the general purpose finite element analysis software ANSYS []. Two kinds of analysis are performed in the ANSYS. Firstly, thermal analysis is conducted and in the second part structural analysis is performed. Thermal analysis is carried out with the help of the PLANE77 element in ANSYS. It possesses thermal degrees of freedom such as temperatures at nodes. Structural analysis is performed using the PLANE82 element. PLANE82 element possesses structural degrees of freedom such as displacements. These two elements are shown in Figure 3.2. (The Gauss points on the PLANE77 and PLANE82 elements for the area and line integrals are shown in the Figures 3.3 and 3.4, respectively.)

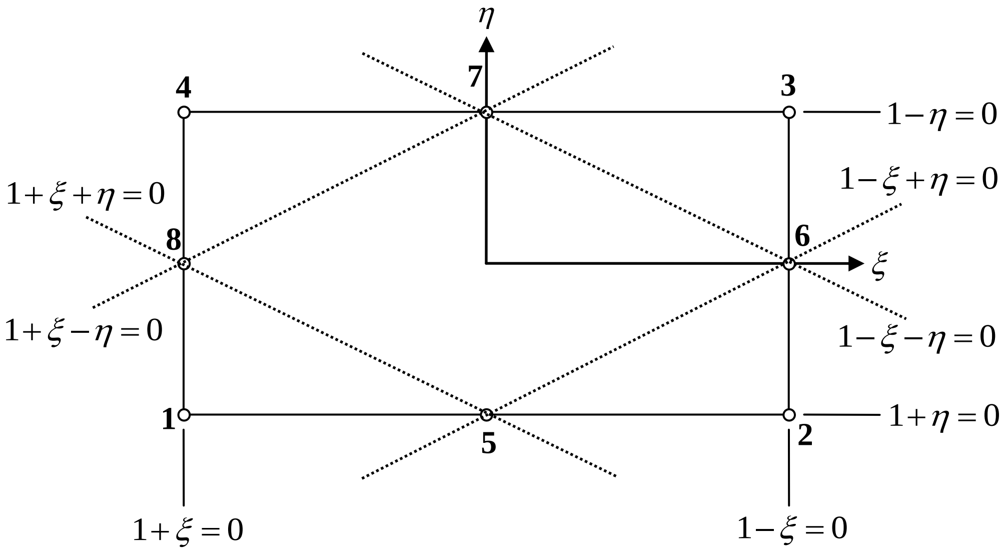

Figure 3.2 PLANE77 and PLANE82 elements.

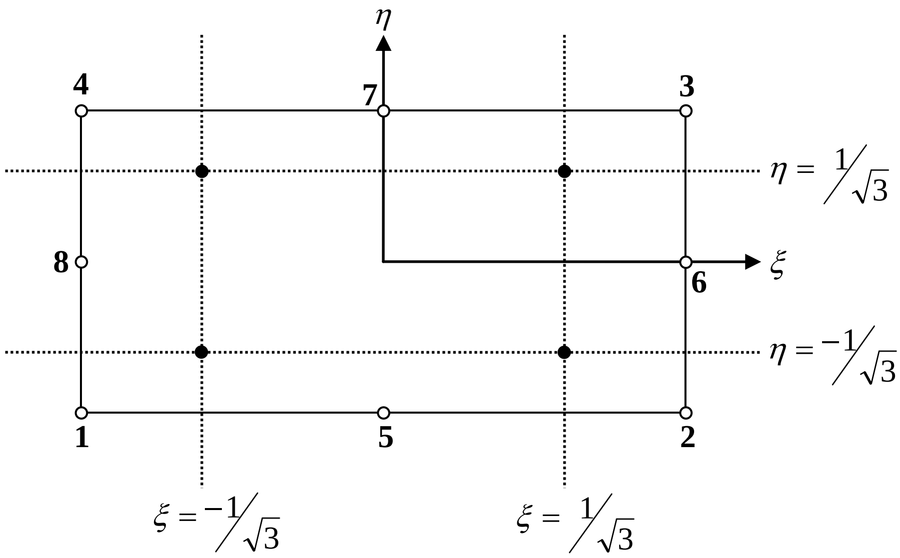

Figure 3.3 Location of the Gauss points for area integrals.

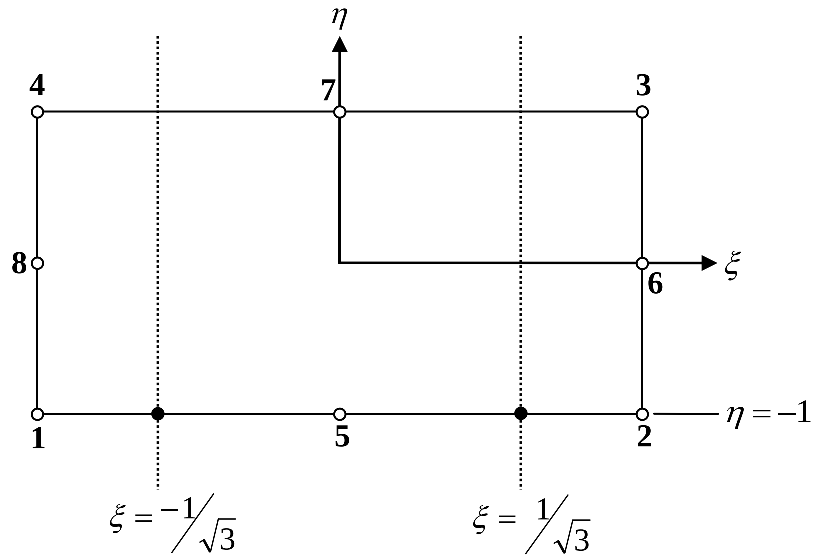

Figure 3.4 Location of the Gauss points for the line integrals.

Shape functions for PLANE77 and PLANE82 elements are given as follows,

$$\psi_1 = -\frac{1}{4}(1-\xi)(1-\eta)(1+\xi+\eta) \qquad \psi_2 = \frac{1}{2}(1-\xi^2)(1-\eta)$$

$$\psi_3 = -\frac{1}{4}(1+\xi)(1-\eta)(1-\xi+\eta) \qquad \psi_4 = \frac{1}{2}(1-\xi)(1-\eta^2) \tag{3.18}$$

$$\psi_5 = \frac{1}{2}(1+\xi)(1-\eta^2) \qquad \psi_6 = -\frac{1}{4}(1-\xi)(1+\eta)(1+\xi-\eta)$$

$$\psi_7 = \frac{1}{2}(1-\xi^2)(1+\eta) \qquad \psi_8 = -\frac{1}{4}(1+\xi)(1+\eta)(1-\xi-\eta)$$

In this study, in order to discretize the functionally graded medium, first the 8-node quadrilateral elements, which are PLANE 77 and PLANE 82 elements, are selected from the Ansys element type menu and then by collapsing the three nodes of these 8-node elements as shown in Figure 3.5, 6-node triangular elements are obtained.

The reason to utilize the triangular elements is to obtain much more accurate results. As a result, the domain is discretized by triangular elements which are actually 8-node quadrilateral elements. Since the triangular elements are 8-node quadrilateral elements in essence, the shape functions and formulations of 8-node quadrilateral elements are utilized throughout this study.

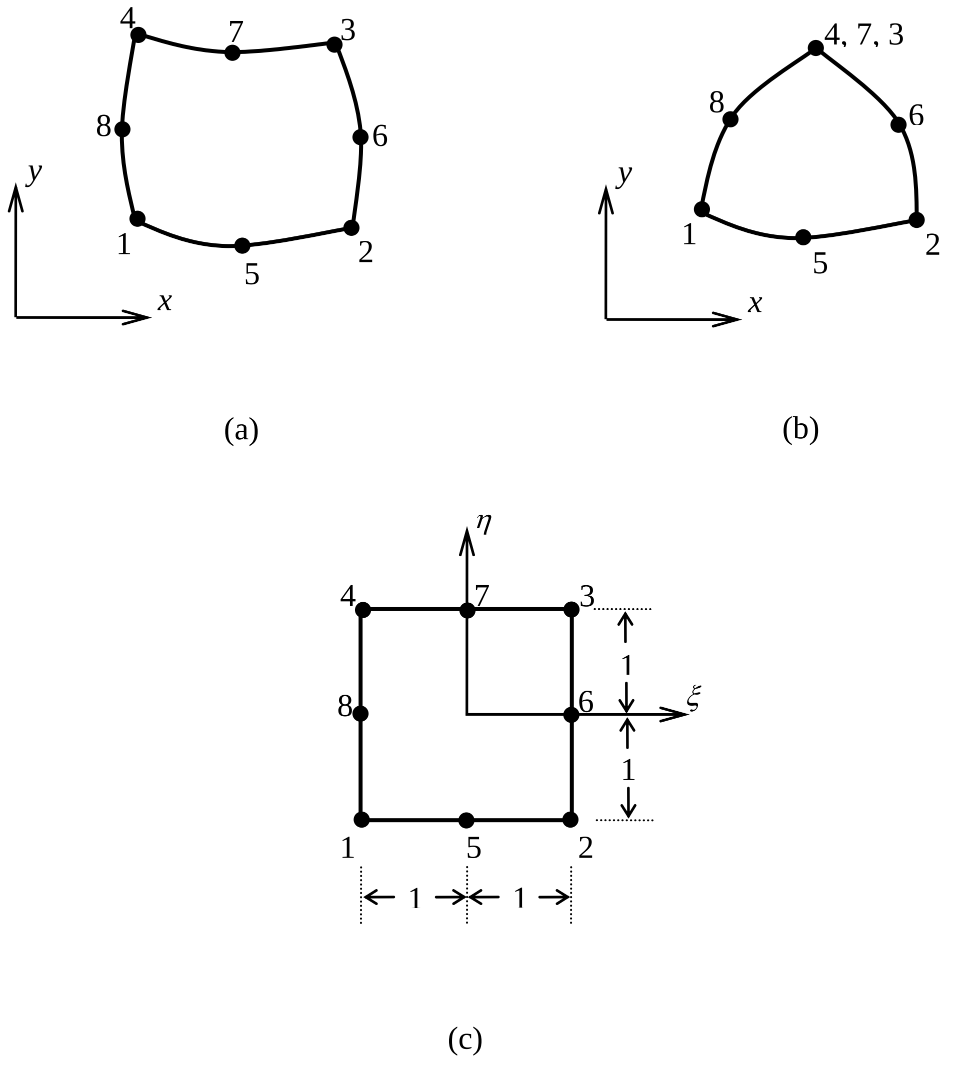

Figure 3.5 (a) Quadrilateral element in the global coordinate system; (b) triangular element in the global coordinate system; (c) quadrilateral and triangular elements in the isoparametric coordinate system.

3.2 Finite Element Procedure

In this study, the J_k-integral method, which is described in Chapter 2, is integrated into an APDL code in ANSYS which is used to solve the problem under consideration. The written APDL code solves the problem in two steps. In the first part, heat transfer problem is solved with the help of ANSYS. In the second part, structural analysis is conducted by utilizing the finite element method described above according to the type of the problem, i.e. plane stress or plane strain. The temperature field obtained in the first part is transferred to the second within the written code. At the end of the second part, all related components of the J_k-integral are calculated. As a result, computation of the stress intensity factors, energy release rate and T-stress is finalized in the written APDL code. It should be mentioned that continuous variations in the thermomechanical properties in the functionally graded medium are incorporated into the finite element model by assigning the material properties at the centroid of each finite element.

In order to calculate the crack tip properties, i.e. stress intensity factors, energy release rate and T-stress, under thermal loading, as mentioned before the orthotropic functionally graded medium is discretized using the triangular elements which are obtained actually from the 8-node quadrilateral elements. Four different circular regions are defined around the crack tip in order to calculate the domain integrals. These circular regions differ from each other by their radii. Although the analysis is independent of the shape of the regions defined, as mentioned before, circular regions will be used in this study.

In the structural analysis part, the line integrals are calculated over the elements which are located on four line segments. Two of the line segments are defined on the upper crack face and two of them are defined on the lower crack face. On the upper crack face the first line segment is confined between the point where the selected circular region intersects the upper crack face and the point δ_1 away from the crack tip. The second line segment is confined between same intersection point and the point δ_2 away from the crack tip. On the lower crack face, same procedure is followed to obtain the two line segments. On the other hand, the domain integrals are calculated over the elements defined within the selected circular region.

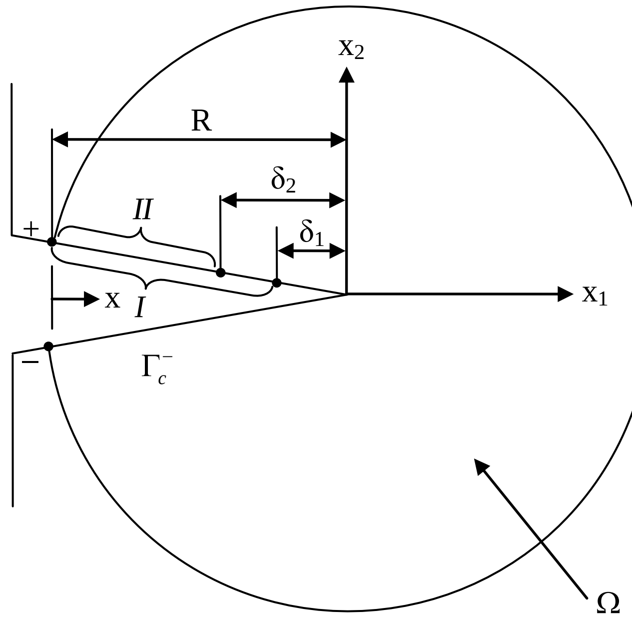

Figure 3.6 Line segments I and II and circular region Ω .

From this point, the finite element procedure of computation of J_1 and $\hat{J}_2$ integrals will be considered. Since the $\hat{J}_2$ integral contains the line integral, let's first deal with this integral.

$\hat{J}_2$ integral is defined in equation (2.65) as

$$\hat{J}_2 = \iint_{\Omega} \left(\sigma_{ij} u_{i,2} - W\delta_{2j}\right) q_{,j} \, d\Omega - \iint_{\Omega} \left(W_{,2}\right)_{\text{expl}} q \, d\Omega - \int_{0}^{R-\delta} \left(W^{+} - W^{-}\right) q \, dx \qquad (i,j=1,2) \tag{3.19}$$

As mentioned above, the line integrals are calculated first with the help of equations (3.7), (3.8), and (3.9). In order to calculate the line integral, the mechanical strain energy density functions are computed by equations (2.16) and (2.20). The function q defined within the line integral and the material properties defined in the equations (2.16) and (2.20) are calculated at both of the gauss points on line elements shown in Figure 3.4. As an example, the line integral calculated at the upper crack face and for $\delta = \delta_1$ is given as follows

$$L_1 = \int_{0}^{R-\delta_1} W^{+} q \, dx \tag{3.20}$$

$$L_1 \approx \sum_{i=1}^{2} W_i^{+} \left(\frac{R - \left| x(\xi_i) \right|}{R} \right) \left| J \right| \tag{3.21}$$

where R is the radius of selected region shown in Figure 3.5, | | represents absolute value and i stands for gauss points.

The Jacobian is computed with the help of the equation (3.9). For the upper crack face L_2 is calculated on line segment II for $\delta = \delta_2$. For lower crack face L_3 and L_4 are calculated for $\delta = \delta_1$ and $\delta = \delta_2$, respectively.

In order to evaluate the domain integral part of the $\hat{J}_2$, the components given in Table 3.1 must be evaluated at the Gauss points of every element within the selected circular region shown in Figure 3.6.

Table 3.1 The components of $\hat{J}_2$-integral

Component	Description	Explicit Form
σ_{ij}	Stress distribution on the element	σ_{11} , σ_{22} , σ_{12}
$u_{i,2}$	Derivative of displacement field with respect to x_2	$\frac{\partial v_1}{\partial x_2}$, $\frac{\partial v_2}{\partial x_2}$
W	Mechanical strain energy density function	(2.16) or (2.20)
$\left(W_{,2}\right)_{\text{expl}}$	Derivative of mechanical strain energy density function with respect to x_2	(2.30) or (2.31)
$\lvert J \rvert$	Jacobian determinant	(3.13)
q	The q function	APPENDIX A
$q_{,j}$	Derivatives of the q function	APPENDIX A

We define $\hat{J}_2^{domain}$ as,

$$\hat{J}_2^{domain} = \iint_{\Omega} \left(\left(\sigma_{ij} u_{i,2} - W \delta_{2j} \right) q_{,j} - \left(W_{,2} \right)_{\text{expl}} q \right) d\Omega , \qquad (i,j=1,2) \qquad (3.22)$$

When the isoparametric formulation of the integrand is carried out, $\hat{J}_2^{domain}$ can be expressed as follows:

$$\hat{J}_2^{domain} = \sum_{k=1}^{2}\sum_{l=1}^{2} \bar{J}_2^{domain}\left(\xi_k, \eta_l\right) \tag{3.23}$$

The stress components σ_{ij} given in equation (3.22) are calculated by means of the constitutive relations given by (2.1) and (2.4) for plane stress and plane strain, respectively. All the stress components are obtained in terms of strain components by using equations (2.1) and (2.4). In order to calculate strains, displacement components are calculated as shown below:

$$\varepsilon_{11} = \frac{\partial u_1}{\partial x_1} = \sum_{i=1}^{8} \frac{\partial \psi_i}{\partial x_1} u_{1i} \tag{3.24}$$

$$\frac{\partial u_1}{\partial x_2} = \sum_{i=1}^{8} \frac{\partial \psi_i}{\partial x_2} u_{1i} \tag{3.25}$$

$$\frac{\partial u_2}{\partial x_1} = \sum_{i=1}^{8} \frac{\partial \psi_i}{\partial x_1} u_{2i} \tag{3.26}$$

$$\varepsilon_{22} = \frac{\partial u_2}{\partial x_2} = \sum_{i=1}^{8} \frac{\partial \psi_i}{\partial x_2} u_{2i} \tag{3.27}$$

$$\varepsilon_{12} = \frac{1}{2}\left(\sum_{i=1}^{8} \frac{\partial \psi_i}{\partial x_2} u_{1i} + \sum_{i=1}^{8} \frac{\partial \psi_i}{\partial x_1} u_{2i} \right) \tag{3.28}$$

where u_1 is the displacement x_1 direction and u_2 is the displacement x_2 direction.

Since the mechanical strain energy density function is represented in terms of strain components and material properties, it can be easily calculated by the equations (2.16) and (2.20) which are given for plane strain and plane stress, respectively.

The derivative of mechanical strain energy density function, $\left(W_{,2}\right)_{\text{expl}}$, requires the calculation of the following terms for plane stress:

$$\frac{\partial W}{\partial E_1}, \frac{\partial W}{\partial E_2}, \frac{\partial W}{\partial \nu_{12}}, \frac{\partial W}{\partial G_{12}}, \frac{\partial W}{\partial \alpha_1}, \frac{\partial W}{\partial \alpha_2}, \frac{\partial W}{\partial (\Delta T)} \tag{3.29}$$

$$\frac{\partial E_1}{\partial x_2}, \frac{\partial E_2}{\partial x_2}, \frac{\partial \nu_{12}}{\partial x_2}, \frac{\partial G_{12}}{\partial x_2}, \frac{\partial \alpha_1}{\partial x_2}, \frac{\partial \alpha_2}{\partial x_2}, \frac{\partial (\Delta T)}{\partial x_2} \tag{3.30}$$

In case of plane strain, the required terms are given below:

$$\frac{\partial W}{\partial E_1}, \frac{\partial W}{\partial E_2}, \frac{\partial W}{\partial \nu_{12}}, \frac{\partial W}{\partial \nu_{13}}, \frac{\partial W}{\partial \nu_{31}}, \frac{\partial W}{\partial \nu_{32}}, \frac{\partial W}{\partial G_{12}}, \frac{\partial W}{\partial \alpha_1}, \frac{\partial W}{\partial \alpha_2}, \frac{\partial W}{\partial \alpha_3}, \frac{\partial W}{\partial (\Delta T)} \tag{3.31}$$

$$\frac{\partial E_1}{\partial x_2}, \frac{\partial E_2}{\partial x_2}, \frac{\partial \nu_{12}}{\partial x_2}, \frac{\partial \nu_{13}}{\partial x_2}, \frac{\partial \nu_{31}}{\partial x_2}, \frac{\partial \nu_{32}}{\partial x_2}, \frac{\partial G_{12}}{\partial x_2}, \frac{\partial \alpha_1}{\partial x_2}, \frac{\partial \alpha_2}{\partial x_2}, \frac{\partial \alpha_3}{\partial x_2}, \frac{\partial (\Delta T)}{\partial x_2} \tag{3.32}$$

The derivatives given in equations (3.29) and (3.31) are given in APPENDIX A. They are represented in terms of strain components and material properties. They can be easily calculated using the equations given in APPENDIX A. The derivatives given in equations (3.30) and (3.32) are calculated as follows:

$$\frac{\partial E_1}{\partial x_2} = \sum_{i=1}^{8} \frac{\partial \psi_i}{\partial x_2} E_{1i} \tag{3.33}$$

$$\frac{\partial E_2}{\partial x_2} = \sum_{i=1}^{8} \frac{\partial \psi_i}{\partial x_2} E_{2i} \tag{3.34}$$

$$\frac{\partial \nu_{12}}{\partial x_2} = \sum_{i=1}^{8} \frac{\partial \psi_i}{\partial x_2} \nu_{12i} \tag{3.35}$$

$$\frac{\partial \nu_{13}}{\partial x_2} = \sum_{i=1}^{8} \frac{\partial \psi_i}{\partial x_2} \nu_{13i} \tag{3.36}$$

$$\frac{\partial \nu_{31}}{\partial x_2} = \sum_{i=1}^{8} \frac{\partial \psi_i}{\partial x_2} \nu_{31i} \tag{3.37}$$

$$\frac{\partial \nu_{32}}{\partial x_2} = \sum_{i=1}^{8} \frac{\partial \psi_i}{\partial x_2} \nu_{32i} \tag{3.38}$$

$$\frac{\partial G_{12}}{\partial x_2} = \sum_{i=1}^{8} \frac{\partial \psi_i}{\partial x_2} G_{12i} \tag{3.39}$$

$$\frac{\partial \alpha_1}{\partial x_2} = \sum_{i=1}^{8} \frac{\partial \psi_i}{\partial x_2} \alpha_{1i} \tag{3.40}$$

$$\frac{\partial \alpha_2}{\partial x_2} = \sum_{i=1}^{8} \frac{\partial \psi_i}{\partial x_2} \alpha_{2i} \tag{3.41}$$

$$\frac{\partial \alpha_3}{\partial x_2} = \sum_{i=1}^{8} \frac{\partial \psi_i}{\partial x_2} \alpha_{3i} \tag{3.42}$$

$$\frac{\partial (\Delta T)}{\partial x_2} = \sum_{i=1}^{8} \frac{\partial \psi_i}{\partial x_2} (\Delta T)_i \tag{3.43}$$

The Jacobian determinant is calculated by using equation (3.13). The q function and its derivatives are given in APPENDIX A.

The derivatives of the shape functions with respect to the global coordinates can be calculated as follows:

$$\frac{\partial \psi_i}{\partial \eta} = \frac{\partial \psi_i}{\partial x_1}\frac{\partial x_1}{\partial \eta} + \frac{\partial \psi_i}{\partial x_2}\frac{\partial x_2}{\partial \eta} \tag{3.44}$$

$$\frac{\partial \psi_i}{\partial \xi} = \frac{\partial \psi_i}{\partial x_1}\frac{\partial x_1}{\partial \xi} + \frac{\partial \psi_i}{\partial x_2}\frac{\partial x_2}{\partial \xi} \tag{3.45}$$

$$\begin{bmatrix} \dfrac{\partial \psi_i}{\partial x_1} \\ \dfrac{\partial \psi_i}{\partial x_2} \end{bmatrix} = \frac{1}{|J|}\begin{bmatrix} \dfrac{\partial x_2}{\partial \xi} & -\dfrac{\partial x_2}{\partial \eta} \\ -\dfrac{\partial x_1}{\partial \xi} & \dfrac{\partial x_1}{\partial \eta} \end{bmatrix}\begin{bmatrix} \dfrac{\partial \psi_i}{\partial \eta} \\ \dfrac{\partial \psi_i}{\partial \xi} \end{bmatrix} \tag{3.46}$$

The J_1 integral is calculated in a similar way as $\hat{J}_2^{Domain}$ integral. J_1 integral is given in equation (2.46) as

$$J_1 = \iint_\Omega \left(\sigma_{ij}\, u_{i,1} - W\delta_{1j}\right) q_{,j} d\Omega - \iint_\Omega \left(W_{,1}\right)_{\text{expl}} q d\Omega \tag{3.47}$$

In order to evaluate J_1-integral, the components given in Table 3.2 must be evaluated at the Gauss points of the element shown in Figure 3.3.

Table 3.2 The components of J_1-integral

Component	Description	Explicit Form
σ_{ij}	Stress distribution on the element	σ_{11} , σ_{22} , σ_{12}
$u_{i,1}$	Derivative of displacement field with respect to x_1	$\frac{\partial v_1}{\partial x_1}$, $\frac{\partial v_2}{\partial x_1}$
W	Mechanical strain energy density function	(2.16) or (2.20)
$(W_{,1})_{\text{expl}}$	Derivative of mechanical strain energy density function with respect to x_1	(2.30) or (2.31)
$\lvert J \rvert$	Jacobian determinant	(3.13)
q	The q function	APPENDIX A
$q_{,j}$	Derivatives of the q function	APPENDIX A

When the isoparametric formulation of the integrand is carried out, J_1 can be reduced to the following form:

$$J_1 = \sum_{k=1}^{2}\sum_{l=1}^{2}\left[\bar{J}_1(\xi_k, \eta_l)\right] \tag{3.48}$$

The stress components σ_{ij} given in equation (3.47) are calculated by means of the constitutive relations given by (2.1) and (2.4) for plane stress and plane strain, respectively. All the stress components are obtained in terms of strain components by using equations (2.1) and (2.4). In order to calculate strains, displacement components are calculated by equations (3.24)-(3.28).

Since the mechanical strain energy density function is represented in terms of strain components and material properties, it can be easily calculated by the equations (2.16) and (2.20) which are given for plane strain and plane stress, respectively.

The derivative of mechanical strain energy density function, $\left(W_{,1}\right)_{\mathrm{expl}}$, requires the calculation of the following terms for plane stress:

$$\frac{\partial W}{\partial E_1}, \frac{\partial W}{\partial E_2}, \frac{\partial W}{\partial \nu_{12}}, \frac{\partial W}{\partial G_{12}}, \frac{\partial W}{\partial \alpha_1}, \frac{\partial W}{\partial \alpha_2}, \frac{\partial W}{\partial(\Delta T)} \tag{3.49}$$

$$\frac{\partial E_1}{\partial x_1}, \frac{\partial E_2}{\partial x_1}, \frac{\partial \nu_{12}}{\partial x_1}, \frac{\partial G_{12}}{\partial x_1}, \frac{\partial \alpha_1}{\partial x_1}, \frac{\partial \alpha_2}{\partial x_1}, \frac{\partial(\Delta T)}{\partial x_1} \tag{3.50}$$

In case of plane strain, the required terms are given below:

$$\frac{\partial W}{\partial E_1}, \frac{\partial W}{\partial E_2}, \frac{\partial W}{\partial \nu_{12}}, \frac{\partial W}{\partial \nu_{13}}, \frac{\partial W}{\partial \nu_{31}}, \frac{\partial W}{\partial \nu_{32}}, \frac{\partial W}{\partial G_{12}}, \frac{\partial W}{\partial \alpha_1}, \frac{\partial W}{\partial \alpha_2}, \frac{\partial W}{\partial \alpha_3}, \frac{\partial W}{\partial (\Delta T)} \tag{3.51}$$

$$\frac{\partial E_1}{\partial x_1}, \frac{\partial E_2}{\partial x_1}, \frac{\partial \nu_{12}}{\partial x_1}, \frac{\partial \nu_{13}}{\partial x_1}, \frac{\partial \nu_{31}}{\partial x_1}, \frac{\partial \nu_{32}}{\partial x_1}, \frac{\partial G_{12}}{\partial x_1}, \frac{\partial \alpha_1}{\partial x_1}, \frac{\partial \alpha_2}{\partial x_1}, \frac{\partial \alpha_3}{\partial x_1}, \frac{\partial (\Delta T)}{\partial x_1} \tag{3.52}$$

The derivatives given in equations (3.29) and (3.30) are calculated as follows:

$$\frac{\partial E_1}{\partial x_1} = \sum_{i=1}^{8} \frac{\partial \psi_i}{\partial x_1} E_{1i} \tag{3.53}$$

$$\frac{\partial E_2}{\partial x_1} = \sum_{i=1}^{8} \frac{\partial \psi_i}{\partial x_1} E_{2i} \tag{3.54}$$

$$\frac{\partial \nu_{12}}{\partial x_1} = \sum_{i=1}^{8} \frac{\partial \psi_i}{\partial x_1} \nu_{12i} \tag{3.55}$$

$$\frac{\partial \nu_{13}}{\partial x_1} = \sum_{i=1}^{8} \frac{\partial \psi_i}{\partial x_1} \nu_{13i} \tag{3.56}$$

$$\frac{\partial \nu_{31}}{\partial x_1} = \sum_{i=1}^{8} \frac{\partial \psi_i}{\partial x_1} \nu_{31i} \tag{3.57}$$

$$\frac{\partial \nu_{32}}{\partial x_1} = \sum_{i=1}^{8} \frac{\partial \psi_i}{\partial x_1} \nu_{32i} \tag{3.58}$$

$$\frac{\partial G_{12}}{\partial x_1} = \sum_{i=1}^{8} \frac{\partial \psi_i}{\partial x_1} G_{12i} \tag{3.59}$$

$$\frac{\partial \alpha_1}{\partial x_1} = \sum_{i=1}^{8} \frac{\partial \psi_i}{\partial x_1} \alpha_{1i} \tag{3.60}$$

$$\frac{\partial \alpha_2}{\partial x_1} = \sum_{i=1}^{8} \frac{\partial \psi_i}{\partial x_1} \alpha_{2i} \tag{3.61}$$

$$\frac{\partial \alpha_3}{\partial x_1} = \sum_{i=1}^{8} \frac{\partial \psi_i}{\partial x_1} \alpha_{3i} \tag{3.62}$$

$$\frac{\partial (\Delta T)}{\partial x_1} = \sum_{i=1}^{8} \frac{\partial \psi_i}{\partial x_1} (\Delta T)_i \tag{3.63}$$

The Jacobian determinant is calculated by using equation (3.13). The q function and its derivatives are given in APPENDIX A.

In summary, the components of the J_k-integral can be evaluated numerically. These results can then be used to compute the thermal fracture parameters.

CHAPTER 4

NUMERICAL EXAMPLE

In this section, temperature distribution profiles and fracture mechanics parameters are calculated by considering the problem of an embedded crack in an FGM layer under steady-state thermal loading. The geometry of the problem and thermal boundary conditions are depicted in Figure 4.1.

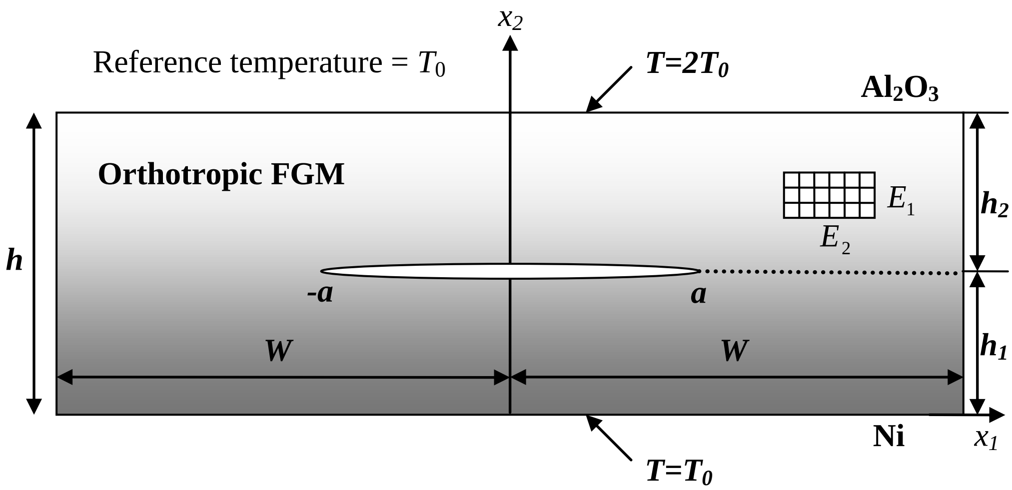

Figure 4.1 An embedded crack in an orthotropic functionally graded layer under thermal loading.

The particular ceramic and metal components of the orthotropic FGM layer are taken as alumina (Al_2O_3) and nickel (Ni). The material properties vary continuously from 100% Ni at $x_2 = 0$ to 100% Al_2O_3 at $x_2 = h$. The embedded crack shown in Figure 4.1 is aligned parallel to the boundaries and perpendicular to the direction of the material property gradation. The length of the embedded crack, which is located at $x_2 = h_1$, equals to $2a$.

Initially, the FGM layer is kept at a reference temperature T_0 at which all the stress components are equal to zero. Then, temperature of the surface at $x_2 = h$ is increased to $2T_0$ and the surface temperature at $x_2 = 0$ is kept at T_0. The crack surfaces and the surfaces at $x_1 = \pm W$ are assumed to be insulated. The presence of the insulated crack disturbs the one dimensional temperature distribution and leads to a two-dimensional temperature distribution field in the vicinity of the crack faces.

The thermomechanical properties of the functionally graded layer are assumed to be continuous functions of the x_2-coordinate. The material property variations are represented by using power functions as follows:

$$E_1(x_2) = E_1^m + \left(E_1^c - E_1^m\right)\left(\frac{x_2}{h}\right)^{\gamma_1} \qquad 0 < x_2 < h \tag{4.1}$$

$$E_2(x_2) = E_2^m + \left(E_2^c - E_2^m\right)\left(\frac{x_2}{h}\right)^{\gamma_2} \qquad 0 < x_2 < h \tag{4.2}$$

$$\nu_{12}(x_2) = \nu_{12}^m + \left(\nu_{12}^c - \nu_{12}^m\right)\left(\frac{x_2}{h}\right)^{\beta_{12}} \qquad 0 < x_2 < h \tag{4.3}$$

$$\nu_{13}(x_2) = \nu_{13}^m + \left(\nu_{13}^c - \nu_{13}^m\right)\left(\frac{x_2}{h}\right)^{\beta_{13}} \qquad 0 < x_2 < h \tag{4.4}$$

$$\nu_{31}(x_2) = \nu_{31}^m + \left(\nu_{31}^c - \nu_{31}^m\right)\left(\frac{x_2}{h}\right)^{\beta_{31}} \qquad 0 < x_2 < h \tag{4.5}$$

$$\nu_{32}(x_2) = \nu_{32}^m + \left(\nu_{32}^c - \nu_{32}^m\right)\left(\frac{x_2}{h}\right)^{\beta_{32}} \qquad 0 < x_2 < h \tag{4.6}$$

$$G_{12}(x_2) = G_{12}^m + \left(G_{12}^c - G_{12}^m\right)\left(\frac{x_2}{h}\right)^{\gamma_{12}} \qquad 0 < x_2 < h \tag{4.7}$$

$$\alpha_1(x_2) = \alpha_1^m + \left(\alpha_1^c - \alpha_1^m\right)\left(\frac{x_2}{h}\right)^{\delta_1} \qquad 0 < x_2 < h \tag{4.8}$$

$$\alpha_2(x_2) = \alpha_2^m + \left(\alpha_2^c - \alpha_2^m\right)\left(\frac{x_2}{h}\right)^{\delta_2} \qquad 0 < x_2 < h \tag{4.9}$$

$$\alpha_3(x_2) = \alpha_3^m + \left(\alpha_3^c - \alpha_3^m\right)\left(\frac{x_2}{h}\right)^{\delta_3} \qquad 0 < x_2 < h \tag{4.10}$$

$$k_1(x_2) = k_1^m + \left(k_1^c - k_1^m\right)\left(\frac{x_2}{h}\right)^{\omega_1} \qquad 0 < x_2 < h \tag{4.11}$$

$$k_2(x_2) = k_2^m + \left(k_2^c - k_2^m\right)\left(\frac{x_2}{h}\right)^{\omega_2} \qquad 0 < x_2 < h \tag{4.12}$$

where the superscripts m and c stand for the properties of metallic and ceramic components namely for the properties of Nickel and Alumina.

The remaining material properties ν_{21}, ν_{23} and E_3 can be calculated with the help of the equation (2.6) and equations (4.1)-(4.6).

The power-law representations of the material property variations given in equations (4.1)-(4.12) are convenient in representing the thermomechanical properties of the FGM layer. The exponents of these equations are positive constants that can be adjusted to attain a required variation profile for the orthotropic FGM layer. If an exponent is greater than unity, the material property variation profile is metal-rich. On the other hand, if an exponent is less than unity the corresponding material property possesses a ceramic-rich variation profile. In this study, the effects of these exponents will be investigated by changing the exponent of one of the material properties from zero to infinity while keeping the other properties constant.

The material properties of 100% alumina surface are given as follows [19]:

$$E_1^c = 90.43\,GPa\,, \qquad E_1^c = 116.36\,GPa\,, \qquad G_{12}^c = 30.21\,GPa \tag{4.13}$$

$$\nu_{12}^c = 0.2176, \;\; \nu_{13}^c = 0.1399, \;\; \nu_{31}^c = 0.14\,, \;\; \nu_{32}^c = 0.21 \tag{4.14}$$

$$k_1^c = 21.25\,W/(m\,K), \;\; k_2^c = 29.82\,W/(m\,K) \tag{4.15}$$

$$\alpha_1^c = 8\,(10)^{-6}\,\left({}^oC\right)^{-1}, \;\; \alpha_2^c = 7.5\,(10)^{-6}\,\left({}^oC\right)^{-1}, \;\; \alpha_3^c = 9\,(10)^{-6}\,\left({}^oC\right)^{-1} \tag{4.16}$$

The material properties of 100% nickel surface are given as follows [19]:

$$E_1^m = E_2^m = E^m = 204\,GPa\,, \;\; \nu_{12}^m = \nu_{13}^m = \nu_{31}^m = \nu_{32}^m = \nu^m = 0.31\,, \tag{4.17}$$

$$G_{12}^m = E^m/\left(2\left(1+\nu^m\right)\right) = 77.9\;GPa\,, \qquad k_1^m = k_2^m = k^m = 70\,W/(m\,K), \tag{4.18}$$

$$\alpha_1^m = \alpha_2^m = \alpha_3^m = \alpha^m = 13.3\,(10)^{-6}\,\left({}^oC\right)^{-1} \tag{4.19}$$

There are certain limitations on the Poisson’s ratios in the orthotropic materials. These limitations are given as follows:

$$\left(1-\nu_{12}\nu_{21}\right) > 0 \qquad \left(1-\nu_{13}\nu_{31}\right) > 0 \qquad \left(1-\nu_{23}\nu_{32}\right) > 0 \tag{4.20}$$

$$\left(1-\nu_{12}\nu_{21} - \nu_{13}\nu_{31} - \nu_{23}\nu_{32} - 2\nu_{12}\nu_{23}\nu_{31}\right) > 0 \tag{4.21}$$

These restrictions hold at every point in the alumina-nickel orthotropic FGM layer.

It must be noted that lateral displacement in the embedded crack shown in Figure 4.1 are anti-symmetric and vertical displacements are symmetric about x_2-axis. Therefore, the relations between the crack tip parameters can be expressed in the following form:

$$K_I(a) = K_I(-a) \qquad K_{II}(a) = -K_{II}(-a) \tag{4.22}$$

$$J_1(a) = J_1(-a) \qquad J_2(a) = -J_2(-a) \qquad T_s(a) = T_s(-a) \tag{4.23}$$

where (a) and $(-a)$ represent the crack tip where the corresponding parameter is calculated. As a result of the symmetry, it is sufficient to model the one-half of the layer. In the present analysis, the region $0 < x_1 < W$ is modeled and crack tip parameters are calculated at $x_1 = a$.

First, the influence of the thermal conductivity variations on the steady-state crack tip temperature will be examined. Figure 4.2 and 4.3 show the variations of crack tip temperature with respect to ω_1 and ω_2, respectively. Crack tip temperature is plotted for various values of h_1/W.

It can be seen from Figure 4.2 that the principal thermal conductivity k_1 has almost no effect on the crack tip temperatures. The effect of the other principal thermal conductivity k_2 can be seen from Figure 4.3. For the different values of the exponent ω_2, different crack tip temperatures are obtained as can be seen from Figure 4.3. In both of the figures, it is also seen that the normalized crack tip temperature values are increasing while the crack is coming closer to the upper surface of the layer. This is also an expected result since the temperature of the upper surface is two times of the temperature of the lower surface. For $h_1/W = 0.2$ crack closure happens. Therefore, as a minimum value 0.23 is taken for h_1/W in the analysis of the influence of ω_1.

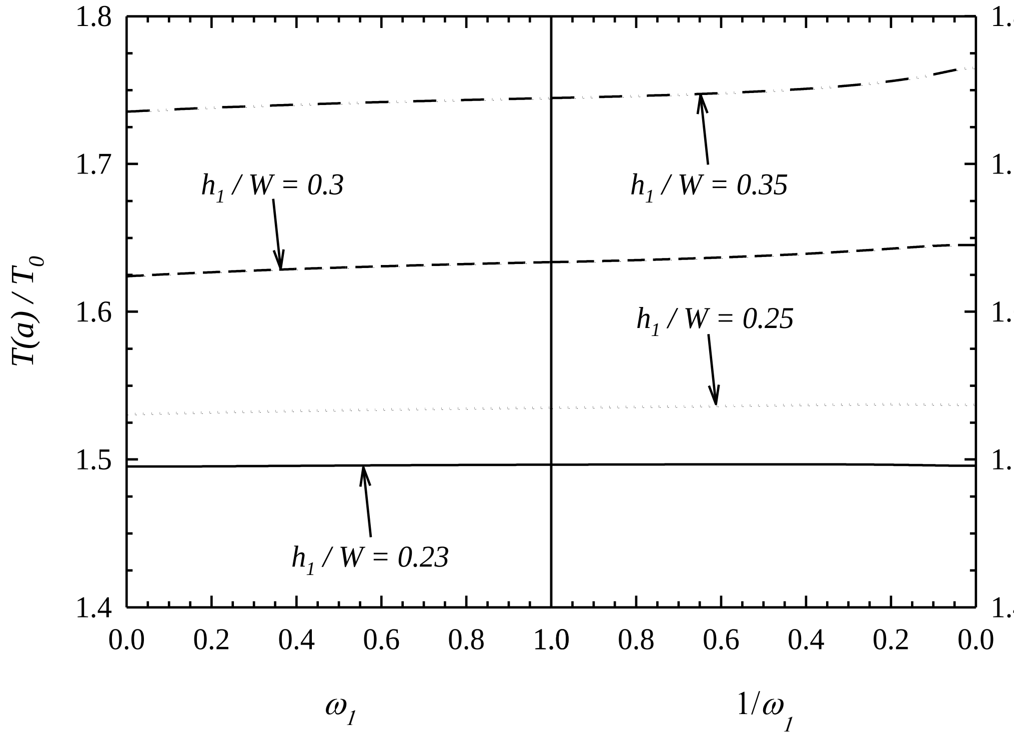

Figure 4.2 Influence of ω_1 on the temperature at the crack tip $x_1 = a$. $a/W = 0.1$, $h/W = 0.4$, $\omega_2 = 4$.

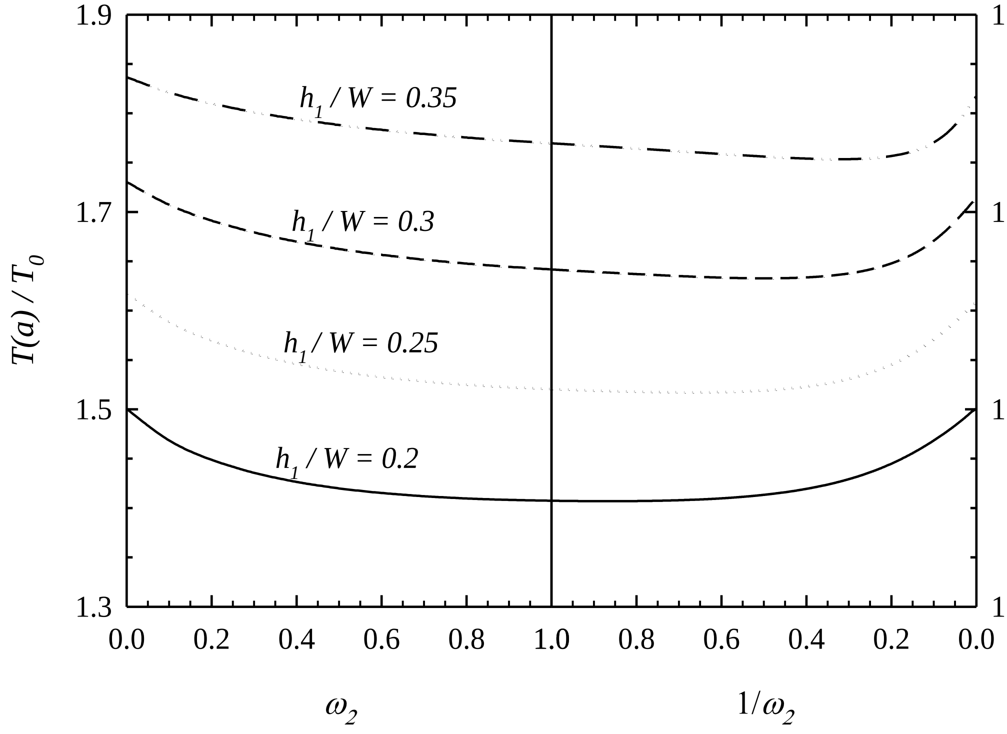

Figure 4.3 Influence of ω_2 on the temperature at the crack tip $x_1 = a$. $a/W = 0.1$, $h/W = 0.4$ $\omega_1 = 4$.

In order to verify the accuracy of the developed procedure, some comparisons of the mode-I and mode-II stress intensity factors calculated using the J_k-integral technique to those calculated by displacement correlation technique [9] will be presented. The details of the formulation and finite element implementation of the J_k-integral technique is given in the previous chapters. Domain independence of J_k-integral method is demonstrated in Tables 4.1 and 4.2 by providing the results for four different domain size values as shown in Figure 4.4 (b). The comparisons are provided for both plane stress and plane strain conditions.

The normalized stress intensity factors given in Tables 4.2 and 4.3 are defined as

$$K_{I\,n} = \frac{K_I(a)}{\sigma_0\sqrt{\pi a}}, \qquad K_{II\,n} = \frac{K_{II}(a)}{\sigma_0\sqrt{\pi a}}, \qquad \sigma_0 = \alpha_1^c E_1^c T_0 \tag{4.24}$$

Table 4.1 Comparisons of the results obtained by J_k-integral to those calculated by DCT. $h_1/W = 0,25$, $a/W = 0.1$, $h/W = 0.4$, $\gamma_1 = \gamma_2 = \gamma_{12} = 2$, $\beta_{12} = \beta_{13} = \beta_{31} = \beta_{32} = 1.5$, $\delta_1 = \delta_3 = 3$, $\omega_1 = \omega_2 = 4$.

			J_k-integral				DCT
			$R/a = 0.1$	$R/a = 0.2$	$R/a = 0.3$	$R/a = 0.4$	
PLANE STRESS	$\delta_2 = \frac{1}{3}$	K_{In}	0.0176	0.0176	0.0176	0.0176	0.0177
		K_{IIn}	0.1197	0.1197	0.1197	0.1197	0.119
	$\delta_2 = 3$	K_{In}	0.0207	0.0207	0.0207	0.0207	0.02088
		K_{IIn}	0.1271	0.1271	0.1271	0.1271	0.1263
PLANE STRAIN	$\delta_2 = \frac{1}{3}$	K_{In}	0.0259	0.026	0.026	0.0261	0.0259
		K_{IIn}	0.1586	0.1587	0.1588	0.1589	0.1579
	$\delta_2 = 3$	K_{In}	0.0294	0.0295	0.0295	0.0296	0.02936
		K_{IIn}	0.1663	0.1664	0.1665	0.1666	0.1656

Table 4.2 Comparisons of the results obtained by J_k-integral to those calculated by DCT. $h_1/W = 0{,}3$, $a/W = 0.1$, $h/W = 0.4$, $\gamma_1 = \gamma_2 = \gamma_{12} = 2$, $\beta_{12} = \beta_{13} = \beta_{31} = \beta_{32} = 1.5$, $\delta_1 = \delta_3 = 3$, $\omega_1 = \omega_2 = 4$.

			J_k-integral				DCT
			$R/a = 0.1$	$R/a = 0.2$	$R/a = 0.3$	$R/a = 0.4$	
PLANE STRESS	$\delta_2 = \frac{1}{3}$	K_{In}	0.0278	0.0278	0.0278	0.0278	0.0279
		K_{IIn}	0.1024	0.1024	0.1024	0.1024	0.1018
	$\delta_2 = 3$	K_{In}	0.0328	0.0328	0.0328	0.0328	0.033
		K_{IIn}	0.1081	0.1081	0.1081	0.1081	0.1074
PLANE STRAIN	$\delta_2 = \frac{1}{3}$	K_{In}	0.0386	0.0386	0.0386	0.0386	0.0387
		K_{IIn}	0.1318	0.1319	0.1321	0.1322	0.1312
	$\delta_2 = 3$	K_{In}	0.044	0.044	0.044	0.044	0.0441
		K_{IIn}	0.1377	0.1379	0.138	0.1382	0.1372

The element and node numbers for these two different h_1/W values are given in Table 4.3.

Table 4.3 Number of elements and nodes used in the analyses.

	Number of Elements	**Number of Nodes**
$h_1/W = 0.25$	93952	189223
$h_1/W = 0.3$	92014	185347

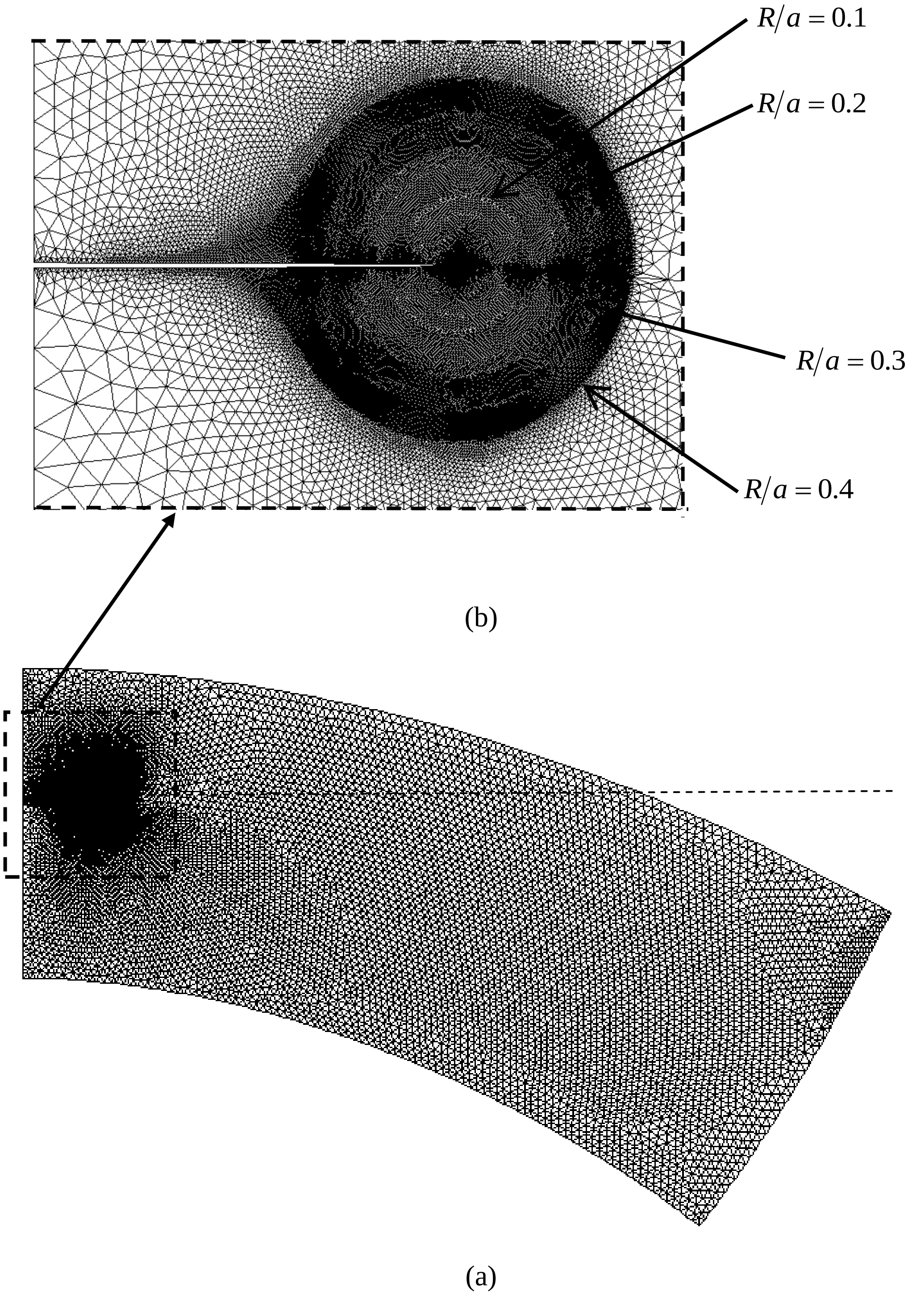

Figure 4.4 (a) Deformed shape of the finite element mesh (b) close-up view of the circular domains around the crack tip. $h_1/W = 0.25$, $a/W = 0.1$, $h/W = 0.4$, $\gamma_1 = \gamma_2 = \gamma_{12} = 2$, $\beta_{12} = \beta_{13} = \beta_{31} = \beta_{32} = 1.5$, $\delta_1 = \delta_2 = \delta_3 = 3$, $\omega_1 = \omega_2 = 4$.

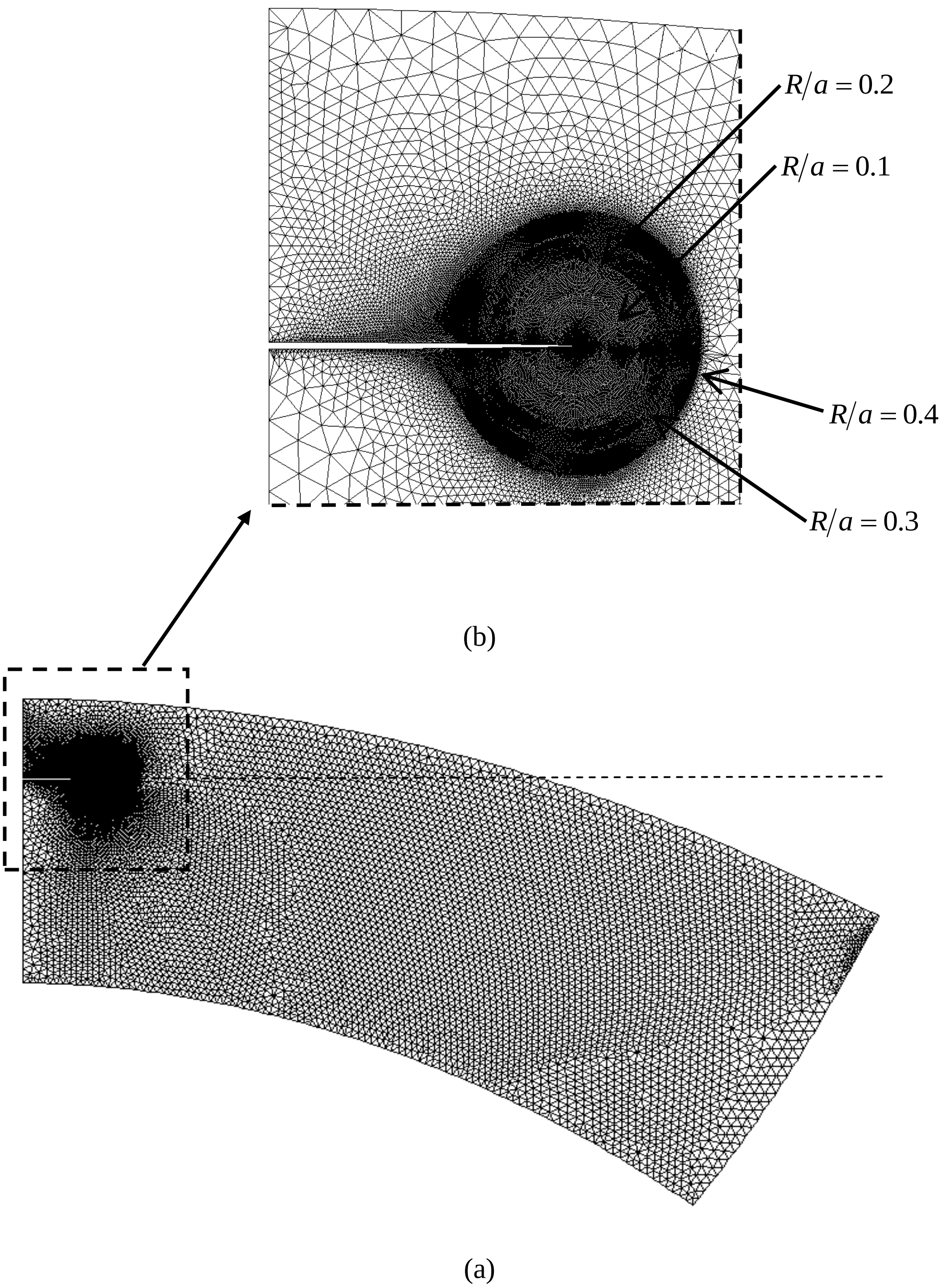

Figure 4.5 (a) Deformed shape of the finite element mesh (b) close-up view of the circular domains around the crack tip. $h_1/W = 0.3$, $a/W = 0.1$, $h/W = 0.4$, $\gamma_1 = \gamma_2 = \gamma_{12} = 2$, $\beta_{12} = \beta_{13} = \beta_{31} = \beta_{32} = 1.5$, $\delta_1 = \delta_2 = \delta_3 = 3$, $\omega_1 = \omega_2 = 4$.

In both J_k-integral method and displacement correlation technique, triangular elements, which are obtained from 8-node quadrilateral elements, are used. In displacement correlation technique special quarter point crack tip elements are used to calculate normalized stress intensity factors. The meshes in the circular domains are especially refined to evaluate the stress intensity factors within a high degree of accuracy. In both Table 4.2 and Table 4.3, it can be seen that the results obtained by J_k-integral method and displacement correlation technique are in excellent agreement for both of the cases of plane stress and plane strain. The results evaluated using different domain sizes also agree quite well which indicates that developed J_k-integral method possesses the required domain independence.

Next, the effects of the thermal conductivities k_1 and k_2, thermal expansion coefficients α_1, α_2 and α_3, Poisson's ratio ν_{12} ,and crack location on the fracture mechanics parameters will be examined. The exponents ω_1, ω_2, δ_1, δ_2, δ_3, and β_{12} govern the variations in k_1, k_2, α_1, α_2, α_3 and ν_{12}, respectively. The variation profiles of fracture mechanics parameters are presented for whole ranges of ω_1, ω_2, δ_1, δ_2, δ_3, and β_{12} by varying of these exponents from zero to infinity. The results illustrated in the following figures are calculated for the condition of plane strain.

In Figure 4.6.1 variation profile of normalized mode-I stress intensity factor is depicted for various values of relative crack position h_1/W . Expressions for the normalized SIFs are given by equation (4.24). For all values of h_1/W considered $K_{In}(a)$ generally decreases as ω_1 is increased. In addition, $K_{In}(a)$ gets its largest value when $h_1/W = 0.3$ and $\omega_1 = 0$ and smallest value when $h_1/W = 0.23$ and ω_1 is between 2-2.5.

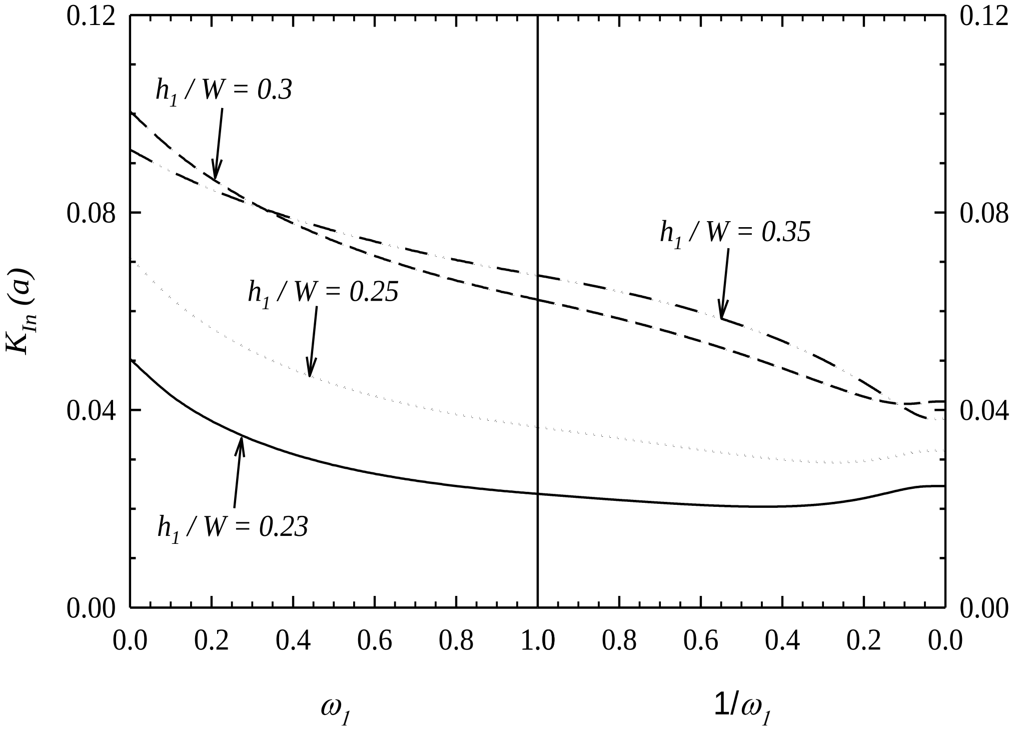

Figure 4.6.1 Influence of ω_1 on normalized mode-I SIF at the crack tip $x_1 = a$. $\gamma_1 = \gamma_2 = \gamma_{12} = 2$, $\beta_{12} = \beta_{13} = \beta_{31} = \beta_{32} = 1.5$, $\delta_1 = \delta_2 = \delta_3 = 3$, $\omega_2 = 4$, $a/W = 0.1$, $h/W = 0.4$.

Variation of $K_{IIn}(a)$ is depicted in Figure 4.6.2. Like $K_{In}(a)$, for all values of h_1/W, in general $K_{IIn}(a)$ decreases as ω_1 is increased. Moreover, $K_{IIn}(a)$ gets larger as h_1/W is decreased from 0.35 to 0.23.

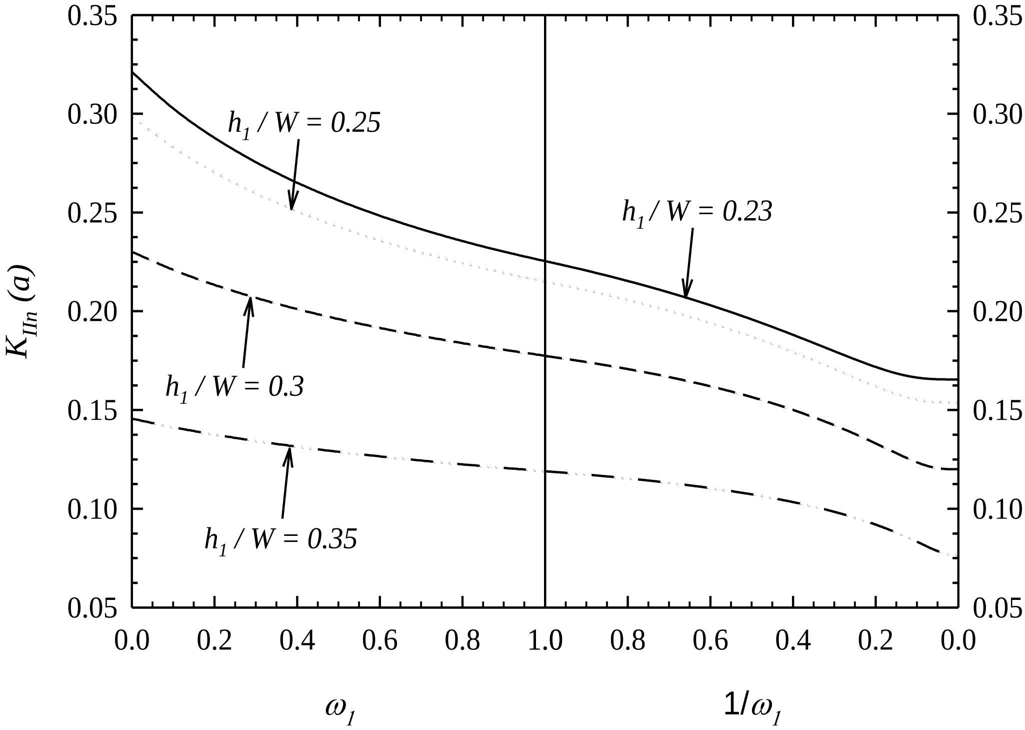

Figure 4.6.2 Influence of ω_1 on normalized mode-II SIF at the crack tip $x_1 = a$. $\gamma_1 = \gamma_2 = \gamma_{12} = 2$, $\beta_{12} = \beta_{13} = \beta_{31} = \beta_{32} = 1.5$, $\delta_1 = \delta_2 = \delta_3 = 3$, $\omega_2 = 4$, $a/W = 0.1$, $h/W = 0.4$.

The computed results for normalized energy release rate $J_{1n}(a)$ and normalized T-stress are presented in Figures 4.6.3 and 4.6.4. The $J_{1n}(a)$ and $T_{sn}(a)$ are defined as

$$J_{1n}(a) = \frac{J_1(a)}{J_0}, \qquad J_0 = \frac{\sigma_0^2(\pi a)}{E_1^c}\left(1 - \left(\nu_{12}^c\right)^2\right), \qquad \sigma_0 = \alpha_1^c E_1^c T_0 \tag{4.25}$$

$$T_{sn}(a) = \frac{T_s(a)}{\sigma_0}, \qquad \sigma_0 = \alpha_1^c E_1^c T_0 \tag{4.26}$$

The variation profiles of $J_{1n}(a)$ are similar to those of $K_{IIn}(a)$. This is an expected result since for given values of ω_1 and h_1/W, $K_{IIn}(a)$ is larger than $K_{In}(a)$.

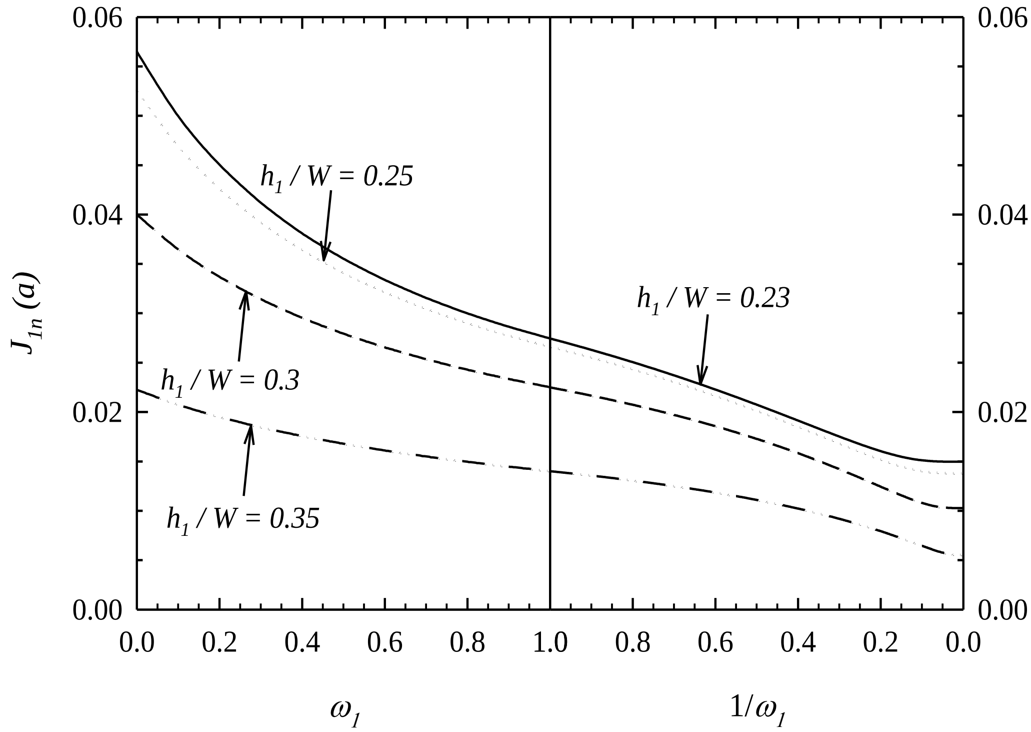

Figure 4.6.3 Influence of ω_1 on normalized energy release rate at the crack tip $x_1 = a$. $\gamma_1 = \gamma_2 = \gamma_{12} = 2$, $\beta_{12} = \beta_{13} = \beta_{31} = \beta_{32} = 1.5$, $\delta_1 = \delta_2 = \delta_3 = 3$, $\omega_2 = 4$, $a/W = 0.1$, $h/W = 0.4$.

The plots obtained for normalized T-stress for various values of h_1/W are almost horizontal which indicates that ω_1 has little influence on T-stress. It is also shown in the Figure 4.6.4 that as h_1/W gets smaller $T_{sn}(a)$ becomes negative.

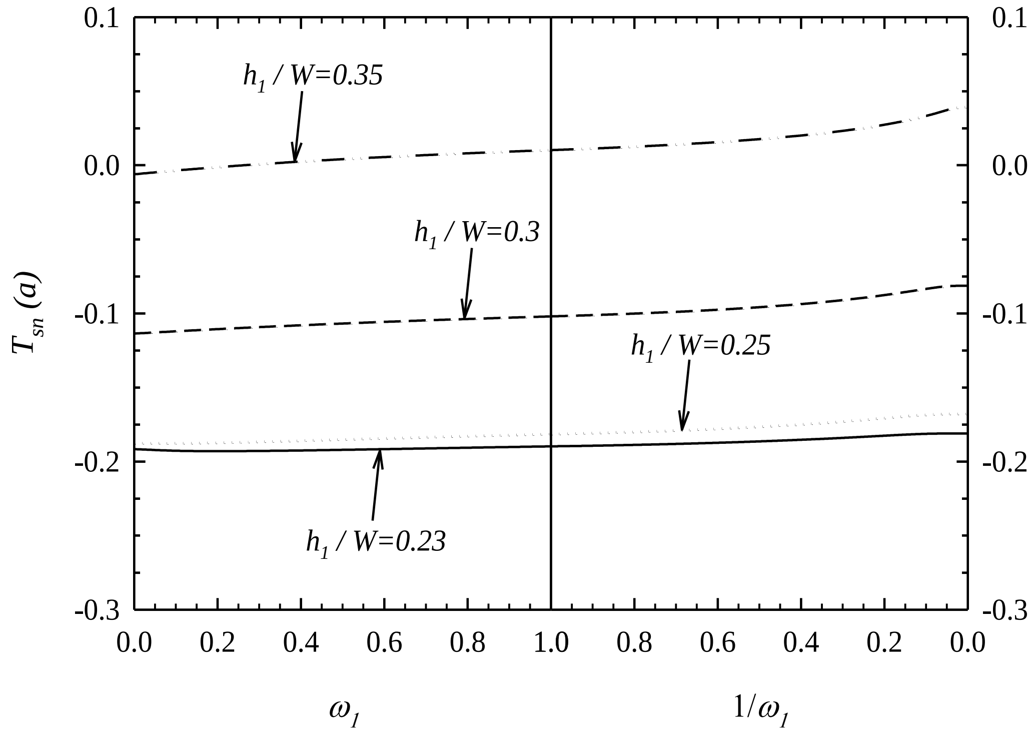

Figure 4.6.4 Influence of ω_1 on normalized T-stress at the crack tip $x_1 = a$. $\gamma_1 = \gamma_2 = \gamma_{12} = 2$, $\beta_{12} = \beta_{13} = \beta_{31} = \beta_{32} = 1.5$, $\delta_1 = \delta_2 = \delta_3 = 3$, $\omega_2 = 4$, $a/W = 0.1$, $h/W = 0.4$.

Figure 4.7.1 presents the influence of the exponent ω_2 and h_1/W on $K_{In}(a)$. It can be seen from the figure that for $h_1/W = 0.2$, $K_{In}(a)$ first goes through a minimum and then increases with increasing values of ω_2. On the other hand, for $h_1/W = 0.25$, 0.3, and 0.35 $K_{In}(a)$ increases as ω_2 increases. Additionally, $K_{In}(a)$ gets larger as h_1/W is increased from 0.2 to 0.35. It can be noted that $K_{In}(a)$ values calculated for $h_1/W = 0.3$, and 0.35 are very close when $1/\omega_2 = 0$.

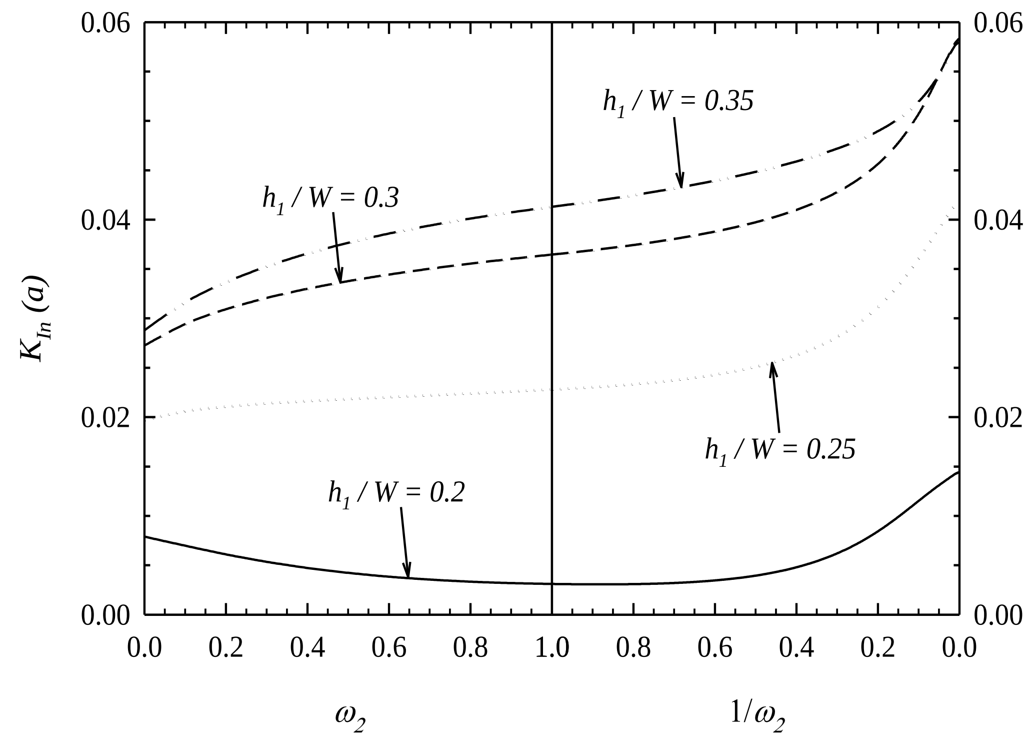

Figure 4.7.1 Influence of ω_2 on normalized mode-I SIF at the crack tip $x_1 = a$. $\gamma_1 = \gamma_2 = \gamma_{12} = 2$, $\beta_{12} = \beta_{13} = \beta_{31} = \beta_{32} = 1.5$, $\delta_1 = \delta_2 = \delta_3 = 3$, $\omega_1 = 4$, $a/W = 0.1$, $h/W = 0.4$.

Variation of the normalized mode-II stress intensity factors with respect to ω_2 is shown in Figure 4.7.2. The variation profiles shown in the figure demonstrate increasing behaviour of $K_{IIn}(a)$ as ω_2 is increased and h_1/W is decreased.

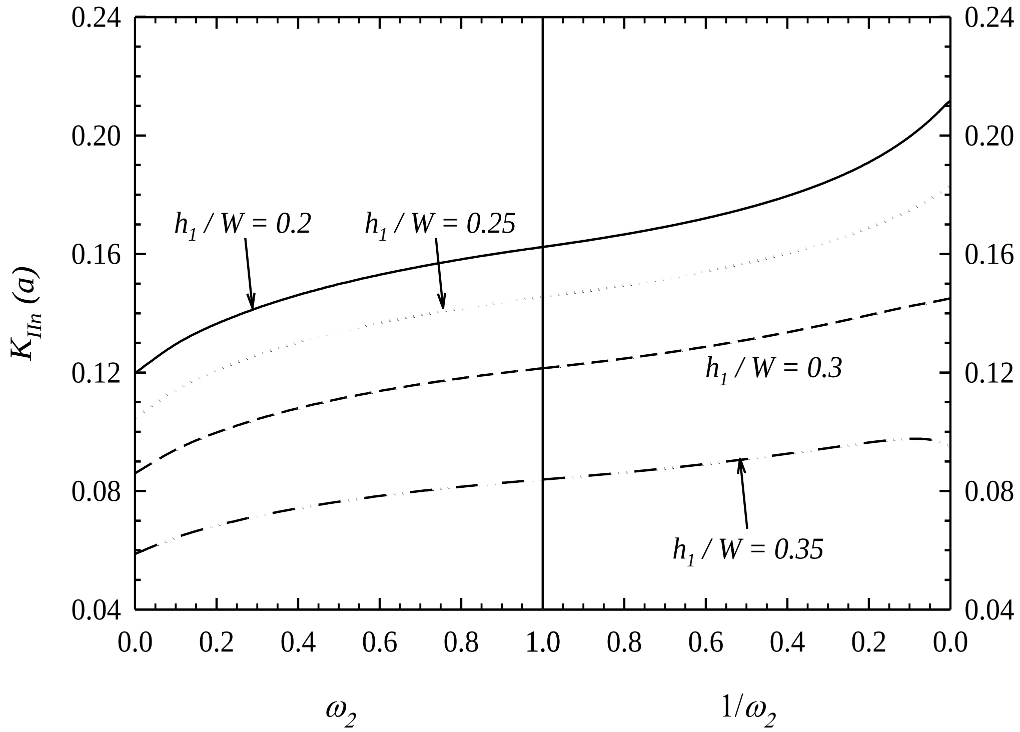

Figure 4.7.2 Influence of ω_2 on normalized mode-II SIF at the crack tip $x_1 = a$. $\gamma_1 = \gamma_2 = \gamma_{12} = 2$, $\beta_{12} = \beta_{13} = \beta_{31} = \beta_{32} = 1.5$, $\delta_1 = \delta_2 = \delta_3 = 3$, $\omega_1 = 4$, $a/W = 0.1$, $h/W = 0.4$.

Figures 4.7.3 and 4.7.4 present the calculated results for $J_{1n}(a)$ and $T_{sn}(a)$, respectively. The variation profile of the $J_{1n}(a)$ is analogous to that of $K_{In}(a)$. This is also an expected result since for given values of ω_2 and h_1/W, $K_{IIn}(a)$ is larger than $K_{In}(a)$. The results shown in Figure 4.7.4 illustrate that T-stress goes through either a maximum or a minimum depending on the value of h_1/W.

T -stress becomes negative when h_1/W is decreased from 0.35 to 0.2. T -stress is more sensitive to variations in ω_2 when $h_1/W = 0.35$, 0.25, and 0.2. When $h_1/W = 0.3$, T -stress is not significantly affected by the variations in ω_2.

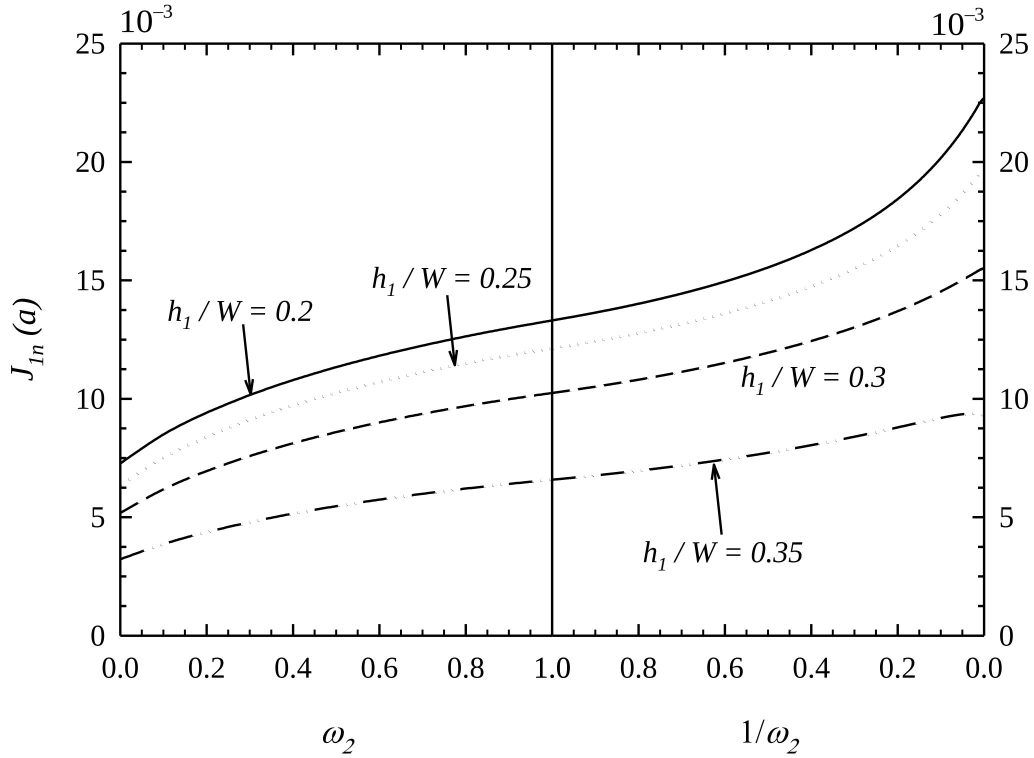

Figure 4.7.3 Influence of ω_2 on normalized energy release rate at the crack tip $x_1 = a$. $\gamma_1 = \gamma_2 = \gamma_{12} = 2$, $\beta_{12} = \beta_{13} = \beta_{31} = \beta_{32} = 1.5$, $\delta_1 = \delta_2 = \delta_3 = 3$, $\omega_1 = 4$, $a/W = 0.1$, $h/W = 0.4$.

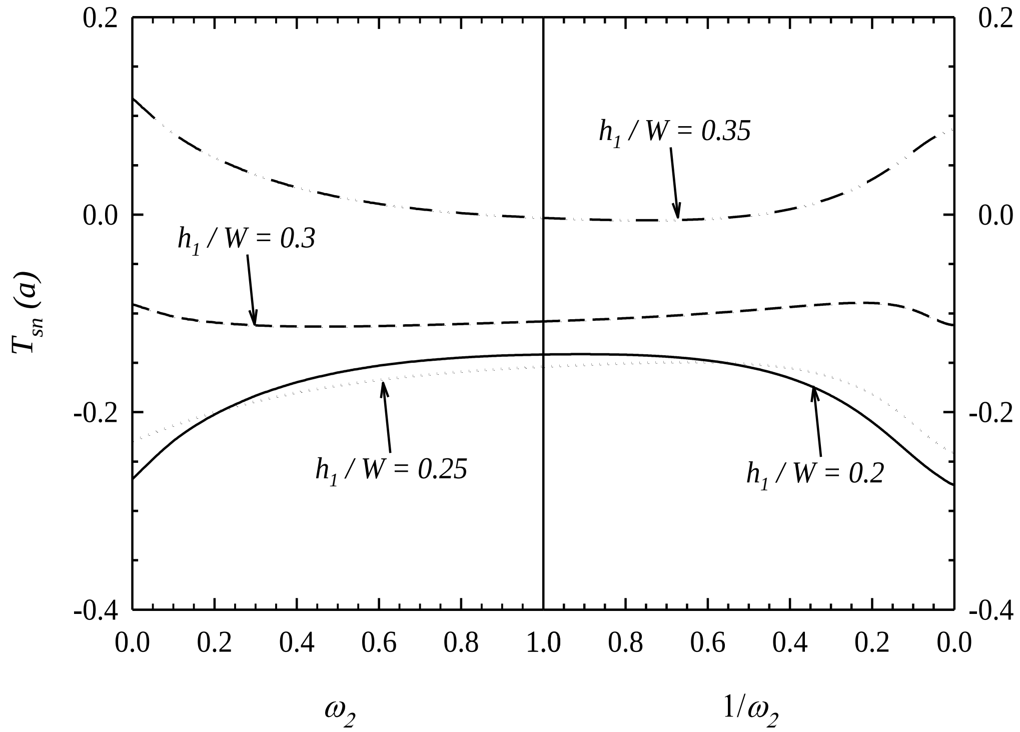

Figure 4.7.4 Influence of ω_2 on T-stress at the crack tip $x_1 = a$. $\gamma_1 = \gamma_2 = \gamma_{12} = 2$, $\beta_{12} = \beta_{13} = \beta_{31} = \beta_{32} = 1.5$, $\delta_1 = \delta_2 = \delta_3 = 3$, $\omega_1 = 4$, $a/W = 0.1$, $h/W = 0.4$.

Figure 4.8.1 shows plots of $K_{In}(a)$ as functions of h_1/W and δ_1. Note that δ_1 controls the variation profile of α_1. It can be seen from the figure that for the values of $h_1/W = 0.2$ and 0.25, $K_{In}(a)$ is not affected significantly by δ_1. But in the cases of $h_1/W = 0.3$ and 0.35, the influence δ_1 on $K_{In}(a)$ is more significant. Moreover, $K_{In}(a)$ gets larger as h_1/W is increased from 0.2 to 0.35.

The effect of δ_1 on the normalized mode-II stress intensity factor is depicted in Figure 4.8.2. Here, for all h_1/W values considered $K_{IIn}(a)$ increases as δ_1 increases. $K_{IIn}(a)$ gets larger values when h_1/W decreases.

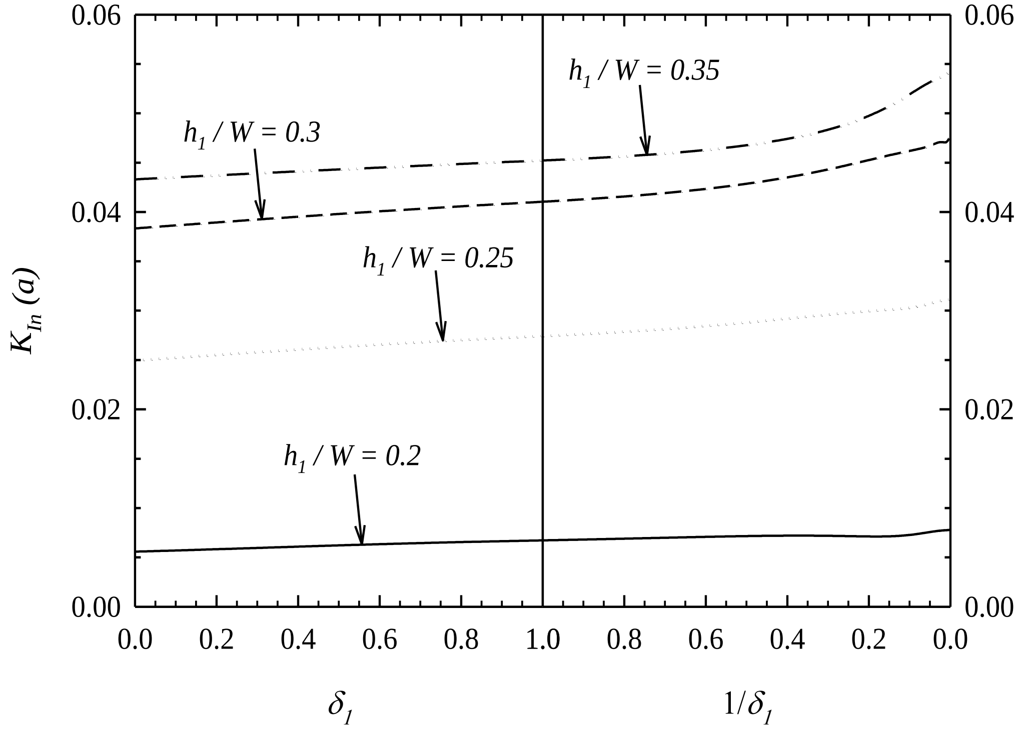

Figure 4.8.1 Influence of δ_1 on normalized mode-I SIF at the crack tip $x_1 = a$. $\gamma_1 = \gamma_2 = \gamma_{12} = 2$, $\beta_{12} = \beta_{13} = \beta_{31} = \beta_{32} = 1.5$, $\delta_2 = \delta_3 = 3$, $\omega_1 = \omega_2 = 4$, $a/W = 0.1$, $h/W = 0.4$.

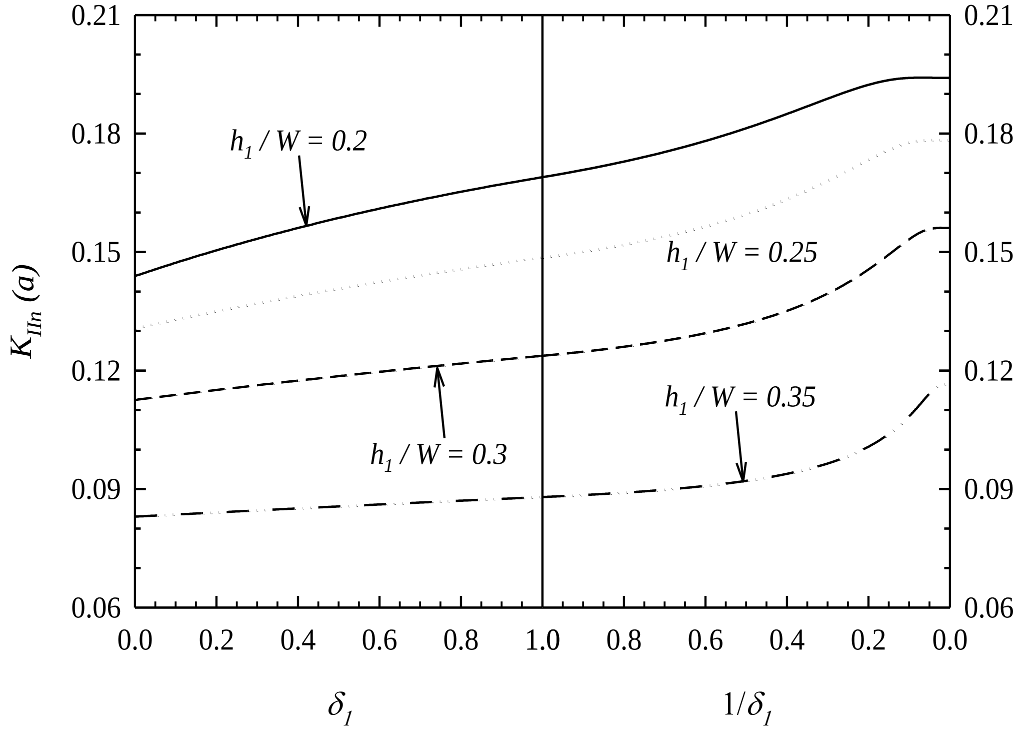

Figure 4.8.2 Influence of δ_1 on normalized mode-II SIF at the crack tip $x_1 = a$. $\gamma_1 = \gamma_2 = \gamma_{12} = 2$, $\beta_{12} = \beta_{13} = \beta_{31} = \beta_{32} = 1.5$, $\delta_2 = \delta_3 = 3$, $\omega_1 = \omega_2 = 4$, $a/W = 0.1$, $h/W = 0.4$.

In Figures 4.8.3 and 4.8.4, the calculated results for $J_{1n}(a)$ and $T_{sn}(a)$ are presented, respectively. The variation profiles of $J_{1n}(a)$ are similar to those of $K_{II\,n}(a)$. This is also an expected result since for given values of δ_1 and h_1/W, $K_{II\,n}(a)$ is larger than $K_{I\,n}(a)$.

It can be seen from the Figure 4.8.4 that h_1/W has a significant influence on the T-stress. For $h_1/W = 0.35$, T-stress first goes through a maximum and then goes through a minimum as δ_1 increases, whereas for smaller values of h_1/W, T-stress goes through a minimum as δ_1 is increased.

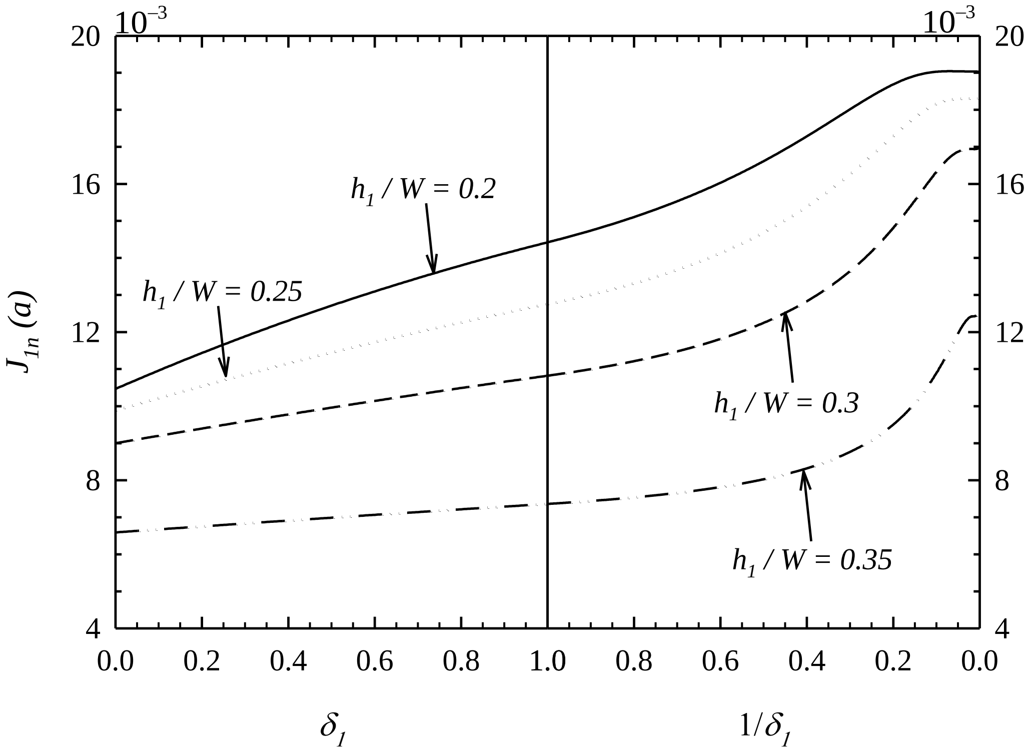

Figure 4.8.3 Influence of δ_1 on normalized energy release rate at the crack tip $x_1 = a$. $\gamma_1 = \gamma_2 = \gamma_{12} = 2$, $\beta_{12} = \beta_{13} = \beta_{31} = \beta_{32} = 1.5$, $\delta_2 = \delta_3 = 3$, $\omega_1 = \omega_2 = 4$, $a/W = 0.1$, $h/W = 0.4$.

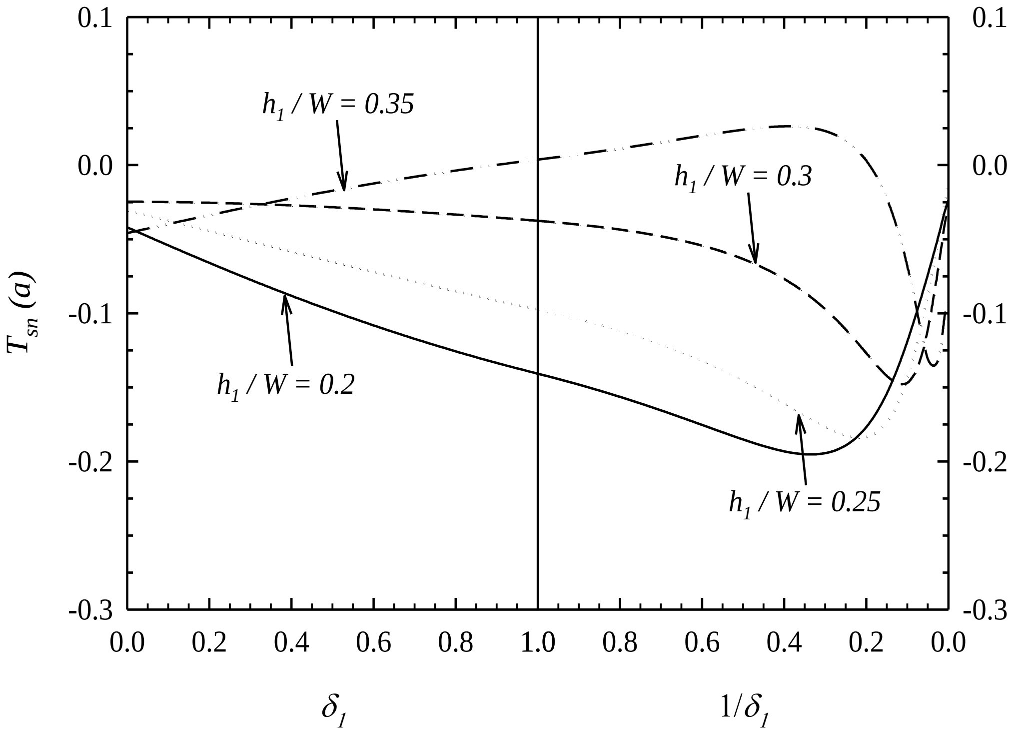

Figure 4.8.4 Influence of δ_1 on T-stress at the crack tip $x_1 = a$. $\gamma_1 = \gamma_2 = \gamma_{12} = 2$, $\beta_{12} = \beta_{13} = \beta_{31} = \beta_{32} = 1.5$, $\delta_2 = \delta_3 = 3$, $\omega_1 = \omega_2 = 4$, $a/W = 0.1$, $h/W = 0.4$.

Variations of the normalized mode-I stress intensity factors with respect to δ_2 are shown in Figure 4.9.1. For all values of h_1/W, $K_{In}(a)$ first increases and then decreases as δ_2 is increased. When $h_1/W = 0.2$, $K_{In}(a)$ decreases at nearly $\delta_2 = 1.125$. When $h_1/W = 0.25$, $K_{In}(a)$ decreases at about $\delta_2 = 4$. When $h_1/W = 0.3$, $K_{In}(a)$ decreases at $\delta_2 = 10$.

Additionally, $K_{In}(a)$ gets larger as h_1/W is increased. It can be seen from the Figure 4.9.2 that $K_{IIn}(a)$ gets larger as δ_2 is increased. Moreover, $K_{IIn}(a)$ increases with a corresponding increase in h_1/W.

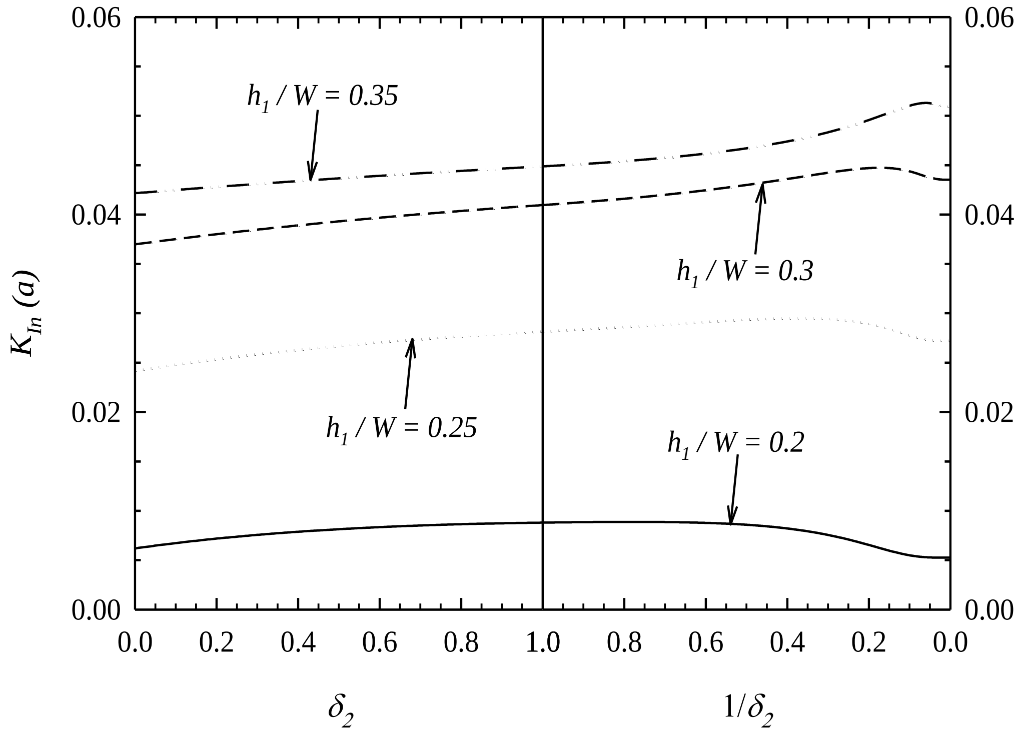

Figure 4.9.1 Influence of δ_2 on normalized mode-I SIF at the crack tip $x_1 = a$. $\gamma_1 = \gamma_2 = \gamma_{12} = 2$, $\beta_{12} = \beta_{13} = \beta_{31} = \beta_{32} = 1.5$, $\delta_1 = \delta_3 = 3$, $\omega_1 = \omega_2 = 4$, $a/W = 0.1$, $h/W = 0.4$.

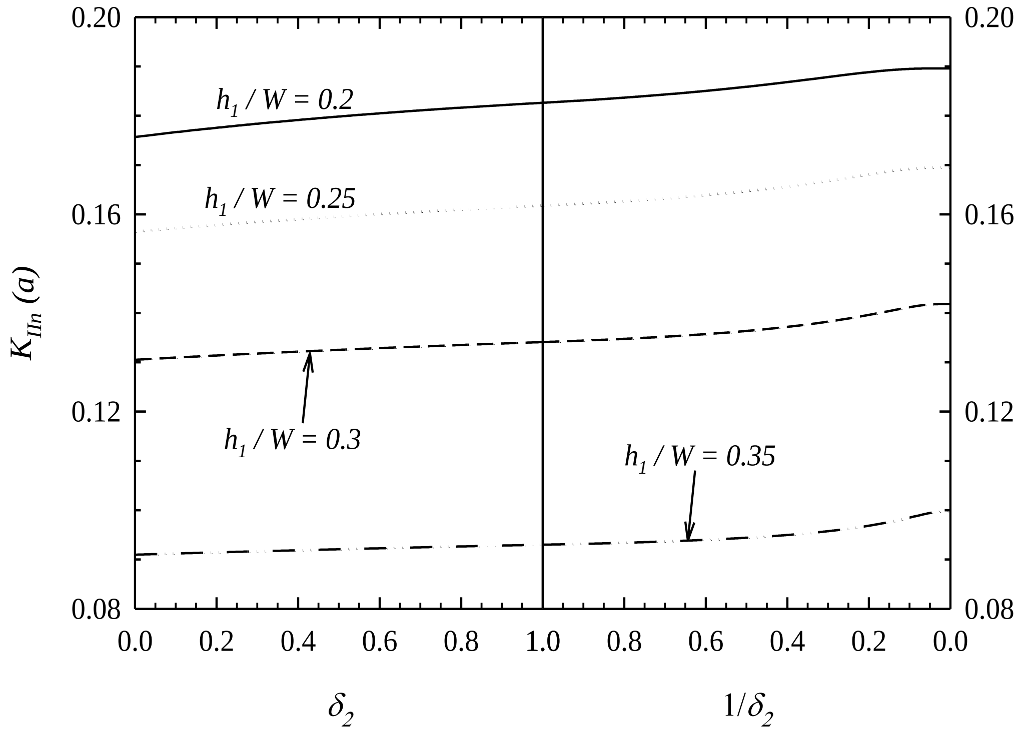

Figure 4.9.2 Influence of δ_2 on normalized mode-II SIF at the crack tip $x_1 = a$. $\gamma_1 = \gamma_2 = \gamma_{12} = 2$, $\beta_{12} = \beta_{13} = \beta_{31} = \beta_{32} = 1.5$, $\delta_1 = \delta_3 = 3$, $\omega_1 = \omega_2 = 4$, $a/W = 0.1$, $h/W = 0.4$.

The variation profiles of the normalized energy release rates which are depicted in Figure 4.9.3 are analogous to the variation profiles of the normalized mode-II stress intensity factors. This is an expected result since for given values of δ_2 and h_1/W, $K_{IIn}(a)$ is larger than $K_{In}(a)$. Interesting results are presented in Figure 4.7.4 which shows the influences of δ_2 and relative crack position on the T-stress. δ_2 is found to have no effect on the T-stress. The only effective parameter is the h_1/W. T-stress increases with a corresponding increase in h_1/W.

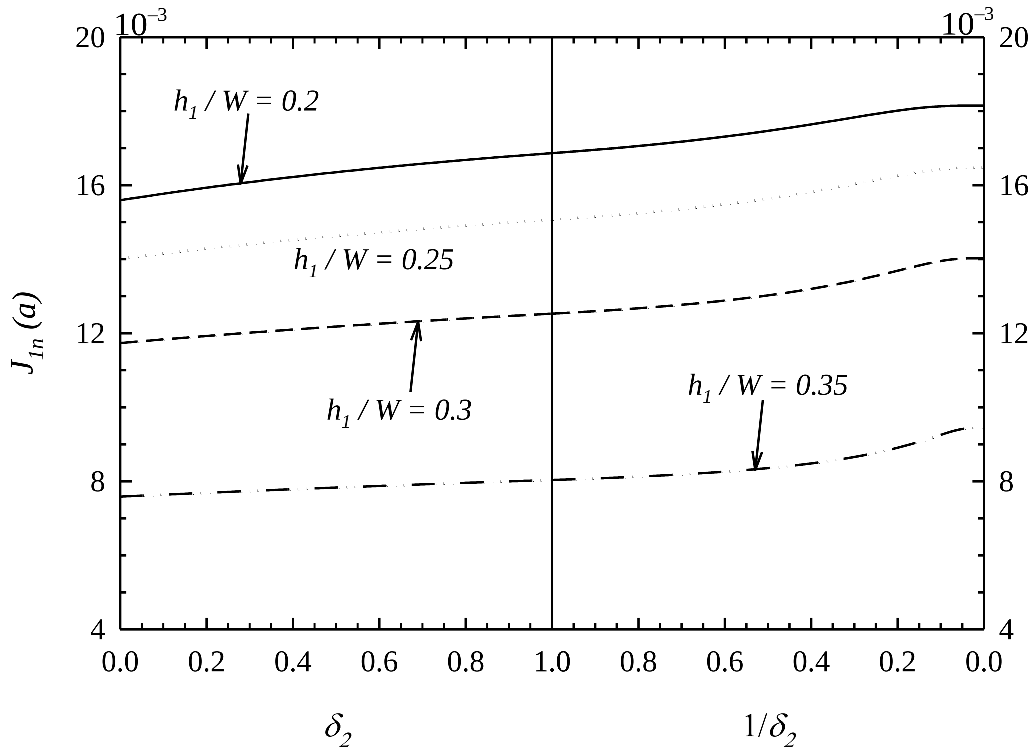

Figure 4.9.3 Influence of δ_2 on normalized energy release rate at the crack tip $x_1 = a$. $\gamma_1 = \gamma_2 = \gamma_{12} = 2$, $\beta_{12} = \beta_{13} = \beta_{31} = \beta_{32} = 1.5$, $\delta_1 = \delta_3 = 3$, $\omega_1 = \omega_2 = 4$, $a/W = 0.1$, $h/W = 0.4$.

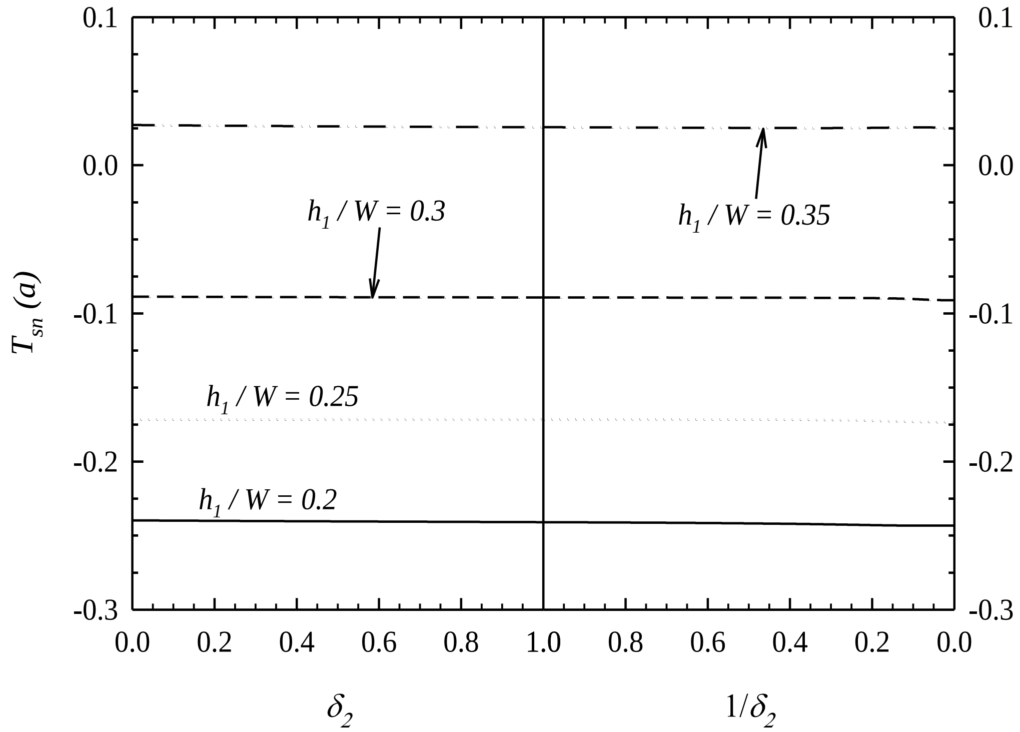

Figure 4.9.4 Influence of δ_2 on normalized T-stress at the crack tip $x_1 = a$. $\gamma_1 = \gamma_2 = \gamma_{12} = 2$, $\beta_{12} = \beta_{13} = \beta_{31} = \beta_{32} = 1.5$, $\delta_1 = \delta_3 = 3$, $\omega_1 = \omega_2 = 4$, $a/W = 0.1$, $h/W = 0.4$.

The influence of the exponent δ_3 on the normalized mode-I stress intensity factor is depicted in Figure 4.10.1. For three values of h_1/W, which are 0.25, 0.3, 0.35, $K_{In}(a)$ increases as δ_3 is increased. For $h_1/W = 0.2$, $K_{In}(a)$ first increases and then decreases. Also, $K_{In}(a)$ gets larger as h_1/W is increased.

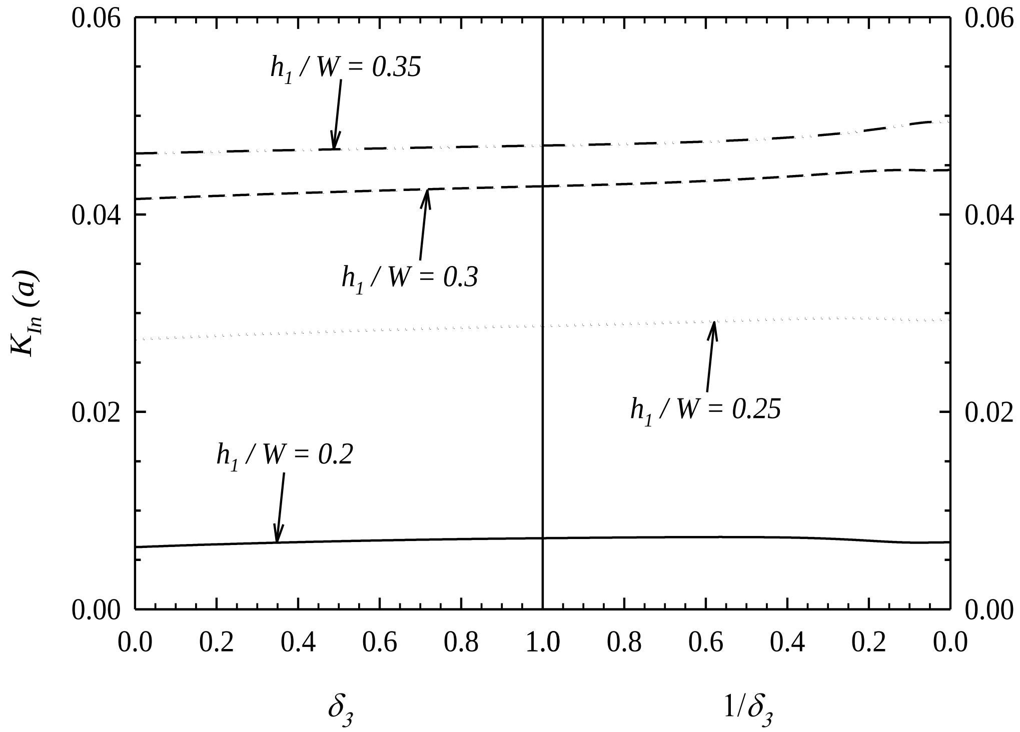

Figure 4.10.1 Influence of δ_3 on normalized mode-I SIF at the crack tip $x_1 = a$. $\gamma_1 = \gamma_2 = \gamma_{12} = 2$, $\beta_{12} = \beta_{13} = \beta_{31} = \beta_{32} = 1.5$, $\delta_1 = \delta_2 = 3$, $\omega_1 = \omega_2 = 4$, $a/W = 0.1$, $h/W = 0.4$.

In Figure 4.10.2, which shows the variation profiles of $K_{IIn}(a)$, it can be seen that for all h_1/W values considered $K_{IIn}(a)$ increases as δ_3 is increased. Moreover, $K_{IIn}(a)$ gets larger values as h_1/W decreases.

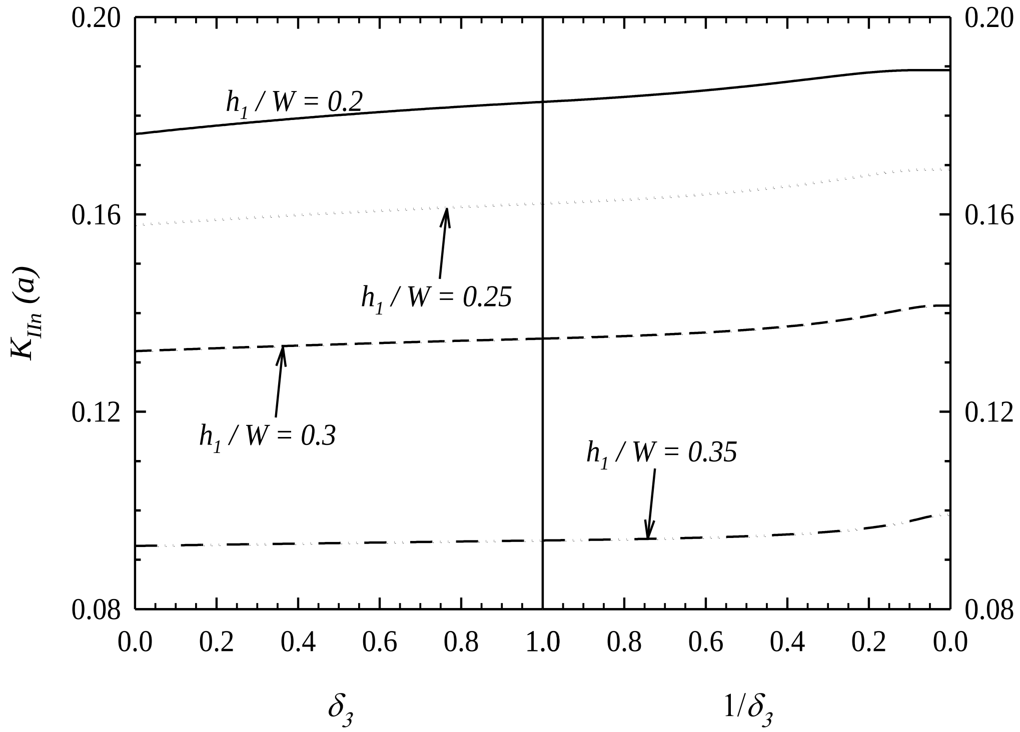

Figure 4.10.2 Influence of δ_3 on normalized mode-II SIF at the crack tip $x_1 = a$. $\gamma_1 = \gamma_2 = \gamma_{12} = 2$, $\beta_{12} = \beta_{13} = \beta_{31} = \beta_{32} = 1.5$, $\delta_1 = \delta_2 = 3$, $\omega_1 = \omega_2 = 4$, $a/W = 0.1$, $h/W = 0.4$.

As also seen in the other analyses, the variation profiles of the normalized energy release rates depicted in Figure 4.10.3 are similar to the variation profiles of normalized mode-II stress intensity factors. This is also an expected result since for given values of δ_3 and h_1/W, $K_{IIn}(a)$ is larger than $K_{In}(a)$.

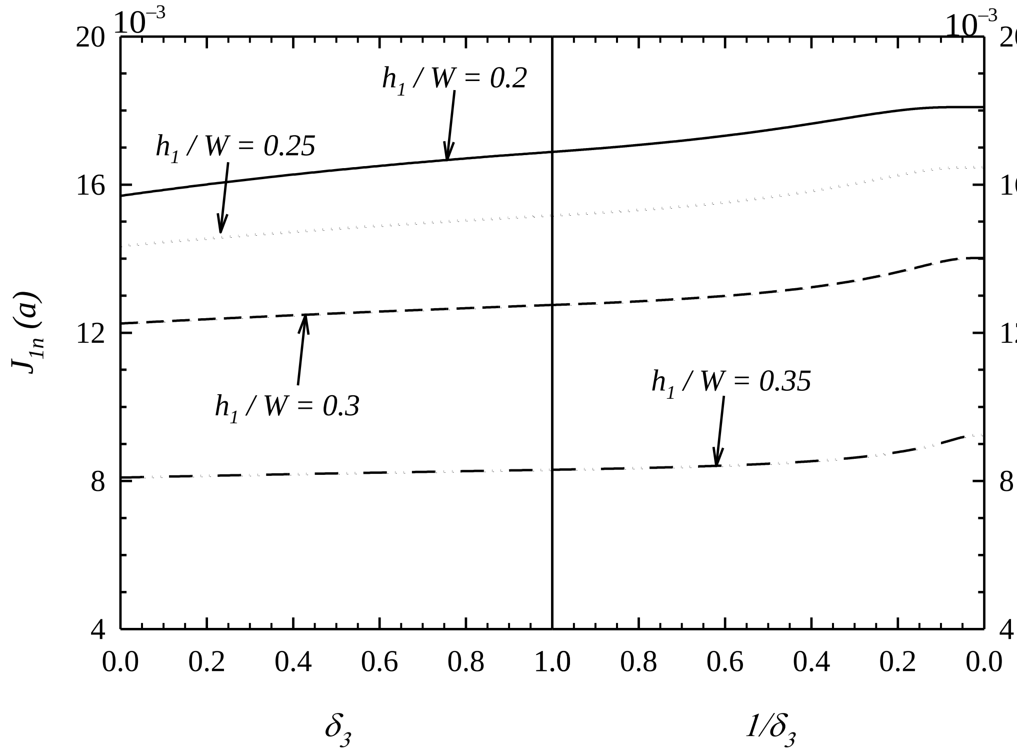

Figure 4.10.3 Influence of δ_3 on normalized energy release rate at the crack tip $x_1 = a$. $\gamma_1 = \gamma_2 = \gamma_{12} = 2$, $\beta_{12} = \beta_{13} = \beta_{31} = \beta_{32} = 1.5$, $\delta_1 = \delta_2 = 3$, $\omega_1 = \omega_2 = 4$, $a/W = 0.1$, $h/W = 0.4$.

It can be seen from the Figure 4.10.4 that crack location has a considerable influence on the T-stress. For $h_1/W = 0.35$, T-stress gets larger until δ_3 nearly equals to 4 and then it decreases. For $h_1/W = 0.2$ and 0.25, T-stress gets smaller until δ_3 nearly equals to 5 and then increases. And, finally for $h_1/W = 0.3$, δ_3 has almost no influence on T-stress until the value where δ_3 equals nearly 2.5. After this point T-stress decreases and then increases to its final value. Additionally, T-stress increases as h_1/W gets larger.

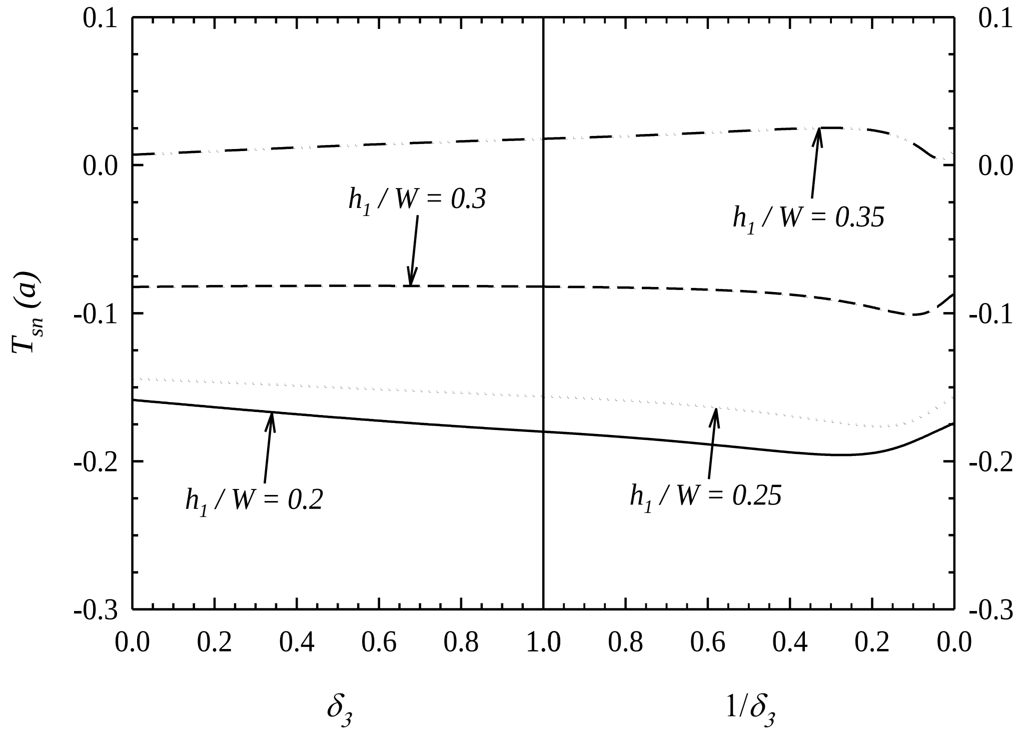

Figure 4.10.4 Influence of δ_3 on T-stress at the crack tip $x_1 = a$. $\gamma_1 = \gamma_2 = \gamma_{12} = 2$, $\beta_{12} = \beta_{13} = \beta_{31} = \beta_{32} = 1.5$, $\delta_1 = \delta_2 = 3$, $\omega_1 = \omega_2 = 4$, $a/W = 0.1$, $h/W = 0.4$.

Plots of the normalized mode-I stress intensity factor, mode-II stress intensity factors and energy release rates as functions of β_{12} are shown in Figures 4.11.1, 4.11.2 and 4.11.3. Note that the exponent β_{12} governs the variation profile of the Poisson's ratio ν_{12}. All the three variation profiles are similar such that they display small variations with respect to β_{12}. The variation profiles of $K_{IIn}(a)$ and $J_{1n}(a)$ are also similar. Both of these quantities get larger values as h_1/W becomes smaller. This is an expected result since for given values of β_{12} and h_1/W, $K_{IIn}(a)$ is larger than $K_{In}(a)$.

On the other hand, $K_{In}(a)$ gets larger values as h_1/W increases. In general, β_{12} has little influence on the fracture mechanics parameters $K_{In}(a)$, $K_{IIn}(a)$ and $J_{1n}(a)$.

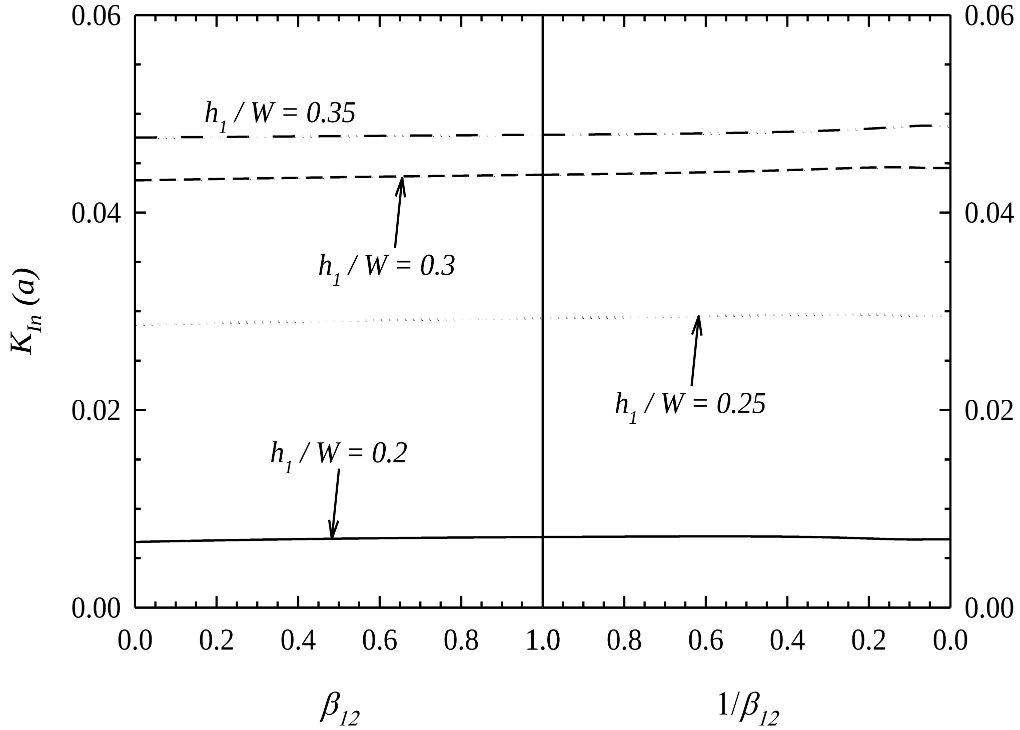

Figure 4.11.1 Influence of β_{12} on normalized mode-I SIF at the crack tip $x_1 = a$. $\gamma_1 = \gamma_2 = \gamma_{12} = 2$, $\beta_{13} = \beta_{31} = \beta_{32} = 1.5$, $\delta_1 = \delta_2 = \delta_3 = 3$, $\omega_1 = \omega_2 = 4$, $a/W = 0.1$, $h/W = 0.4$.

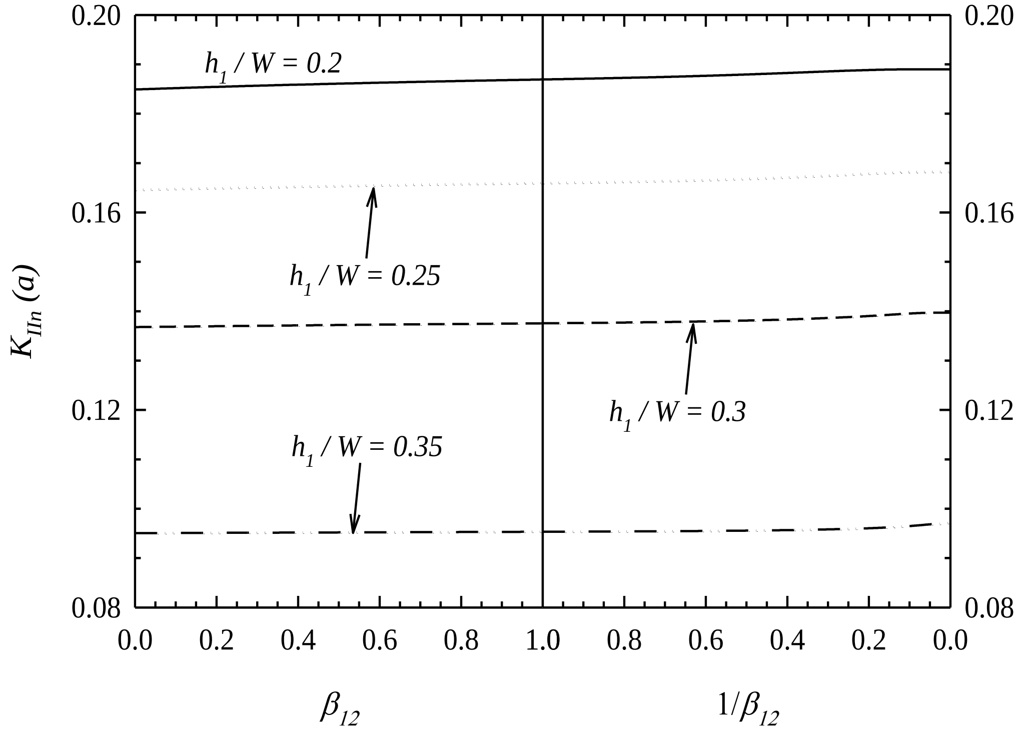

Figure 4.11.2 Influence of β_{12} on normalized mode-II SIF at the crack tip $x_1 = a$. $\gamma_1 = \gamma_2 = \gamma_{12} = 2$, $\beta_{13} = \beta_{31} = \beta_{32} = 1.5$, $\delta_1 = \delta_2 = \delta_3 = 3$, $\omega_1 = \omega_2 = 4$, $a/W = 0.1$, $h/W = 0.4$.

.

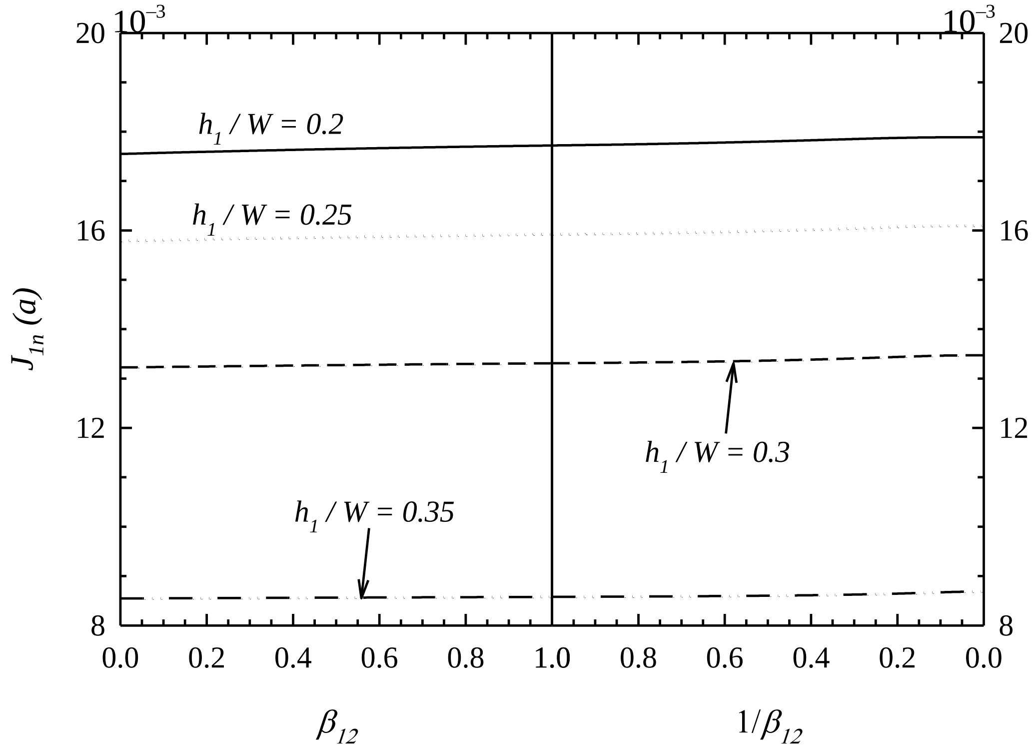

Figure 4.11.3 Influence of β_{12} on normalized energy release rate at the crack tip $x_1 = a$. $\gamma_1 = \gamma_2 = \gamma_{12} = 2$, $\beta_{13} = \beta_{31} = \beta_{32} = 1.5$, $\delta_1 = \delta_2 = \delta_3 = 3$, $\omega_1 = \omega_2 = 4$, $a/W = 0.1$, $h/W = 0.4$.

The influences of the β_{12} and h_1/W on the T-stresses are depicted in Figure 4.11.4. For all values of h_1/W T-stress is found to be almost not affected from the increasing values of β_{12}.

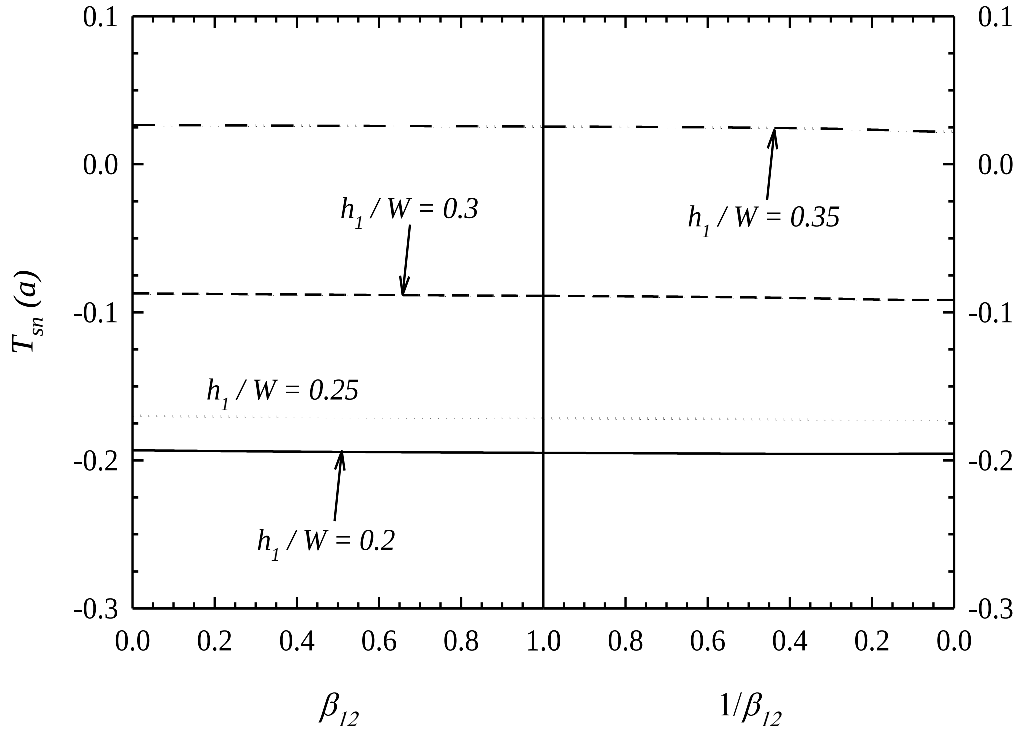

Figure 4.11.4 Influence of β_{12} on T-stress at the crack tip $x_1 = a$. $\gamma_1 = \gamma_2 = \gamma_{12} = 2$, $\beta_{13} = \beta_{31} = \beta_{32} = 1.5$, $\delta_1 = \delta_2 = \delta_3 = 3$, $\omega_1 = \omega_2 = 4$, $a/W = 0.1$, $h/W = 0.4$.

CHAPTER 5

CONCLUDING REMARKS

In this study, a computational method based on the J_k -integral method is used to calculate fracture mechanics parameters under thermal stress conditions. An embedded crack is considered in an orthotropic functionally graded medium. The problem is formulated using the plane orthotropic thermoelasticity constitutive relations. The orthotropic medium is under thermal loading condition. The upper surface of the FGM layer is at 2 times the reference temperature T_0 and the lower surface of the layer is kept at the reference temperature. The other surfaces of the model are assumed to be insulated. Therefore, the temperature distribution within the model is two dimensional. The principal axes of the orthotropy coincide with the axes of the model created. Because of the symmetry about x_2 axis, one half of the model is used in the finite element analysis. In order to represent the material property gradation, power-law is utilized. Power-law is a flexible method and frequently used in the analysis of FGMs. A general purpose finite element software ANSYS is utilized to perform thermal and structural analysis. In order to implement the J_k -integral method in ANSYS, Ansys Parametric Design Language (APDL) is utilized. With the help of the code written by means of APDL, normalized mode-I stress intensity factor (K_{In}), mode-II stress intensity factor (K_{IIn}), normalized energy release rate (J_{1n}), and normalized T -stress (T_{sn}) are calculated at the crack tip.

The fracture mechanics parameters are calculated for different values of exponents of the power functions and for different values of relative crack locations.

The other parameters used in the analysis are ω_1, ω_2, δ_1, δ_2, δ_3, and β_{12} which are the exponents of power functions representing thermal conductivity k_1, thermal conductivity k_2, thermal expansion coefficient α_1, thermal expansion coefficient α_2, thermal expansion coefficient α_3, and Poisson's ratio ν_{12}, respectively.

The variation profiles of fracture mechanics parameters for different values of the exponents and relative crack locations are depicted in the figures. In addition, temperature analyses are performed by the changing values ω_1 and ω_2 . The figures depicting the temperature distributions are also given in this study. Moreover, in order to show the domain independence and accuracy of the J_k-integral method, normalized mode-I stress intensity factors, and mode-II stress intensity factors are compared to those evaluated by the displacement correlation technique (DCT).

The temperature distribution is two dimensional within the FGM layer. The temperature distribution at the crack tip is primarily affected by the exponent of thermal conductivity k_2. The thermal conductivity k_1 has almost no effect on the temperature distribution at the crack tip. The normalized stress intensity factors obtained for the cases of plane stress and plane strain show the great agreement with results obtained from DCT. This agreements demonstrate the accuracy and domain independence of the J_k-integral method. Among the exponents ω_1, ω_2, δ_1, δ_2, δ_3 and β_{12} has no effect on the fracture mechanics parameters. The other five exponents possess different influences on the fracture mechanics parameters as depicted in the figures.

It must be noted that the used method in this study can be applicable to CASE I and CASE II type problems as mentioned in section 2.1. In order to obtain stress intensity factors for CASE III, iteration must be utilized in conjunction with DCT.

REFERENCES

[1] Nikishkov, G.P., Atluri, S.N., 1987. “An Equivalent domain integral method for computing crack-tip integral parameters in non-elastic, thermo-mechanical fracture”. *Engineering Fracture Mechanics*, Vol. 26, pp.851-867.

[2] Kim, J.H., Paulino, G.H., 2003. “Mixed mode *J*-integral formulation and implementation using graded elements for fracture analysis of nonhomogeneous orthotropic materials”. *Mechanics of Materials*, Vol. 35, pp.107-128.

[3] Walters M.C, Paulino G.H., Dodds R.H. Jr., 2004. “Stress-intensity factors for surface cracks in functionally graded materials under mode-I thermomechanical loading”. *International Journal of Solids and Structures*, Vol. 41, pp.1081–1118.

[4] Kim, J.H., Paulino, G.H., 2004. “T-stress in orthotropic functionally graded materials: Lekhnitskii and Stroh formalisms”. International Journal of Fracture, Vol. 126, pp. 345-384.

[5] Abanto-Bueno, J., Lambros, J., 2006. “Parameters controlling fracture resistance in functionally graded materials under mode I loading”. *International Journal of Solids and Structures*, Vol. 43, pp.3920-3939.

[6] Dağ, S. “Thermal fracture analysis of orthotropic functionally graded materials using an equivalent domain integral approach”, *Engineering Fracture Mechanics*, Vol. 73, pp. 2802-2828.

[7] Dağ, S. “Mixed-mode fracture analysis of functionally graded materials under thermal stresses: a new approach using J_k-integral”. Journal of Thermal Stresses, Vol. 30, pp. 269-296.

[8] Amit, K.C., Kim, J.H., 2008. "Interaction integrals for thermal fracture of functionally graded materials". *Engineering Fracture Mechanics*, Vol. 75, pp. 2542-2565.

[9] Dağ, S., İlhan, K.A., 2008 "Mixed-mode fracture analysis of FGM coatings using analytical and computational methods". Journal of Applied Mechanics, Vol. 75, Article number: 051104.

[10] Lekhnitskii J.D., 1968. "Anisotropic Plates" Gordon and Breach Science Publishers, New York, London, Paris.

[11] Rice J.R.,1968. "A path independent integral and approximate analysis of strain concentration by notches and cracks". *Journal of Applied Mechanics*, Vol. 35, pp. 379-386.

[12] Eischen, J.W. 1987. "Fracture of nonhomogeneous materials". *International Journal of Fracture*, Vol. 34, pp. 3-22.

[13] Obata, M., Nemat-Nasser, S., Goto, Y., 1989. "Branched cracks in anisotropic elastic solids". *ASME Journal of Applied Mechanics*, Vol. 56, pp. 858-864.

[14] Ma, H., Chen, Y.H. 1996. "The explicit formulation for the J_k vector in both isotropic and anisotropic cases". *International Journal of Fracture*, Vol. 75, pp. R25-R28.

[15] Kim, J.H., Paulino, G.H., 2002. "Finite element evaluation of mixed mode stress intensity factors in functionally graded materials". *International Journal for Numerical Methods in Engineering,* Vol. 53, pp.1903-1935.

[16] Eischen, J.W. 1987. "An improved method for computing the J_2 integral". *Engineering Fracture Mechanics*, Vol. 26, pp. 691-700.

[17] Reddy, J.N., *"An introduction to the Finite Element Method"* 3rd Edition, McGraw Hill, 2006.

[18] Cook, R., Malkus, D., Plesha, M., *"Concepts and applications of finite element analysis"* 3rd Edition, John Wiley & Sons, 1989.

[19] Callister, WD., *"Materials science and engineering an introduction"* John Wiley & Sons, 2000.

APPENDIX A

DIVERGENCE THEOREM

Let $\vec{\nabla}$ denote the Laplace Operator in the two-dimensional Cartesian rectangular coordinate system *(x, y)* shown in Figure A.1,

$$\vec{\nabla} = \hat{e}_x \frac{\partial}{\partial x} + \hat{e}_y \frac{\partial}{\partial y} \tag{A.1}$$

where $\hat{e}_x$ and $\hat{e}_y$ denote the unit basis vectors along the *x* and *y* coordinates, respectively. If *G(x,y)* is a scalar function of class $C^0(\Omega)$ in the two-dimensional domain Ω shown in the Figure A.1, the following divergence theorem holds.

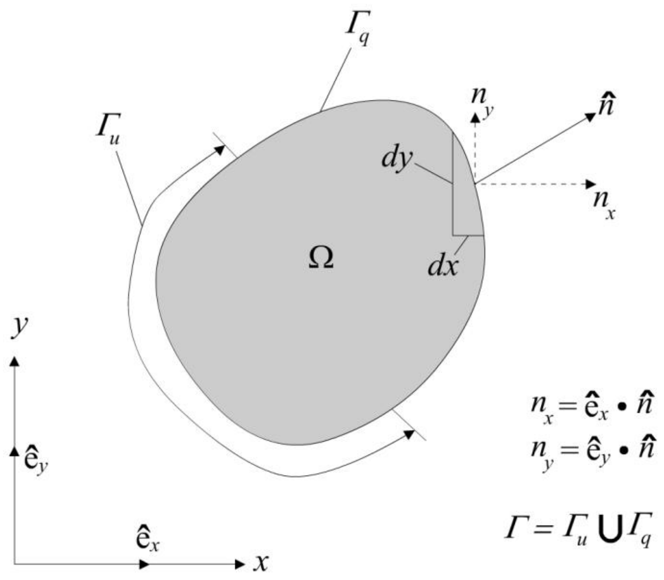

Figure A.1 Divergence theorem in two dimensional domain.

$$\int_{\Omega} div\mathrm{G}\ dx\,dy \equiv \int_{\Omega} \nabla \cdot \mathrm{G}\,dx\,dy = \oint_{\Gamma} \hat{n} \cdot \mathrm{G}\,ds \tag{A.2}$$

$$\int_{\Omega} \left(\frac{\partial G_x}{\partial x} + \frac{\partial G_y}{\partial y} \right) dx\,dy = \oint_{\Gamma} \left(n_x\, G_x + n_y\, G_y \right) ds \tag{A.3}$$

or in indicial notation,

$$\int_{\Omega} \left(\frac{\partial G_i}{\partial x_i} \right) dx\,dy = \oint_{\Gamma} \left(n_i\, G_i \right) ds \tag{A.4}$$

Here the dot denotes the scalar product of vectors, $\hat{n}$ denotes the unit vector normal to the surface Γ of the domain Ω; n_x and n_y (G_x and G_y) are the rectangular components of $\hat{n}(G)$; and the circle on the boundary integral indicates that the integration is taken over the entire boundary.

APPENDIX B

ASYMPTOTIC EXPRESSIONS FOR THE STRESS COMPONENTS

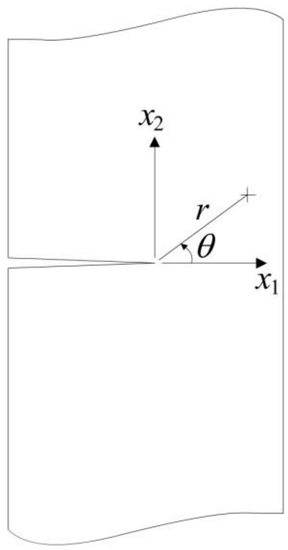

Figure B.1 Crack tip coordinate system.

The asymptotic stress field for crack shown in Figure A.2 is given as follows,

$$\sigma_{ij}\left(r,\theta\right)=\frac{K_I}{\sqrt{2\pi r}}\,f_{ij}^{I}\left(\theta\right)+\frac{K_{II}}{\sqrt{2\pi r}}\,f_{ij}^{II}\left(\theta\right)+T_{str}\,\delta_{1i}\,\delta_{1j} \qquad \textbf{(B.1)}$$

where T_{str} is the non-singular stress, or so called *T*-stress.

The explicit form of asymptotic stress field in the vicinity of the crack tip for mixed-mode is given as follows:

$$\sigma_{11}(r,\theta)=\frac{K_I}{\sqrt{2\pi r}}\mathrm{Re}\left[\frac{\mu_1^{tip}\mu_2^{tip}}{\mu_1^{tip}-\mu_2^{tip}}\left\{\frac{\mu_2^{tip}}{\sqrt{\cos\theta+\mu_2^{tip}\sin\theta}}-\frac{\mu_1^{tip}}{\sqrt{\cos\theta+\mu_1^{tip}\sin\theta}}\right\}\right]$$
$$+\frac{K_{II}}{\sqrt{2\pi r}}\mathrm{Re}\left[\frac{1}{\mu_1^{tip}-\mu_2^{tip}}\left\{\frac{\left(\mu_2^{tip}\right)^2}{\sqrt{\cos\theta+\mu_2^{tip}\sin\theta}}-\frac{\left(\mu_1^{tip}\right)^2}{\sqrt{\cos\theta+\mu_1^{tip}\sin\theta}}\right\}\right]+T_{str}$$

$$\sigma_{22}(r,\theta)=\frac{K_I}{\sqrt{2\pi r}}\mathrm{Re}\left[\frac{1}{\mu_1^{tip}-\mu_2^{tip}}\left\{\frac{\mu_1^{tip}}{\sqrt{\cos\theta+\mu_2^{tip}\sin\theta}}-\frac{\mu_2^{tip}}{\sqrt{\cos\theta+\mu_1^{tip}\sin\theta}}\right\}\right]$$
$$+\frac{K_{II}}{\sqrt{2\pi r}}\mathrm{Re}\left[\frac{1}{\mu_1^{tip}-\mu_2^{tip}}\left\{\frac{1}{\sqrt{\cos\theta+\mu_2^{tip}\sin\theta}}-\frac{1}{\sqrt{\cos\theta+\mu_1^{tip}\sin\theta}}\right\}\right] \qquad \textbf{(B.2)}$$

$$\sigma_{12}(r,\theta)=\frac{K_I}{\sqrt{2\pi r}}\mathrm{Re}\left[\frac{\mu_1^{tip}\mu_2^{tip}}{\mu_1^{tip}-\mu_2^{tip}}\left\{\frac{1}{\sqrt{\cos\theta+\mu_1^{tip}\sin\theta}}-\frac{1}{\sqrt{\cos\theta+\mu_2^{tip}\sin\theta}}\right\}\right]$$
$$+\frac{K_{II}}{\sqrt{2\pi r}}\mathrm{Re}\left[\frac{1}{\mu_1^{tip}-\mu_2^{tip}}\left\{\frac{\mu_1^{tip}}{\sqrt{\cos\theta+\mu_1^{tip}\sin\theta}}-\frac{\mu_2^{tip}}{\sqrt{\cos\theta+\mu_2^{tip}\sin\theta}}\right\}\right]$$

The μ_1^{tip} and μ_2^{tip} are given by equation (2.8).

APPENDIX C

q-FUNCTION

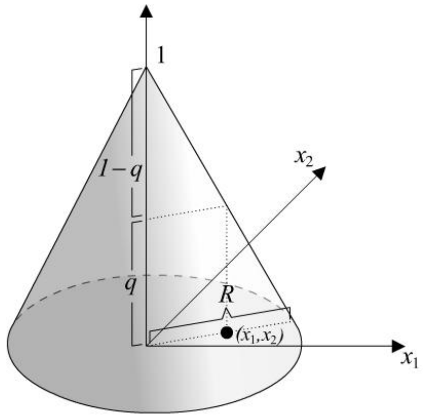

Figure C.1 Orientation of the q- function.

$$q = 1 - \frac{\sqrt{x_1^2 + x_2^2}}{R} \qquad \textbf{(C.1)}$$

The derivatives of the function q with respect to coordinates x_1 and x_2 are as follows

$$q_{,1} = -\frac{x_1}{R\sqrt{x_1^2 + x_2^2}} \qquad \textbf{(C.2)}$$

$$q_{,2} = -\frac{x_2}{R\sqrt{x_1^2 + x_2^2}} \qquad \textbf{(C.3)}$$

It is clear in the Figure A.4 that

$$\frac{q}{1} = \frac{x}{R} \tag{C.4}$$

$$q = \frac{x}{R} \tag{C.5}$$

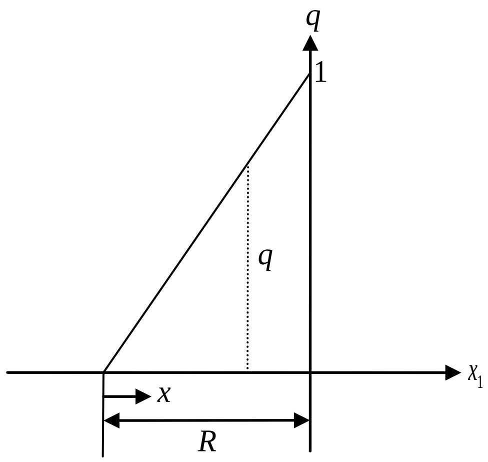

Figure C.2 *q*- function for a circular path around the crack tip.

APPENDIX D

DERIVATIVES OF THE MECHANICAL STRAIN ENERGY DENSITY FUNCTION W.

The derivatives of mechanical strain energy density function for the case of plane stress are obtained as [6]

$$\frac{\partial W}{\partial E_1} = \frac{-\left\{\left(2E_2\nu_{12}^2 - E_1\right)\varepsilon_{11}^m + \nu_{12}E_2\varepsilon_{22}^m\right\}\left\{\nu_{12}E_2\varepsilon_{22}^m + E_1\varepsilon_{11}^m\right\}}{2\left(E_1 - \nu_{12}^2 E_2\right)^2} \quad \textbf{(D.1)}$$

$$\frac{\partial W}{\partial E_2} = \frac{E_1^2\left(\nu_{12}\varepsilon_{11}^m + \varepsilon_{22}^m\right)^2}{2\left(E_1 - \nu_{12}^2 E_2\right)^2} \quad \textbf{(D.2)}$$

$$\frac{\partial W}{\partial \nu_{12}} = \frac{E_1E_2\left(\nu_{12}\varepsilon_{11}^m + \varepsilon_{22}^m\right)\left(\nu_{12}E_2\varepsilon_{22}^m + E_1\varepsilon_{11}^m\right)}{\left(E_1 - \nu_{12}^2 E_2\right)^2} \quad \textbf{(D.3)}$$

$$\frac{\partial W}{\partial G_{12}} = \varepsilon_{12}^2 + \varepsilon_{21}^2 \quad \textbf{(D.4)}$$

$$\frac{\partial W}{\partial \alpha_1} = \frac{-E_1\left(\nu_{12}E_2\varepsilon_{22}^m + E_1\varepsilon_{11}^m\right)\Delta T}{E_1 - \nu_{12}^2 E_2} \quad \textbf{(D.5)}$$

$$\frac{\partial W}{\partial \alpha_2} = \frac{-E_1E_2\left(\nu_{12}\varepsilon_{11}^m + \varepsilon_{22}^m\right)\Delta T}{E_1 - \nu_{12}^2 E_2} \quad \textbf{(D.6)}$$

$$\frac{\partial W}{\partial \Delta T} = \frac{-E_1\left\{\left(E_1\alpha_1 + \nu_{12}E_2\alpha_2\right)\varepsilon_{11}^m + \left(E_2\alpha_2 + \nu_{12}E_2\alpha_1\right)\varepsilon_{22}^m\right\}}{E_1 - \nu_{12}^2 E_2} \quad \textbf{(D.7)}$$

In case of plane strain, the derivatives of mechanical strain energy density function are given as follows [6]

$$\frac{\partial W}{\partial E_1}=\frac{1}{2\Lambda}\left\{(A_1\nu_{31}+2A_2E_1)\bar{\varepsilon}_{11}^2+b_1E_2\bar{\varepsilon}_{11}\bar{\varepsilon}_{22}+(b_1\bar{\varepsilon}_{11}+b_2\bar{\varepsilon}_{22})E_2\bar{\varepsilon}_{22}\right\}$$
$$-\frac{E_1b_2}{2\Lambda^2}\left\{(A_2E_1\bar{\varepsilon}_{11}+b_1E_2\bar{\varepsilon}_{22})\bar{\varepsilon}_{11}+(b_1\bar{\varepsilon}_{11}+b_2\bar{\varepsilon}_{22})E_2\bar{\varepsilon}_{22}\right\}+\frac{\nu_{31}\bar{\varepsilon}_{33}^2}{2\nu_{13}} \tag{D.8}$$

$$\frac{\partial W}{\partial E_2}=\frac{E_1}{2\Lambda}\left\{\left(b_1\bar{\varepsilon}_{22}-\frac{\nu_{32}^2\nu_{13}\bar{\varepsilon}_{11}}{\nu_{31}}\right)\bar{\varepsilon}_{11}+(b_1\bar{\varepsilon}_{11}+b_2\bar{\varepsilon}_{22})\bar{\varepsilon}_{22}\right\}$$
$$+\frac{E_1}{2\Lambda^2}\left\{(A_2E_1\bar{\varepsilon}_{11}+b_1E_2\bar{\varepsilon}_{22})\bar{\varepsilon}_{11}+(b_1\bar{\varepsilon}_{11}+b_2\bar{\varepsilon}_{22})E_2\bar{\varepsilon}_{22}\right\}\left(\nu_{12}^2+2\nu_{12}\nu_{13}\nu_{32}+\frac{\nu_{32}^2\nu_{13}}{\nu_{31}}\right) \tag{D.9}$$

$$\frac{\partial W}{\partial G_{12}}=\varepsilon_{12}^2+\varepsilon_{21}^2 \tag{D.10}$$

$$\frac{\partial W}{\partial \nu_{12}}=\frac{E_1E_2b_1}{\Lambda^2}\left\{(A_2E_1\bar{\varepsilon}_{11}+b_1E_2\bar{\varepsilon}_{22})\bar{\varepsilon}_{11}+(b_1\bar{\varepsilon}_{11}+b_2\bar{\varepsilon}_{22})E_2\bar{\varepsilon}_{22}\right\}$$
$$+\frac{E_1E_2\bar{\varepsilon}_{11}\bar{\varepsilon}_{22}}{\Lambda} \tag{D.11}$$

$$\frac{\partial W}{\partial \nu_{31}}=\frac{E_1}{2\Lambda}\left\{(A_1\bar{\varepsilon}_{11}+A_2E_1\bar{\varepsilon}_{33})\bar{\varepsilon}_{11}-(A_2E_1\bar{\varepsilon}_{11}+b_1E_2\bar{\varepsilon}_{22})\bar{\varepsilon}_{33}-(b_1\bar{\varepsilon}_{33}+\nu_{13}\bar{\varepsilon}_{22})E_2\bar{\varepsilon}_{22}\right\}$$
$$-\frac{E_1(A_1-E_1\nu_{13})}{2\Lambda^2}\left\{(A_2E_1\bar{\varepsilon}_{11}+b_1E_2\bar{\varepsilon}_{22})\bar{\varepsilon}_{11}+(b_1\bar{\varepsilon}_{11}+b_2\bar{\varepsilon}_{22})E_2\bar{\varepsilon}_{22}\right\}+\frac{E_1\bar{\varepsilon}_{33}^2}{2\nu_{13}} \tag{D.12}$$

$$\frac{\partial W}{\partial \nu_{13}} = \frac{E_1 E_2}{2\Lambda}\left\{\left(\nu_{32}\bar{\varepsilon}_{22} - \frac{\nu_{32}^2 \bar{\varepsilon}_{11}}{\nu_{31}}\right)\bar{\varepsilon}_{11} + \left(\nu_{32}\bar{\varepsilon}_{11} - \nu_{31}\bar{\varepsilon}_{22}\right)\bar{\varepsilon}_{22}\right\}$$

$$+ \frac{E_1}{2\Lambda^2}\left\{\left(A_2 E_1 \bar{\varepsilon}_{11} + b_1 E_2 \bar{\varepsilon}_{22}\right)\bar{\varepsilon}_{11} + \left(b_1 \bar{\varepsilon}_{11} + b_2 \bar{\varepsilon}_{22}\right)E_2 \bar{\varepsilon}_{22}\right\}\left(E_1 \nu_{31} + E_2\left(\frac{\nu_{32}^2}{\nu_{31}} + 2\nu_{12}\nu_{32}\right)\right)$$

$$- \frac{E_1 \nu_{31} \bar{\varepsilon}_{33}^2}{2\nu_{13}^2}$$

(D.13)

$$\frac{\partial W}{\partial \nu_{32}} = \frac{E_1 E_2}{2\Lambda}\left\{\left(\nu_{13}\bar{\varepsilon}_{22} - b_1 \bar{\varepsilon}_{33} - \frac{2\nu_{32}\nu_{13}\bar{\varepsilon}_{11}}{\nu_{31}}\right)\bar{\varepsilon}_{11} + \nu_{13}\bar{\varepsilon}_{11}\bar{\varepsilon}_{22} - 2b_2 \bar{\varepsilon}_{33}\bar{\varepsilon}_{22} - b_1 \bar{\varepsilon}_{33}\bar{\varepsilon}_{11}\right\}$$

$$+ \frac{E_1 E_2}{\Lambda^2}\left\{\left(A_2 E_1 \bar{\varepsilon}_{11} + b_1 E_2 \bar{\varepsilon}_{22}\right)\bar{\varepsilon}_{11} + \left(b_1 \bar{\varepsilon}_{11} + b_2 \bar{\varepsilon}_{22}\right)E_2 \bar{\varepsilon}_{22}\right\}\left(\frac{\nu_{32}\nu_{13}}{\nu_{31}} + \nu_{12}\nu_{13}\right)$$

(D.14)

$$\frac{\partial W}{\partial \alpha_1} = -\frac{E_1 \Delta T}{\Lambda}\left\{A_2 E_1 \bar{\varepsilon}_{11} + b_1 E_2 \bar{\varepsilon}_{22}\right\}$$ **(D.15)**

$$\frac{\partial W}{\partial \alpha_2} = -\frac{E_1 E_2 \Delta T}{\Lambda}\left\{b_1 \bar{\varepsilon}_{11} + b_2 \bar{\varepsilon}_{22}\right\}$$ **(D.16)**

$$\frac{\partial W}{\partial \alpha_3} = -\frac{E_1 \Delta T}{\Lambda}\left\{\left(A_2 E_1 \nu_{31} + b_1 E_2 \nu_{32}\right)\bar{\varepsilon}_{11} + \left(b_1 E_2 \nu_{31} + b_2 E_2 \nu_{32}\right)\bar{\varepsilon}_{22}\right\}$$

$$+ \frac{E_1 \nu_{31} \bar{\varepsilon}_{33} \Delta T}{\nu_{13}}$$ **(D.17)**

$$\frac{\partial W}{\partial (\Delta T)} = -\frac{E_1 \bar{\varepsilon}_{11}}{\Lambda}\left\{A_2 E_1\left(\nu_{31}\alpha_3 + \alpha_1\right) + b_1 E_2\left(\nu_{32}\alpha_3 + \alpha_2\right)\right\} + \frac{E_1 \nu_{31}\alpha_3 \bar{\varepsilon}_{33}}{\nu_{13}}$$

$$- \frac{E_1 E_2 \bar{\varepsilon}_{22}}{\Lambda}\left\{b_1\left(\nu_{31}\alpha_3 + \alpha_1\right) + b_2\left(\nu_{32}\alpha_3 + \alpha_2\right)\right\}$$ **(D.18)**

where

$$A_1 = \frac{\nu_{32}^2 \nu_{13}}{\nu_{31}^2} E_2 , \qquad A_2 = 1 - \frac{\nu_{32}^2 \nu_{13}}{\nu_{31}} \frac{E_2}{E_1} \tag{D.19}$$

$$b_1 = \nu_{12} + \nu_{13}\nu_{32} , \qquad b_2 = 1 - \nu_{31}\nu_{13} \tag{D.20}$$

$$\bar{\varepsilon}_{22} = \varepsilon_{22} - (\nu_{32}\alpha_3 + \alpha_1)\Delta T , \quad \bar{\varepsilon}_{11} = \varepsilon_{11} - (\nu_{31}\alpha_3 + \alpha_1)\Delta T , \quad \bar{\varepsilon} = \alpha_3(\Delta T) \tag{D.21}$$

$$\Lambda = E_1(1 - \nu_{31}\nu_{13}) - E_2\left(\frac{\nu_{32}^2 \nu_{13}}{\nu_{31}} + \nu_{12}^2 + 2\nu_{12}\nu_{13}\nu_{32} \right) \tag{D.22}$$